Results and discussion

Chapter (3)
Results and discussion

3.1 Mossbauer effect results.

In the few last decads , Mossbauer effect (ME) spectroscopy has been classified to be an effective tool for investigating the structure of different solids and compounds . Therefore , many applied articles have been published dealing with different branches of material science [physics , chemistry and geology] as well as many other important applications in various branches such as biology and medicen[92,93,94] . Therefore ME was applied to study the structural role of iron ions in the studied glass samples as well as the effect of the enviromental changes around the iron ions [as it usually named Mossbauer ions].

Figure (3.1) shows the obtained ME spectra for the investigated glass samples of the composition $(50\text{-}x)P_2O_5\text{-}xAgI\text{-}40Ag_2O\text{-}10Fe_2O_3$, [x = 0 , 5 , 10 , 15, 20, 30] at room temperature.It is observed that,all of the obtained spectra exhibit an asymmetric paramagnetic doublet with broadend line width (LW). According to the computer fitting and analysis , the values of all the ME parameters were calculated and presented in Table (3.1) .It was concluded also that , each spectrum are composed of a single paramagnetic doublet which mains that all samples are considered paramagnetic host glass around the iron ions [ME ions or ME probes][95] . The appeared single double of each Mossbauer spectra indicated that iron ions occupy only the ferric state [Fe^{3+}]. The calculated parameters showed that most of the iron ions occupy the tetrahedral coordination state [96] and revealed also that iron ions are most probably occupy the network forming positions in these glasses.

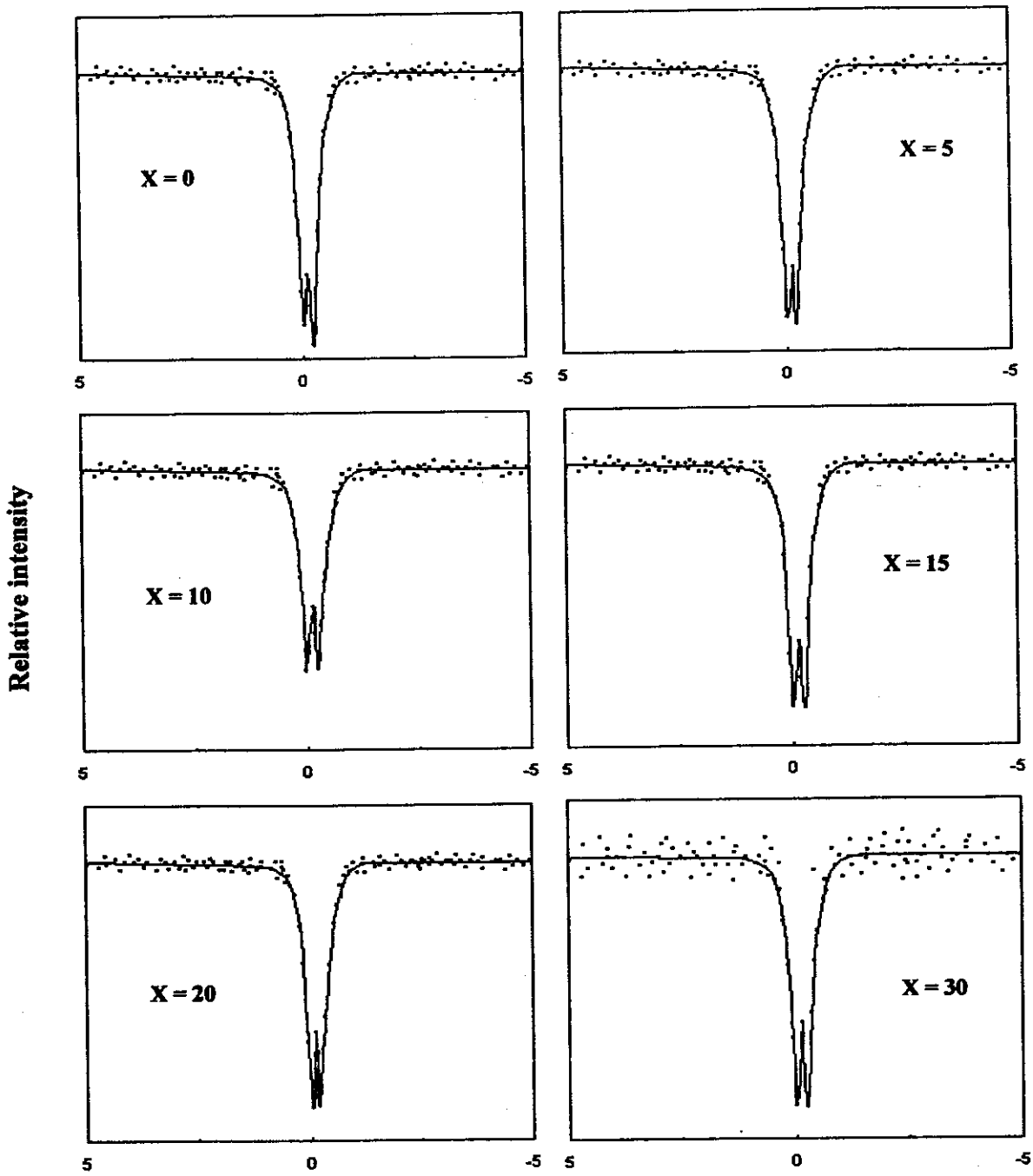

Figure (3.1) : ME spectra for the investigated glass samples (50-x)P_2O_5-xAgI-40Ag_2O-10Fe_2O_3 , [x = 0 , 5 , 10 , 15, 20, 30].

Table (3.1) : Mossbauer parameters of iron ions.

xAgI	LW mm/s	IS mm/s	QS mm/s
0	0.665	0.238	0.718
5	0.729	0.176	0.841
10	0.688	0.173	0.798
15	0.701	0.157	0.811
20	0.576	0.189	0.656
30	0.621	0.074	0.782

Figure (3.2) exhibit the variation of the line width (LW) values as a function of AgI content. The values of the LW are found to fluctuate between 0.576 and 0.729 mm/sec .These values appeared to be highly broadened in comparesion to the natural LW , which confirmed the homogenity of the amorphous state of the prepared glass samples[92] . Accordingly , it can be supposed that these values reflect the stability and the homogenity of the network structure of these glasses in spite of the replacement of oxygen by iodine anions.It can be also supposed that iodine ions when replace oxygen ions in the glass network increase the dangling iodine atoms gradually up to the sample x=20 mole % . The appered differences in the ME parameters at this point may be due to the higher ammount of dangling iodine ions . The approximate stability of the ME parameter after this point confirm such supposition . In addition to the similar behaviour of density and molar volume resultes .

Figure (3.3) showed the change in the isomer shift (IS) values over the range of increasing AgI content . by fitting the plotted IS (distributed) values a decreasing straight line was appeared , except the sample x=20 mole % AgI , which reflect the highest value . This line showed a decreasing trend with the increase in the AgI content . This means that the effect of the d-iron electron act to increase the s-electron wave function around the iron nucleus[97] .

Figure (3.4) shows the change in the quadrupole splitting (QS) values as the AgI content was gradually increased . The computer fitting of the distributed QS values resulted in a decreasing trend with a lower value for the sample x=20 mole % AgI . It can be stated that the electric field gradient

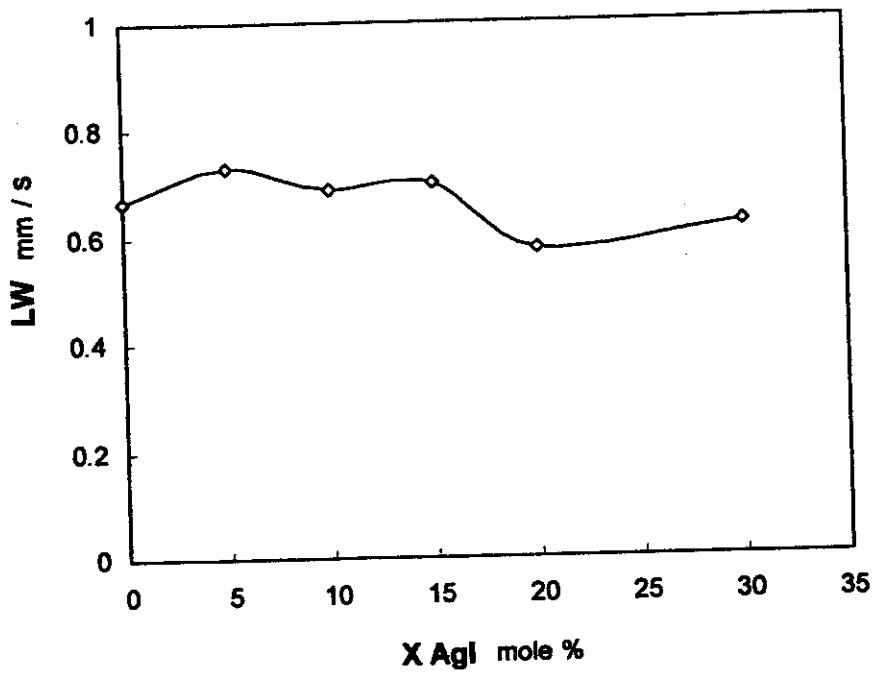

Figure (3.2) : Relation between Line width (LW) and xAgI mole% for the glass system $(50-x)P_2O_5$-xAgI-$40Ag_2O$-$10Fe_2O_3$, [x = 0,5,10,15,20,30] .

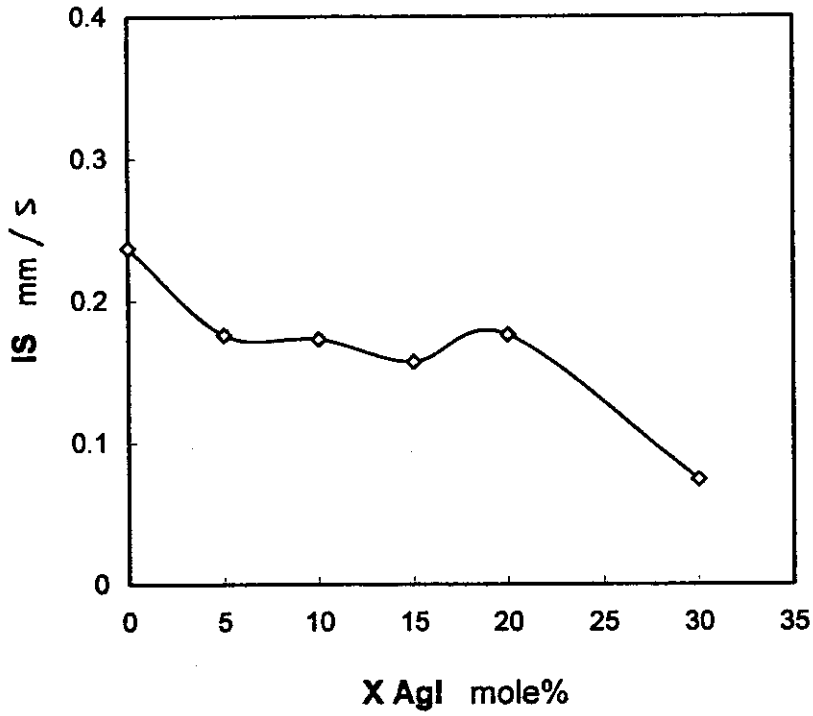

Figure (3.3) : Relation between Isomer shift (IS) and xAgI mole% for the glass system (50-x)P_2O_5-xAgI-40Ag_2O-10Fe_2O_3 , [x = 0,5,10,15,20,30] .

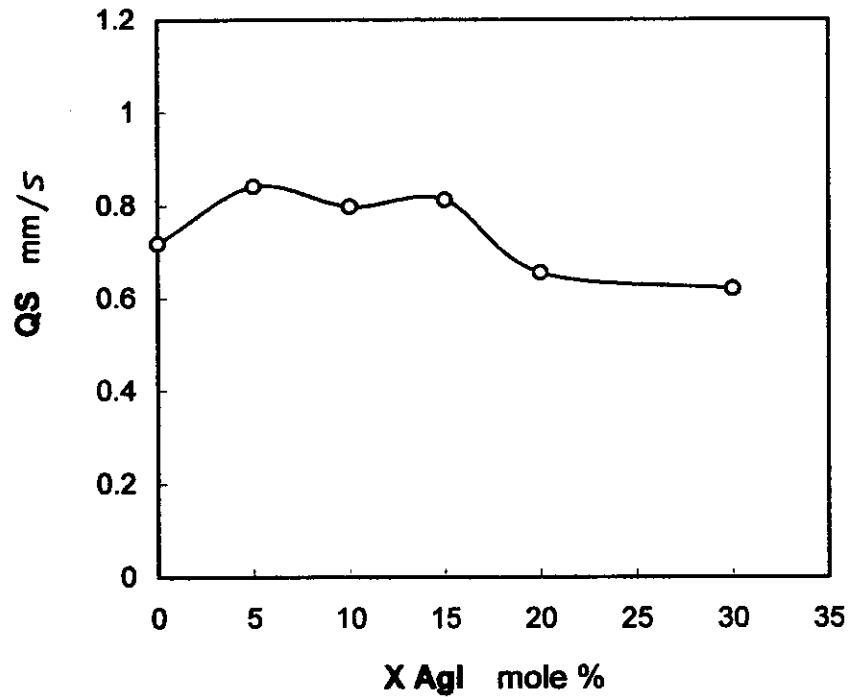

Figure (3.4) : Relation between Quadrupole splitting (QS) and xAgI mole% for the glass system (50-x)P_2O_5-xAgI-40Ag_2O-10Fe_2O_3 , [x = 0,5,10,15,20,30] .

(EFG) due to the lattice around the iron nucleus decreases gradually , but for the mentioned sample , it reflect a lower EFG value[98,99]

It is obvious from the obtained resultes that , the sample which contains 20 mole % AgI undergo some structural changes . This could be show from : *(i)* The lower LW value in comparesion to the others , *(ii)* The higher IS value in comparesion to the others , *(iii)* The lower QS value .This structural change in the sample x=20 mole % AgI was confirmed from the resultes of other techniques (density and molar volume) .

3.2 Density and Molar volume .

Density of glass is considered as an important property specially for industrial control , since any change in the density of glass reflects fine structural changes , phase separation or some crystal precipitation . Therefore the density of studied glasses were measured and they are presented in Figure (3.5) as a function of AgI content . It showed approximately linear increasing trend in the range from 0 to 20 mole % AgI and appeared to be stable until 30 % AgI .

It is interested to calculate the molar volume (V_m) which of interest for reflecting the spatial structure of a glass network . Figure (3.6) showed the change in the molar volume values as a function of the AgI content . It is noticed that , as the AgI increased from 0 to 20 mole % , the molar volume decreased linearly , while in between 20 to 30 mole % AgI , it seems to be stable[100] .

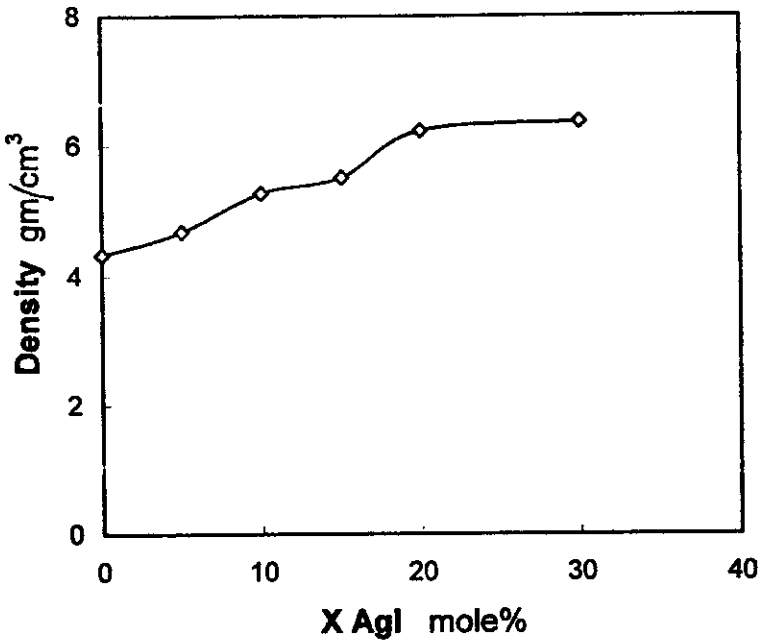

Figure (3.5) : Relation between Density and xAgI mole% for the glass system $(50-x)P_2O_5$-xAgI-$40Ag_2O$-$10Fe_2O_3$, [x = 0,5,10,15,20,30] .

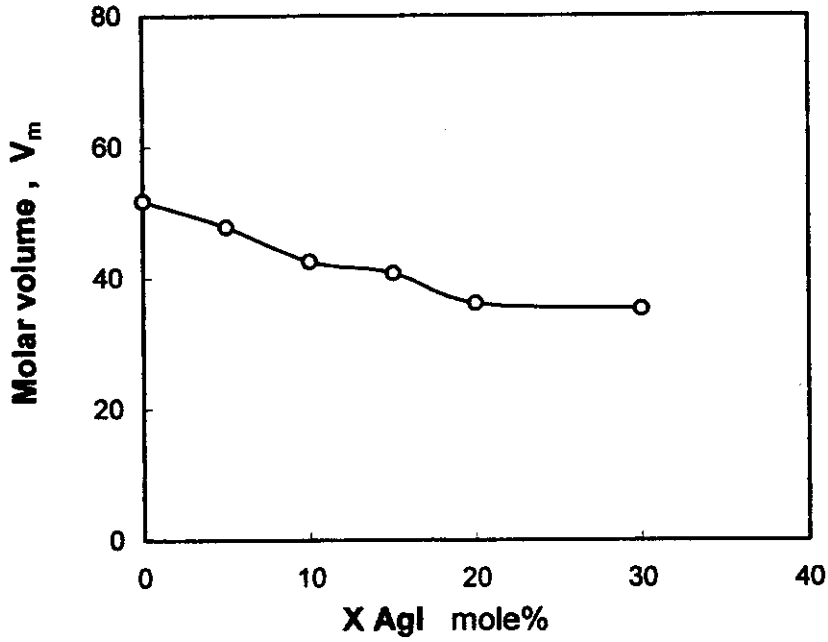

Figure (3.6) : Relation between Molar Volume (V_m) and xAgI mole% for the glass system $(50-x)P_2O_5$-xAgI-$40Ag_2O$-$10Fe_2O_3$, [x = 0,5,10,15,20,30].

3.3 General discussion on the structure of glass .

It is known from the preparation of the glass samples $(50-x)P_2O_5$-xAgI-$40Ag_2O$-$10Fe_2O_3$, [x = 0 , 5 , 10 , 15, 20, 30] that , AgI increases and P_2O_5 decreases gradually in molecular weight % . this means that , the number of the oxygen decreased gradually when Ag and I increased. Therefore it can be supposed that , the sample (xAgI = 0) contians many non-bridging oxygen and no Ag-P bonds was founed . In addition , the most of iron ions occupy the network forming positions as concluded from IR and Mossbauer (ME) techniques which confirm each other . Consequently , the most of Ag cations prefer to occupy the network modifying positions in this sample . Increasing AgI content at the expense of P_2O_5 indicates the approximate gradual decrease in the ratio of [(P+Fe)/(O+I)] , since Fe acts as a network former . This reaveld that , the non-bridging oxygen may decreased and the Ag-P bonds may increased. The addition of AgI (increasing silver cations and introducing I anions) may also increase the dangling bonds between I and P or Fe atoms of the form PO_3-I or FeO_3-I. In addition some silver cations may appeared as an isolated (AgI_4) groups.

According to the density and the molar volume , the change in their values in the range from 0 up to 20 mol % appeared to be small which may reflect the formation of some AgI_4 clusters . The stability of the density and molar volume in the range from 20 and 30 % AgI may reflect the stability of the glass network in this range and the increase in silver cations as AgI was gradually increased may increase the P-Ag bonds. The formation of these bonds reflect no change in the network structure of these glasses. This stability was confermed in agreement with the results of both line width (LW) and quadrupole splitting (QS) values concluded from ME.

From the IR interpretation , the P=O bond at1200 cm^{-1} apperead in the samples contianing AgI from 0 to 10 mole % and disappeared completely in the samples contianing AgI from 15 to 30 mole % . This result confirm the above supposition that at low AgI content , the excess oxygen form large non-bridging oxygens as well as the formation of some phosphrous double bond oxygens (P=O) [49] . The disappearance of this bond confirm also the decrease of non-bridging oxygen due to the difficiency of the oxygen anions

3.4 Electrical characterization (conduction and dielectric properties).

3.4.1 The frequency dependence of the total conductivity.

Figure [(3.7)A,B] illustrates the logarithmic plots of $\sigma_{tot}(\omega)$ against frequency F in the frequency range (50 Hz - 5 MHz) for the glass system $(50\text{-}x)P_2O_5\text{-}xAgI\text{-}40Ag_2O\text{-}10Fe_2O_3$, [x = 0 , 5 , 10 , 15, 20, 30] at different ambient temperatures. It is noticed that, the total conductivity is nearly constant at the lower frequency range for the glass samples of the xAgI content (x = 0,5,10) but it obeys a power relation at the higher frequency range. At higher temperature range , $\sigma_{tot}(\omega)$ is nearly unchanged with increasing frequency over all the frequency range. For the higher xAgI content , an anomalous behaviour [a minimum in $\sigma_{tot}(\omega)$-F relation] is observed. The variation of $\sigma_{tot}(\omega)$ with frequency could be expressed by the following relation[101];

$$\sigma_{tot} = \sigma_{dc} + \sigma`(\omega) \qquad (3.1)$$

where σ_{dc} , the dc conductivity, which is independent of frequency (extrapolation of σ_{tot} at $\omega = 0$) and $\sigma'(\omega)$ is the ac conductivity .

Recently the jump relaxation model of Funke[102] has been used to account for the frequency dependence of the conductivity in disordered systems . Funke proposed that in the case of structurally disordered materials, if an ion performes a hop to neighbouring vacant sites , there is high probability for that ion to hop back to its previous position (an unsuccessful hop) but if the neighbourhood then becomes relaxed with

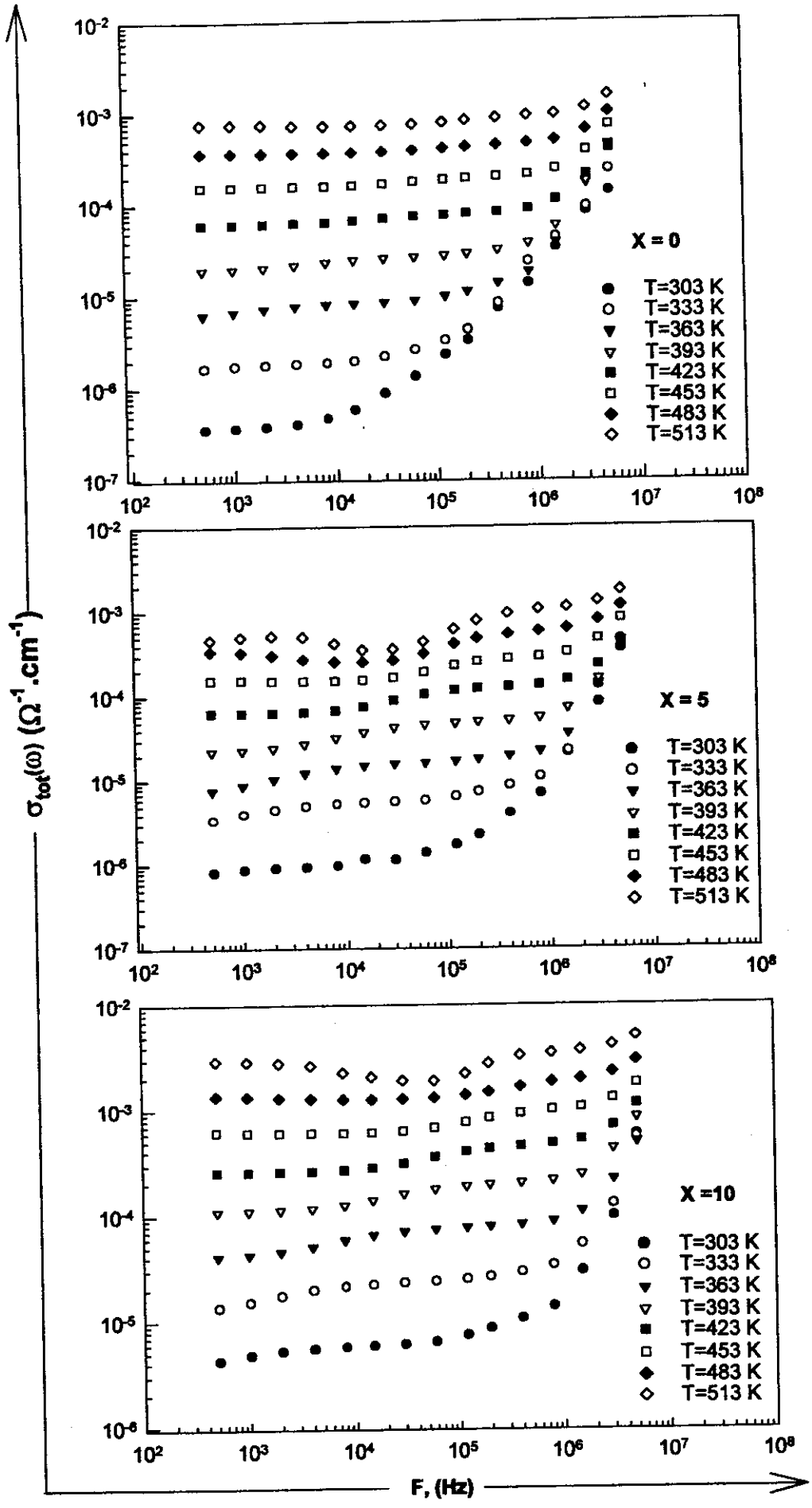

Figure [3.7(A)] : The frequency dependence of σ_{tot} (ω) for the glass system (50-x)P_2O_5-xAgI-40Ag_2O-10Fe_2O_3 ,(x=0,5,10) at different ambient temperatures

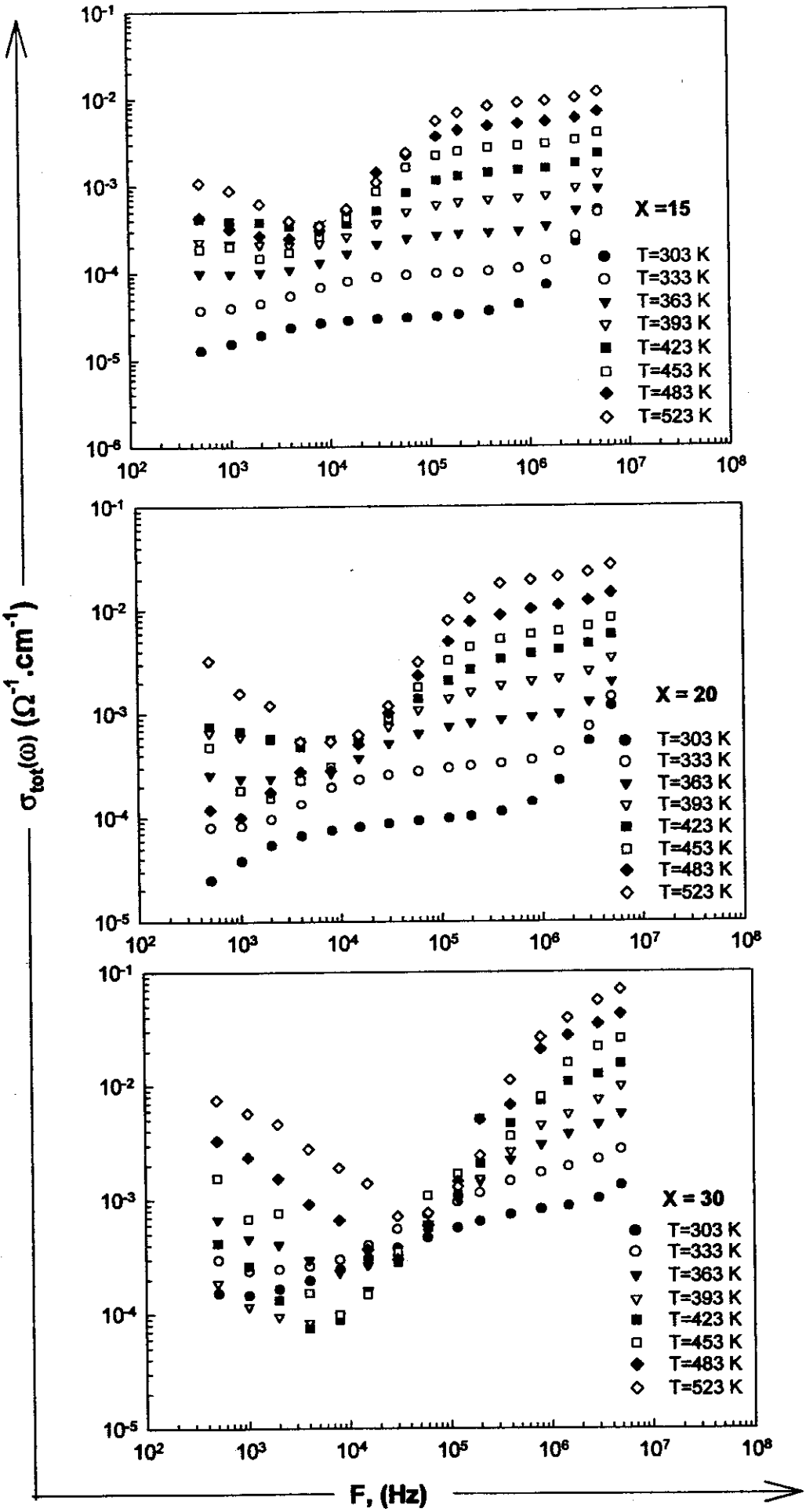

Figure [3.7(B)] : The frequency dependence of σ_{tot} (ω) ,for the glass system (50-x)P_2O_5-xAgI-40Ag_2O-10Fe_2O_3 ,(x=15,20,30) at different ambient temperatures .

respect to the ion position , the ion stays on the new site , the initial forward hop has proved successful. In the plateau region , the dc conductivity is determined entirely by the successful hops . In the region above the plateau , many hops are unsuccessful and,as the frequency increased ,the proportion of these unsuccessful hops rises ; this change in the ratio of successful to unsuccessful hops that results in the dispersive conductivity . The predictions of this jump relaxation model apply to the temperature dependence of the ac conductivity , different activation energies being associated with unsuccessful and successful hoping process.

In line with the model predictions , the frequency dependences of the conductivity of the ionic glasses studied can be fitted , as shown in Figure [(3.7)A,B] using a power law[49],

$$\sigma'(\omega) = A\,\omega^{S} \qquad (3.2)$$

where A is temperature-dependence parameter and ω is the angular frequency.The values of the exponent s have been estimated from relation (3.2) by means of the least square method at different temperatures . The obtained values of power s and pre-factor A are given in Table (3.2). It is noticed that , the exponent $s<1$ corresponds to the translational hopping motion and its values does not depend on the AgI content of these glasses . The observed anomalous behaviour in σ_{tot} (ω)- F relation at x =15,20,30 (decreases of σ_{tot} at lower values of frequncy) can be attributed to increase of the interfacial polarization (polarizing conductivity) as a result of presence of microdomains structure and subsequently the opposing field was increased which will reduce the resultant effective field at the domain

Table (3.2) : The values of the power S and pre-factor A for the glass system $(50\text{-}x)P_2O_5\text{-}xAgI\text{-}40Ag_2O\text{-}10Fe_2O_3$, *[x=0,5,10,15,20,30].*

x AgI	X=0		X=5		X=10		X=15		X=20		X=30	
T , K	S	A	S	A	S	A	S	A	S	A	S	A
303	0.58	5.1×10^{-9}	0.78	2.1×10^{-10}	1.28	4.2×10^{-13}	0.86	3.8×10^{-10}	0.64	2.6×10^{-8}	0.48	8.1×10^{-7}
333	0.85	6.1×10^{-7}	1.05	8.0×10^{-12}	1.09	1.1×10^{-11}	0.95	1.6×10^{-10}	0.95	5.2×10^{-10}	0.38	6.6×10^{-6}
363	0.94	6.1×10^{-11}	0.89	1.4×10^{-10}	1.04	4.1×10^{-11}	0.86	1.3×10^{-9}	0.81	7.1×10^{-9}	0.41	9.9×10^{-6}
393	1.01	4.0×10^{-11}	0.87	3.1×10^{-10}	0.85	1.3×10^{-9}	0.60	1.1×10^{-7}	0.51	1.1×10^{-6}	0.53	2.6×10^{-8}
423	0.61	2.3×10^{-8}	0.92	2.3×10^{-10}	0.79	5.7×10^{-9}	0.49	1.0×10^{-6}	0.49	1.3×10^{-5}	0.43	1.9×10^{-5}
453	0.47	3.3×10^{-7}	1.03	9.8×10^{-11}	0.51	6.0×10^{-7}	0.37	1.2×10^{-5}	0.39	3.4×10^{-5}	0.70	5.4×10^{-7}
483	0.59	9.5×10^{-8}	0.75	1.1×10^{-8}	0.50	1.1×10^{-6}	0.36	2.7×10^{-5}	0.38	4.1×10^{-5}	0.45	4.2×10^{-5}
513	0.53	3.7×10^{-7}	0.56	2.9×10^{-7}	0.45	9.2×10^{-6}	0.35	5.1×10^{-5}	0.39	6.5×10^{-5}	0.50	3.2×10^{-5}

interfaces and subsequently reduce the ionic diffusion (the increase of scattering polarization).

Regarding to the general behaviour of $\sigma_{tot}(\omega)$ against frequency , it consists of two regions discribed by equation (3.1) . There is a critical frequency ω_p after which the conductivity obeys the mentioned power relation.The crossover frequency from the dc to the dispersive region ,ω_p, increases with increasing temperature.Almond et al[103] have assumed that, the total conductivity reaches twice σ_{dc} at such critical frequency ω_p [which is defined as the ionic hopping rate] , and is given by,

$$\omega_p = [\sigma_{dc}/A]^{1/S} \qquad (3.3)$$

The values of ω_p are deduced at different ambient temperatures for the glass system under investigation, it is noticed that ω_p values lie in the same range of those obtained by Almond et al[103] for silver iodoarsenate ionic glasses (10^3-10^6 Hz) . Figure (3.8) illustrates the temperature dependence for the hopping rate ω_p for all glass samples,which obey the following Arrhenius relation ;

$$\omega_p = \omega_o \exp (- E_\omega / KT) \qquad (3.4)$$

where E_ω is an activation energy term concerning the variation of ω_p with temperature, and $\omega_p = \omega_o$ at $T = \infty$ K. The values of E_ω and ω_o are deduced by using the least square fitting of relation (3.4) and listed in Table (3.3). The observed activation of ω_p with increasing temperature can be explained as follows. The increase of ambient temperature leads to an increase of the dc

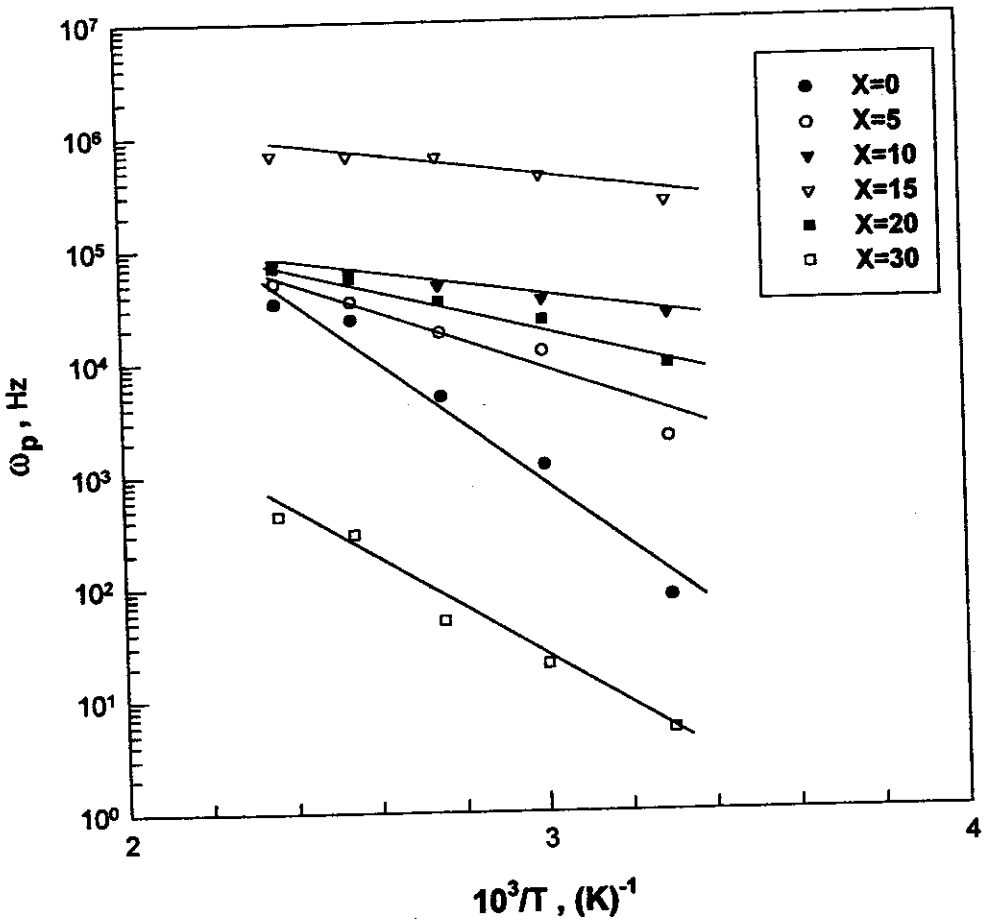

Figure (3.8) : The temperature dependence of ω_p for the glass system $(50-x)P_2O_5$-$xAgI$-$40Ag_2O$-$10Fe_2O_3$,[x=0,5,10,15,20,30].

Table (3.3) : The values E_ω and ω_o for the glass system $(50\text{-}x)P_2O_5\text{-}xAgI\text{-}40Ag_2O\text{-}10Fe_2O_3$, [x=0,5,10,15,20,30].

xAgI	E_ω , eV	ω_o , Hz
0	0.585	7×10^{12}
5	0.262	8×10^{8}
10	0.028	9×10^{5}
15	0.038	8×10^{6}
20	0.150	3×10^{7}
30	0.475	5×10^{8}

conductivity of the glasses which competes the influence of the polarizing conductivity leading to the apparent shift of $\sigma_{tot}(\omega)$- F curves up right.

The temperature dependence of dc conductivity for the glass system $(50\text{-}x)P_2O_5\text{-}xAgI\text{-}40Ag_2O\text{-}10Fe_2O_3$, [x = 0 , 5 , 10 , 15, 20, 30] were studied in the temperature range from room temperature to 500 K , Figure (3.9). The temperature dependence of dc conductivity in the whole temperature range can be discribed by the following relation[104];

$$\sigma_{dc}T = A` \exp(-E_{dc}/KT) \qquad (3.5)$$

where E_{dc} is the apparent activation energy. It is noticed that, the general behaviour is the activation of conductivity with increasing temperature. Also there is one region in $\sigma_{dc}(T)\text{-}10^3/T$ relation appears and the conductivity increases with the increasing xAgI content . The obtained values of the E_{dc} are listed in Table (3.4). It clear that, E_{dc} lie in the range (0.21 - 0.42 eV) and show regular decrease with increasing xAgI content.

The activation of dc conductivity with increasing temperature may be attributed to the fast diffusion involving low-energy barriers for the motion of Ag^+ ions in the microdomains of AgI_4 clusters[57] which are embedded in the glass matrix. Also, the total interaction between the Ag^+ and I^- ions including both ionic and covalent bonding in the AgI_4 cluster, is very small. This characteristic electronic state [73] of the Ag^+ ion is one of the causes of the fast movement of Ag^+ ions in AgI-based superionic glasses.In addition , the Ag^+ ion has a $(4d)^{10}$ configuration of electrons which results in "soft outer shell" and may be distorted and fitted to the conduction pass . This flexibility of the outer shell is belived to be one of the origins of the hight

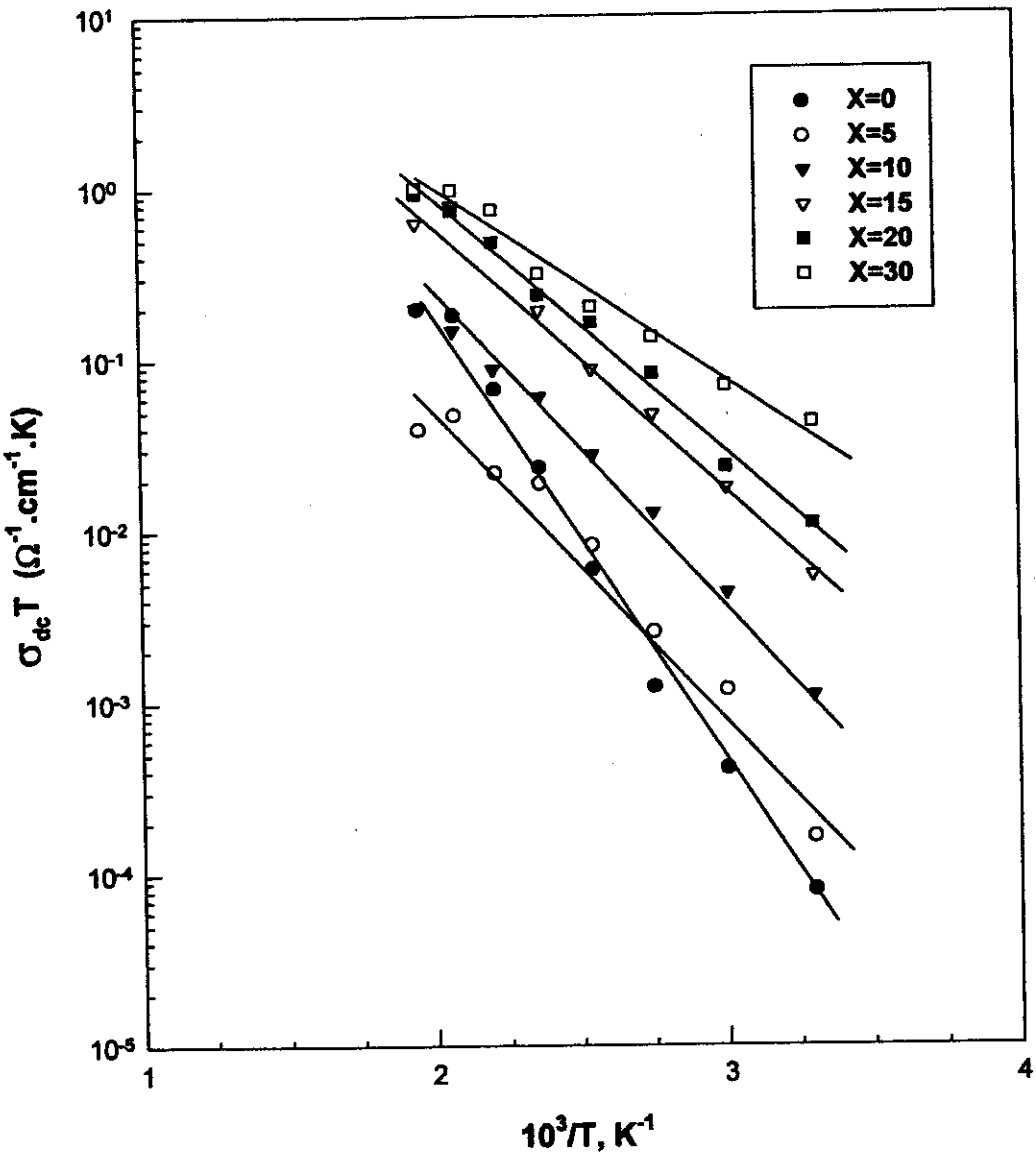

Figure (3.9): The temperature dependence of σ_{dc} for the glass system $(50-x)P_2O_5$-$xAgI$-$40Ag_2O$-$10Fe_2O_3$ (x=0,5,10,15,20,30).

Table (3.4): The values E_{dc} for the glass system$(50-x)P_2O_5$-$xAgI$-$40Ag_2O$-$10Fe_2O_3$,[x=0,5,10,15,20,30].

xAgI	E_{dc} , eV
0	0.423
5	0.347
10	0.323
15	0.317
20	0.284
30	0.209

ionic conductivity of AgI related compounds . As the concentration of the xAgI content increases, the concentration of the microdomains increases which leads to an increase of the conductivity.

3.4.2 The temperature dependence of the total conductivity.

The total conductivity $\sigma_{tot}(\omega)$ was studied as a function of reciprocal temperature at different frequencies (0.5 KHz, 100 KHz, 5 MHz) for the glass system $(50-x)P_2O_5$-xAgI-$40Ag_2O$-$10Fe_2O_3$, [x = 0 , 5 , 10 , 15, 20, 30] , Figure [(3.10)A,B,C] . It is noticed that, the total conductivity $\sigma_{tot}(\omega)$ is found to be thermally activated. One region in $[\sigma_{tot}T\text{-}10^3/T]$ relation are observed in the case of the frequences 0.5 KHz, 100KHz where as at 5 MHz there are two regions for all samples except the case x =30. This behaviour could be described by the following relation[51] ;

$$\sigma_{tot}(\omega)T = A` \exp (-\Delta E_1/KT) + B \exp (-\Delta E_2/KT) \qquad (3.6)$$

where A` and B are temperature independent parameters and ΔE_1 and ΔE_2 are low and high temperature activation energies listed in Table (3.5). The observed behaviour of $\sigma_{tot}(\omega)T\text{-}10^3/T$ relation can be explained as follows ; when the temperature was increased, $\sigma_{tot}(\omega)$ increases because of structure relaxation and the Ag^+ ions attached to the non-bridging oxygens are released and become mobile leading to the increase of the mobile ion concentration. In addition, the increase of $\sigma_{tot}(\omega)$ with increasing xAgI content may be due to the contribution of silver salt (AgI) and glass modifier oxide (Ag_2O) through the following dissociation reaction[105] ;

$$AgI = Ag^+ + I^- \quad \text{and} \quad Ag_2O = Ag^+ + OAg^- \ .$$

At low temperature region , Figure [(3.10)C], a very low energy (about 0.02 eV) characterizing this region shows only a weak dependence on the xAgI content.Hence the process involved could be related to the topological

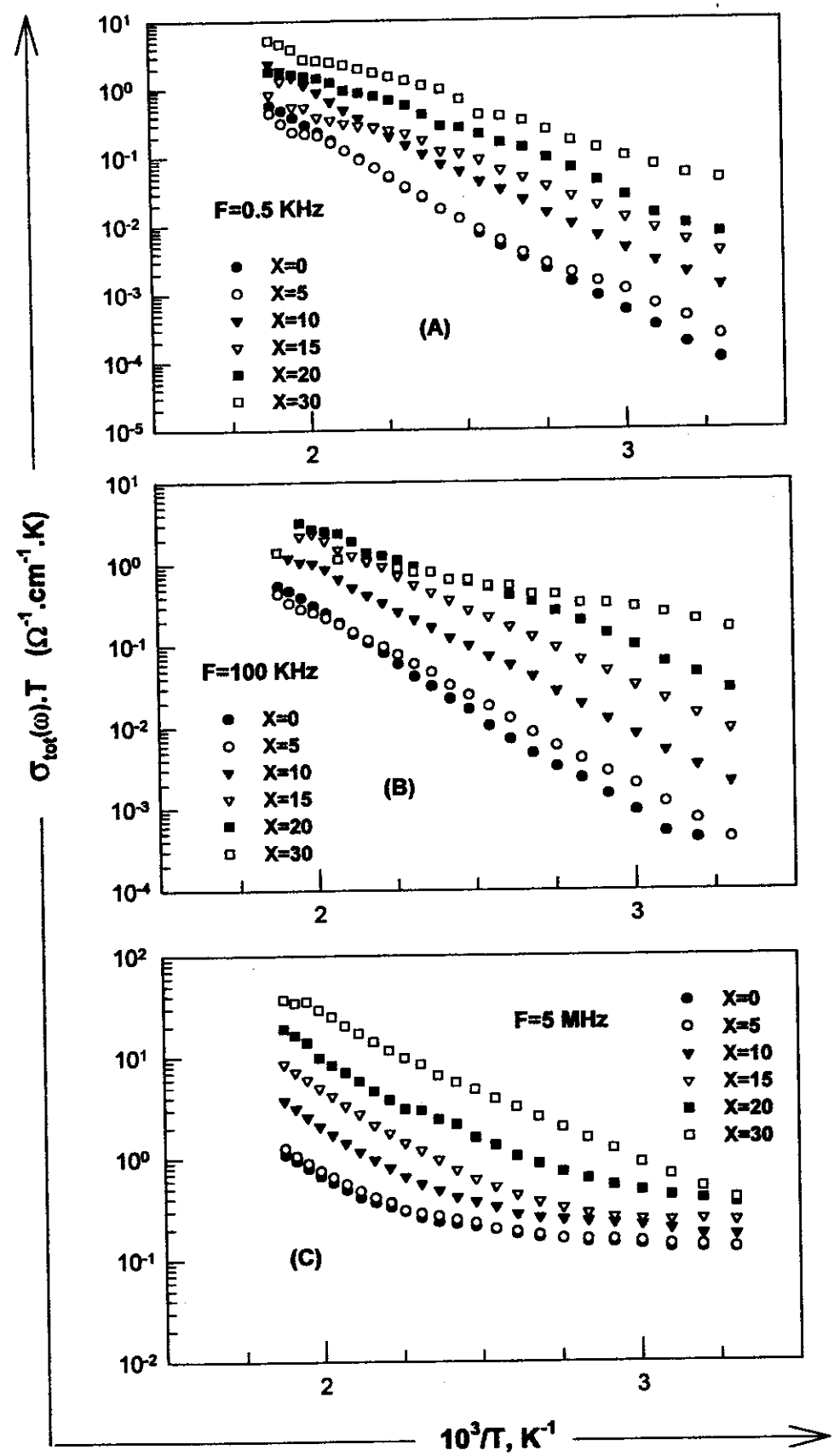

Figure [3.10(A,B,C)] : The temperature dependence of $\sigma_{tot}(\omega)$ for the glass system $(50-x)P_2O_5$-$xAgI$-$40Ag_2O$-$10Fe_2O_3$ (x=0,5,10,15,20,30) at different frequencies.

Table (3.5) : The values of the activation energy for the glass system $(50-x)P_2O_5$-$xAgI$-$40Ag_2O$-$10Fe_2O_3$,[x=0,5,10,15,20,30] at different frequencies.

Frequency	0.5 KHz	100 KHz	5 MHz	
xAgI	ΔE_1 , eV	ΔE_1 , eV	ΔE_1 , eV	ΔE_2 , eV
0	0.49	0.46	0.02	0.26
5	0.42	0.38	0.03	0.27
10	0.42	0.36	0.26	0.28
15	0.31	0.32	0.02	0.27
20	0.38	0.24	0.06	0.26
30	0.22	0.05	0.25	----

disorder typifying disordered materials . At higher temperatures an activation energy $0.26 < \Delta E > 0.28$ eV characterizing a second relaxation process whose onset shifts towards higher temperatures with increasing frquency and whose value does depend on the xAgI content.

3.4.3 Complex Impedence results.

The bulk conductivity for the glass system,$(50-x)P_2O_5$-xAgI-$40Ag_2O$-$10Fe_2O_3$,[x=0,5,10,15,20,30],was estimated using the complex impedene method[106] in the range between room temperature and 500 K and the frequency range (50Hz–5MHz) . The plots of Z``, (imaginary part of impedence), against Z`, (real part of impedence) , for the glass system, ,showed two arcs , Figure(3.11) . The arc corresponds to the lower frequency values of complex impedence (right-hand side of each plot) is incomplete and is determined by interfacial capacetance C_i and resistance R_i . As the temperature is increased, the interfacial resistance increases . The arc corresponds to the higher frequency values (left-hand side of each plot) in the frequency range investigated determined by the bulk resistance R_{bl} and geometrical capacetance C_{bl} .The intersection of the semicircle with Z`axis gives the bulk resistance R_{bl} from which bulk conductivity σ_{bl} can be obtained. The obtained values of σ_{bl} are thermally activated with increasing temperature and obeys Arrhenius equation which can be expressed by the following relation ;

$$\sigma_{bL}T = A` \exp(-E_{bL} / KT) \qquad (3.7)$$

where E_{bL} is the apparent activation energy.Figure (3.12) illustrates semilogarithmic plot of $\sigma_{bl}T$ versus $10^3/T$. The activation energies are determined by the least square fitting of relation (3.7) and listed in Table (3.6).It is also noticed that , the bulk conductivity σ_{bl} increases with increase the xAgI content.

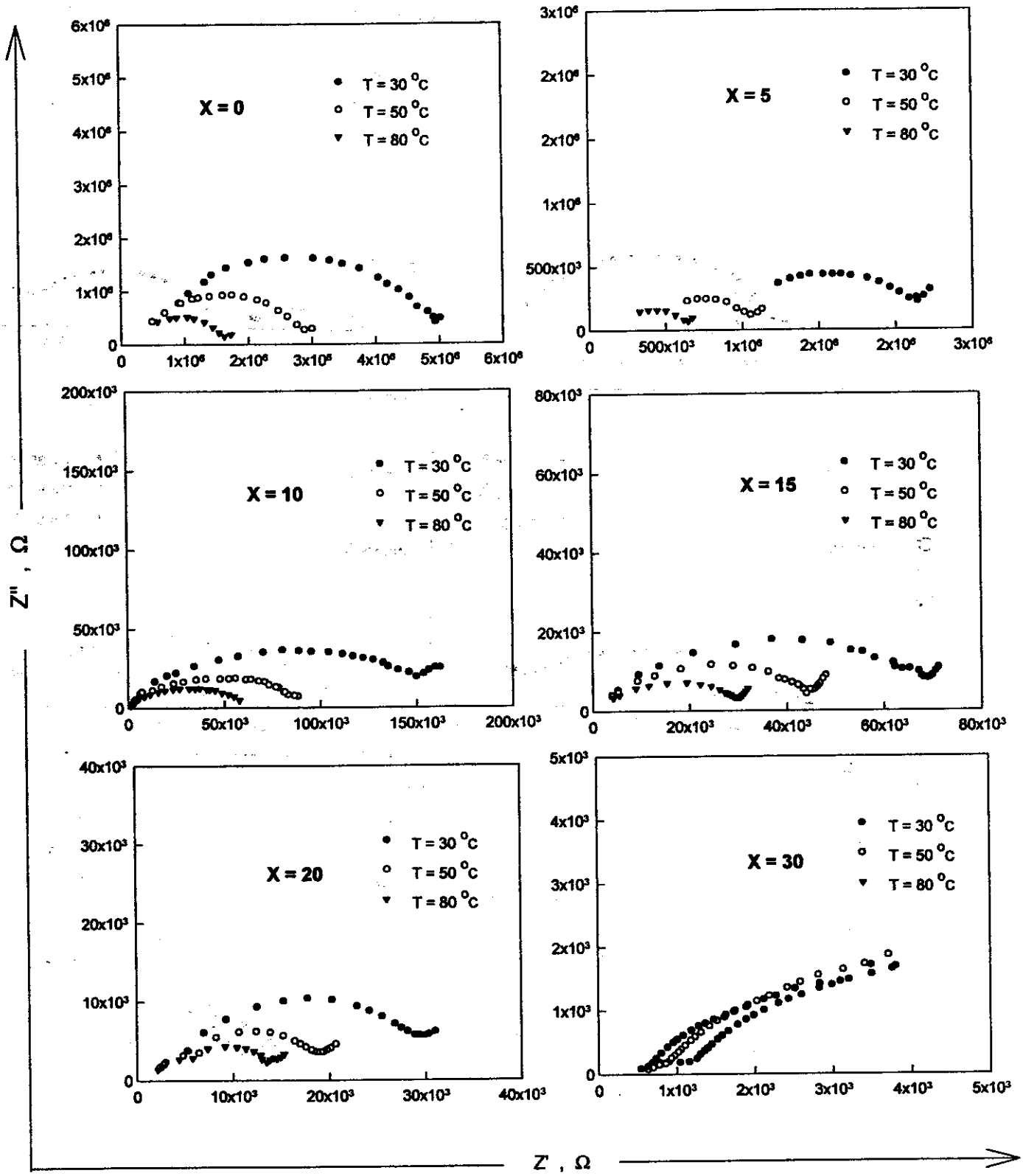

Figure (3.11) : Plots of Z'' vs Z' for the glass system $(50\text{-}x)P_2O_5\text{-}xAgI\text{-}40Ag_2O\text{-}10Fe_2O_3$ (x=0,5,10,15,20,30) at different temperatures .

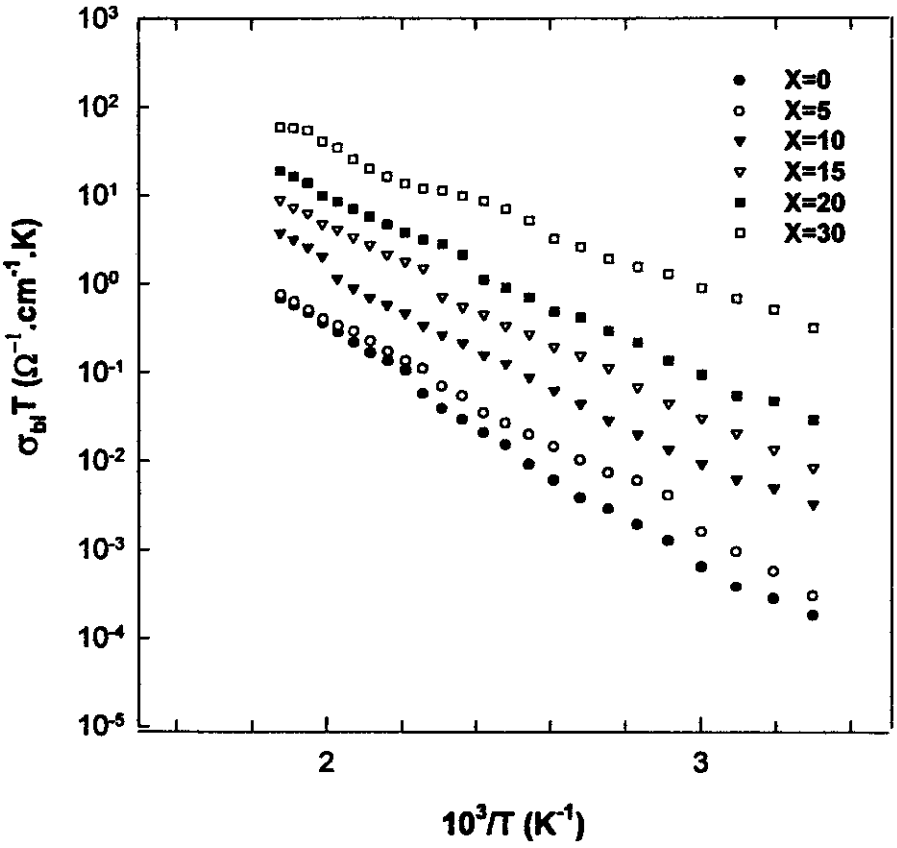

Figure (3.12) : The temperature dependence of σ_{bl} ,for the glass system $(50\text{-}x)P_2O_5$- $xAgI$-$40Ag_2O$-$10Fe_2O_3$, (x=0,5,10,15,20,30) .

Table (3.6) : The values E_{bi} for the glass system $(50-x)P_2O_5$-$xAgI$-$40Ag_2O$-$10Fe_2O_3$,[x=0,5,10,15,20,30]

x AgI	E_{bi} , eV
0	0.488
5	0.432
10	0.397
15	0.393
20	0.366
30	0.282

Figure (3.13) illustrates the semilogarithnic plot of $\sigma_{bl}T$ versus xAgI content at different temperatures which obeying the following emperical relation ;

$$\sigma_{bL}(x) = \sigma_{bL}(0) \exp(x/\alpha) \qquad (3.8)$$

where the factor $\sigma_{bl}(0)$ is constant equal to the bulk conductivity at $x \rightarrow 0.0$, $(1/\alpha)$ is a characteristic concentration depends on the Ag^+ ion content .The pre-exponential factor $\sigma_{bl}(0)$ lie in the range $(5x10^{-7}\text{-}8x10^{-4})$ and the characteristic concentration constant $(1/\alpha)$ lie in the range (3.71 - 5.89) see Table (3.7).

The activation of bulk conductivity (σ_{bl}) with increasing temperature can be interpreted by the following structure model which was suggested by T.Minami[12]. This model suggested the occurance of Ag^+ ions with different mobilities in AgI-based superionic glasses in three types of Ag^+ ions: (i) Ag^+ ions are bonded to the oxygen atoms of the network, (ii) Ag^+ ions interact weakly with the network oxygen atoms and (iii) Ag^+ ions are surrounded by I^- ions only. Silver ions of the last type have maximum mobility and contribute mostly to ionic conduction. When the temperature was increased to higher values, the conductivity reaches to higher values because of Ag^+ ions (which interact weakly to the oxygen atoms of the network) may release and contribute in conduction with the Ag^+ ions (which surrounded by I^- ions) leads to increase the concentration of Ag^+ mobile ions.

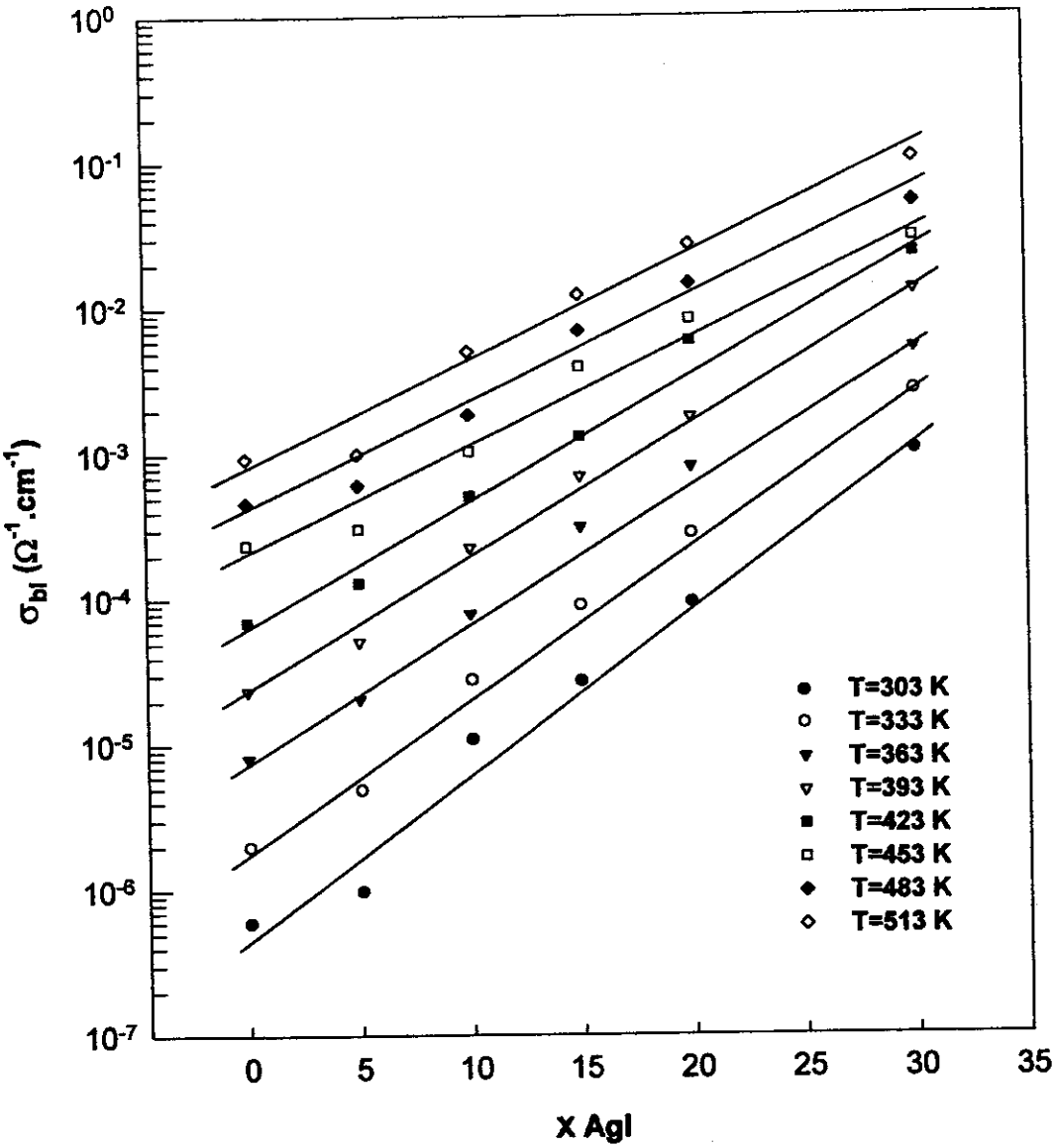

Figure (3.13) : The composition dependence of σ_{bl} for the glass system (50-x)P_2O_5-xAgI-40Ag_2O-10Fe_2O_3 at different temperatures.

Table (3.7) : The values $\sigma(0)$ and $1/\alpha$ for the glass system $(50-x)P_2O_5$ $-xAgI-40Ag_2O-10Fe_2O_3$,[x=0,5,10,15,20,30] at different temperatures.

T , K	σ (0)	$1/\alpha$
303	5×10^{-7}	3.71
333	2×10^{-6}	4.06
363	7×10^{-6}	4.22
393	2×10^{-5}	4.64
423	6×10^{-5}	4.88
453	2×10^{-4}	5.42
483	4×10^{-4}	5.51
513	8×10^{-4}	5.89

3.4.4 Effect of frequency and temperature on the dielectric constant ε`.

Figure [(3.14)A,B] illustrates the plot of real part of dielectric constant ε' against frequency for the glass system $(50\text{-}x)P_2O_5\text{-}xAgI\text{-}40Ag_2O\text{-}10Fe_2O_3$, [x = 0 , 5 , 10 , 15, 20, 30] at different ambient temperatures. It is noticed that, the general feature is the decrease of ε` with increasing frequency to asympototic value. According to Deby's theory of intrinsic relaxtion time, ε` can be expressed by following relation[107];

$$\varepsilon` = \varepsilon_\infty + [\ (\varepsilon_s - \varepsilon_\infty) / (1 + \omega^2 \tau^2)\ ] \qquad (3.9)$$

where ε_s and ε_∞ are the static and infinite dielectric constant respectively. The attenuation of dielectric constant ε` with increasing frequency can be explained as follows. When the frequency was increased, the dipoles will no longer be able rotate sufficiently rapidly so that their oscillations begin to lag behined field . It is noticed also that,the observed large values of ε` at lower frequency over the whole temperature range interfacial polarization effect[53,108,109].

The dielectric constant ε` of the glass system $(50\text{-}x)P_2O_5\text{-}xAgI\text{-}40Ag_2O\text{-}10Fe_2O_3$ , [x = 0 , 5 , 10 , 15, 20, 30] was studied in the temperature range between room temperature and 500 K at different fixed frequencies , Figure [(3.15)A,B] . It is noticed that , ε` increases, in general , with increasing temperature , some decrease of ε` is also observed beyond a certain temperature .This anomalous behaviour can be attributed to the glass transsition temperature ,T_g (see DTA thermograms).

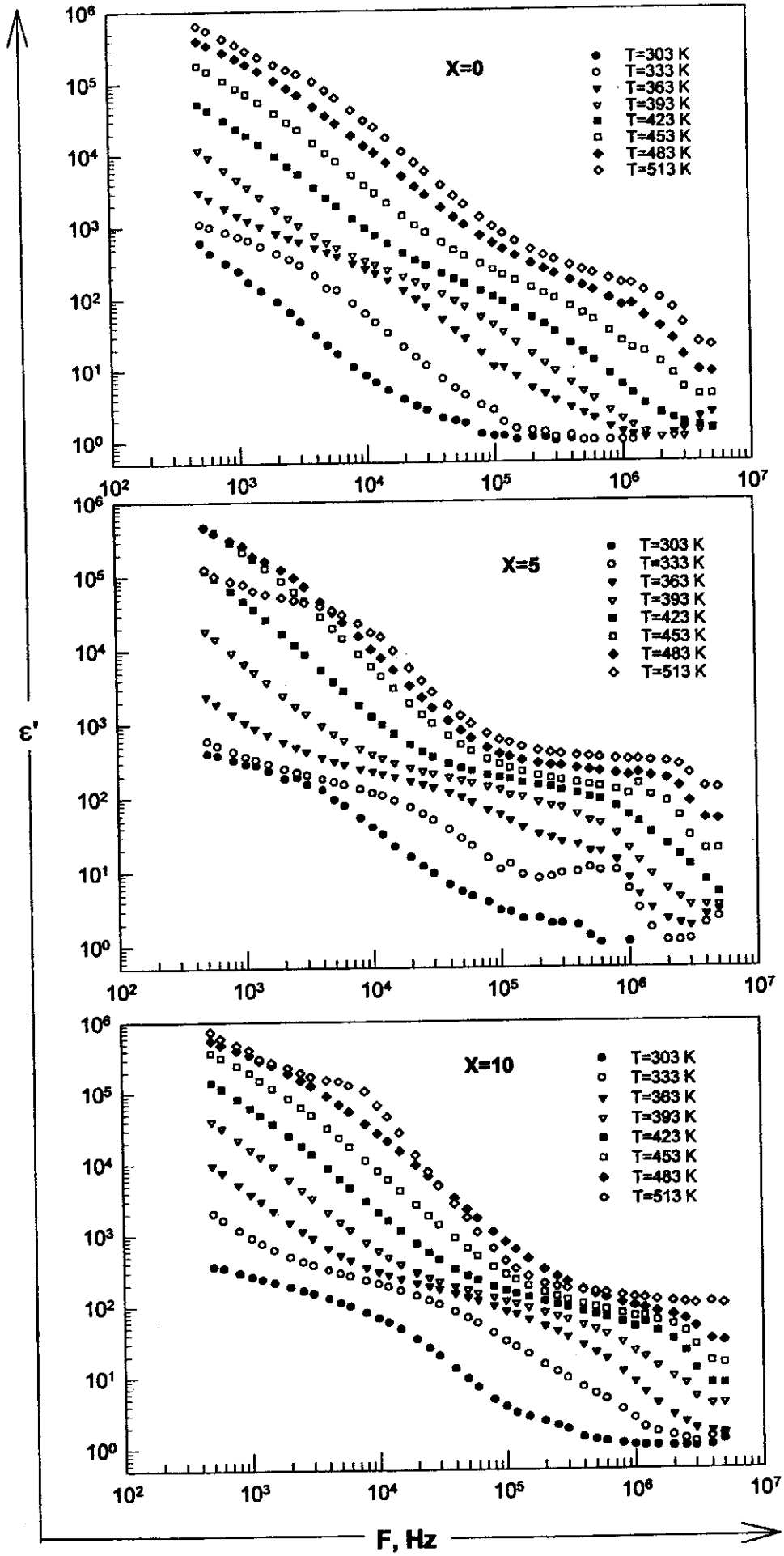

Figure [(3.14(A)] : The frequency dependence of ε' for the glass system (50-x)P_2O_5-xAgI- 40Ag_2O-10Fe_2O_3 ,(x=0,5,10) at different ambient temperatures.

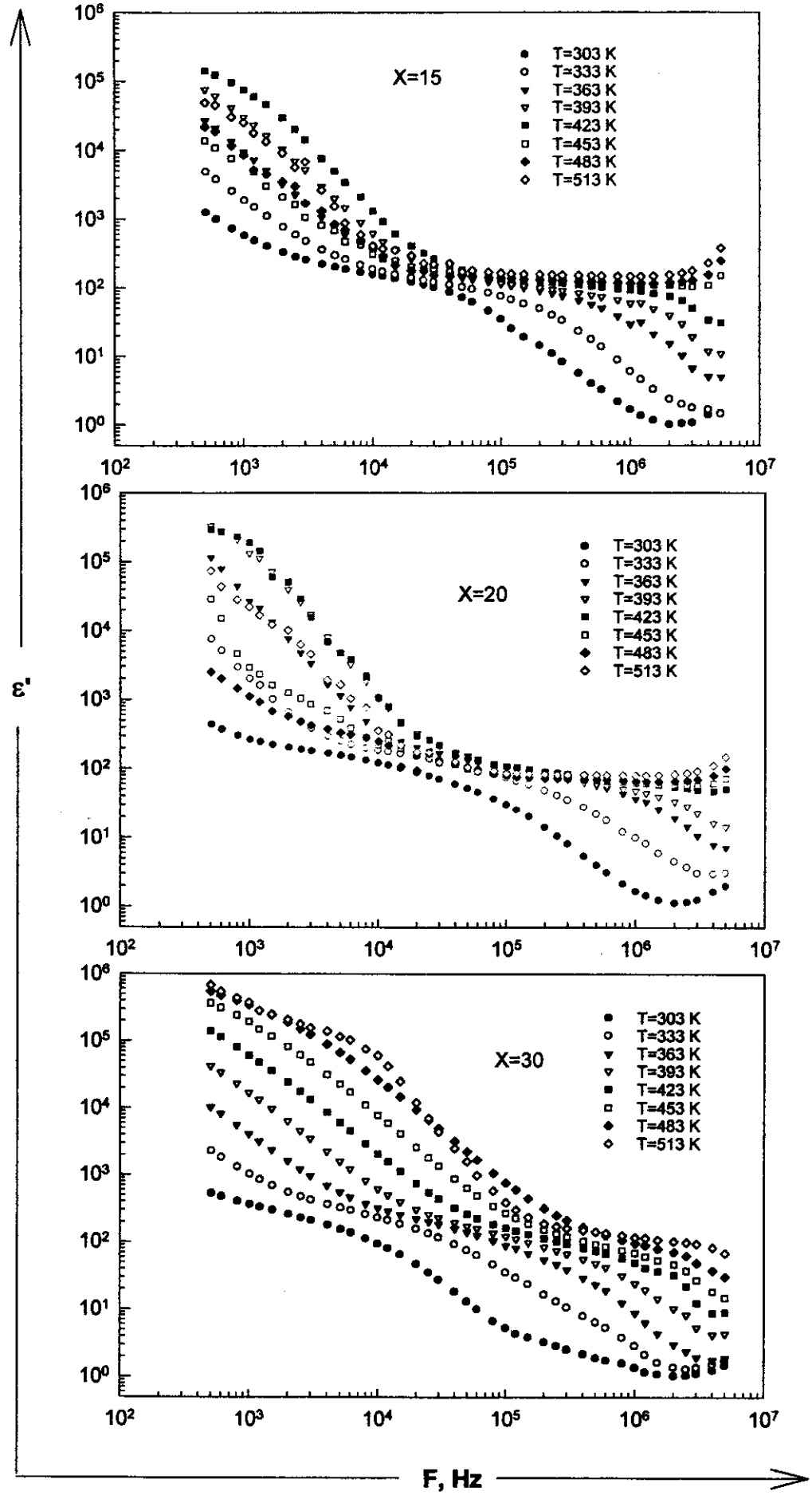

Figure [3.14(B)] : The frequency dependence of ε' for the glass system (50-x)P_2O_5-xAgI- 40Ag_2O-10Fe_2O_3 , (x=15,20,30) at different ambient temperatures.

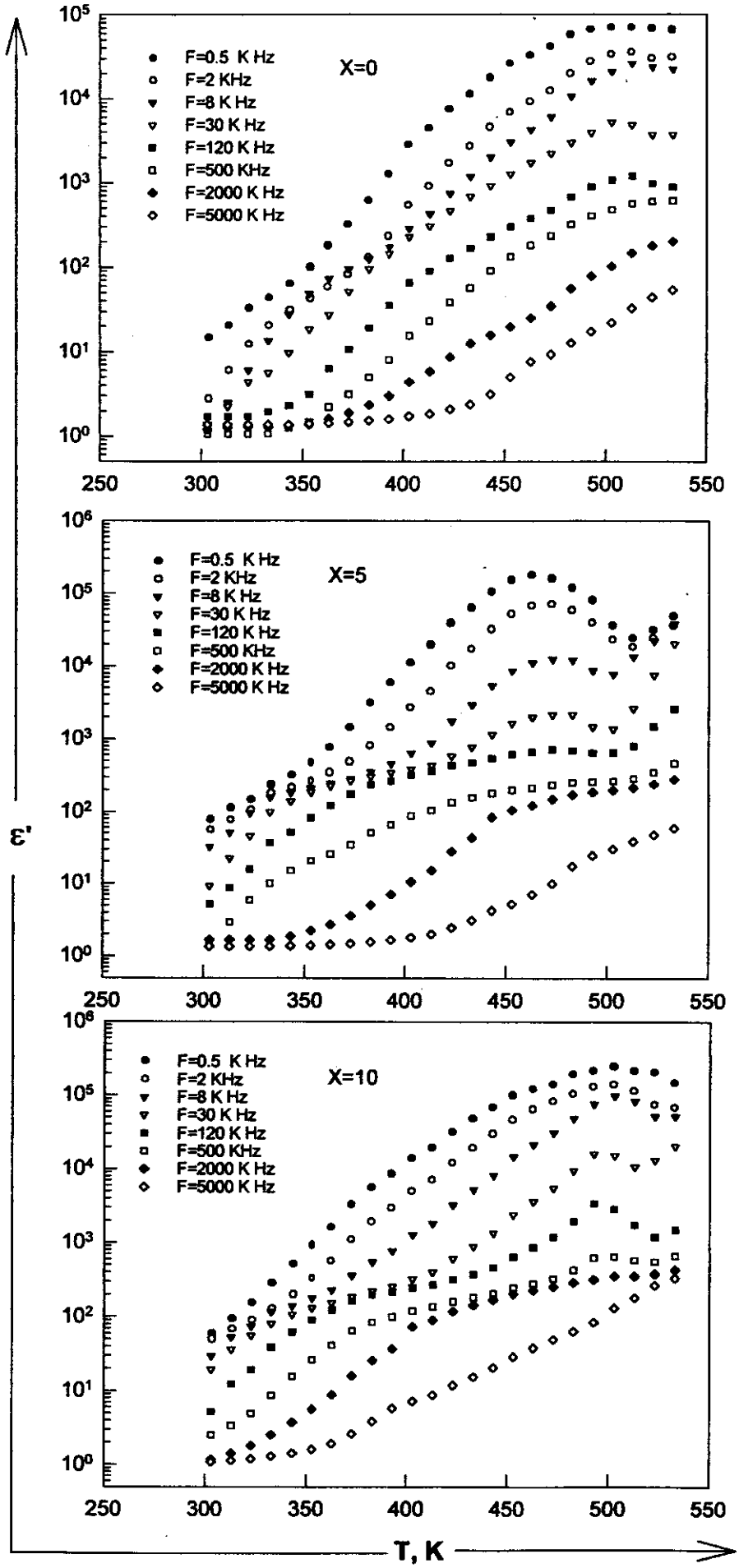

Figure [3.15(A)] : The temperature dependence of ε' for the glass system (50-x)P_2O_5-xAgI-40Ag_2O-10Fe_2O_3 ,(x=0,5,10) at fixed frequencies.

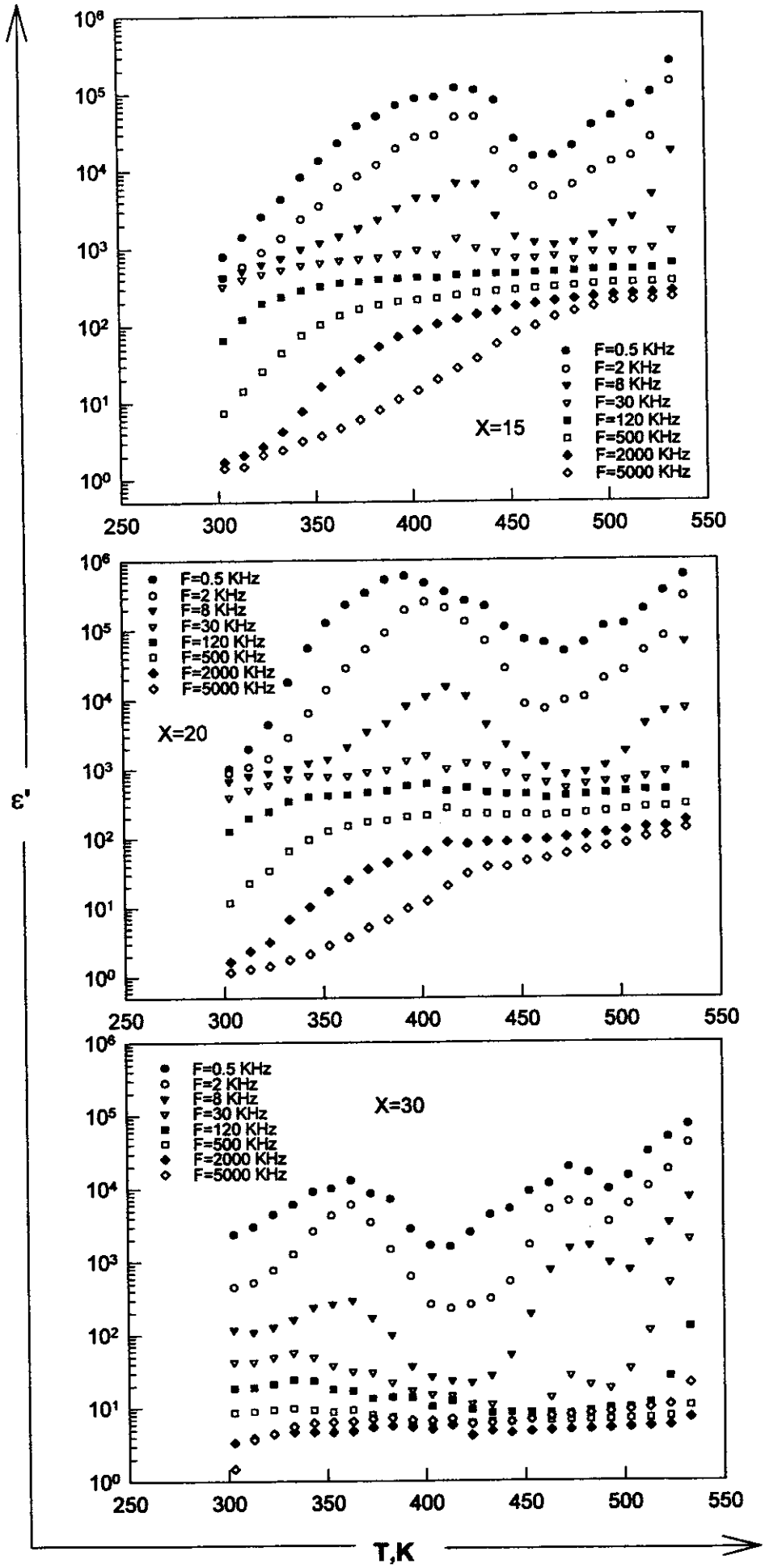

Figure [3.15(B)] : The temperature dependence of ε' for the glass system (50-x)P_2O_5-xAgI-40Ag_2O-10Fe_2O_3 , (x=15,20,30) at fixed frequencies.

The dielectric properties in ion conductive glasses mainly arise from the ionic motions. The free energy barriers impeding the ionic diffusion , however , can be expected to vary from site to site , so there are different ionic motions in glasses[110]. The first is the rotation of ions around their negative sites, the second is short-distance transport, i.e. ions hop out of sites with low free-energy barriers and tend to pile up at sites with high free-energy barriers in the electric field direction in dc or low frequency electric field or oscillate between the sites with high free-energy barriers in an ac electric field. Both the first and the second motions make a contribution to the dielectric constant ε` of glasses. The third ionic motion is that the ions with higher energy can penetrate the glasses, i.e. conduct electricity and cause the dielectric loss ε``. In the case of blocking electrodes and or domain interface or even low-frequency conduction can easily lead to electrode polarization. Thus, it will not only cause dielectric loss ε`` but also lead to a sharp increase of the apparent dielectric constant ε` of glasses.

When the temperature was increased the dielectric constant ε` increases because of the glass network relaxation and ionic motion becomes easier. This increase is also expected to be more pronounced at low frequency range, since the ions have more time to participate in the motion . At a certain temperature the dc ionic conductivity dominates leading to the apparent decrease of the dielectric constant .

3.4.5 Effect of frequency and temperature on the dielectric loss ε``.

The frequency dependence of the dielectric loss ε`` is studied for the glass system $(50-x)P_2O_5$-xAgI-$40Ag_2O$-$10Fe_2O_3$ , [x = 0 , 5 , 10 , 15, 20, 30] at different ambient temperatures, Figure [(3.16)A,B] . It is noticed that, the general behaviour shows a decrease of ε`` with increasing frequency which can be expressed according to Guntini et al[54] in the range $\omega\tau >> 1$ by the following relation ;

$$\varepsilon`` \sim (\varepsilon_s - \varepsilon_\infty)\, 2\pi^2 N [ne^2/\varepsilon_s]^3 KT\, \tau_0^m\, w_M^{-4}\, \omega^{-m} \qquad (3.10)$$

where m = (-4KT /W_M) , W_M being the energy required to librate a carrier, n is the concentration of the charge carriers that hop and N is the concentration of localized sites. However the relation (3.10) can be reformulated as;

$$\varepsilon`` = A\, \omega^m \qquad (3.11)$$

The values of the exponent m are obtained by using the least square fitting of equation (3.11). The values of m,A, W_M is listed in Table [(3.8)A,B] .

More information can be obtained from the relation between conductivity and ε`` as follows ,

$$\varepsilon``(\omega) = \sigma / \varepsilon_o \omega \quad \propto \quad \omega^{S-1}$$

where ε_o is the permittivity of vacuum . It is clear that a value S = 1 means constant ε``, or a constant loss per cycle.

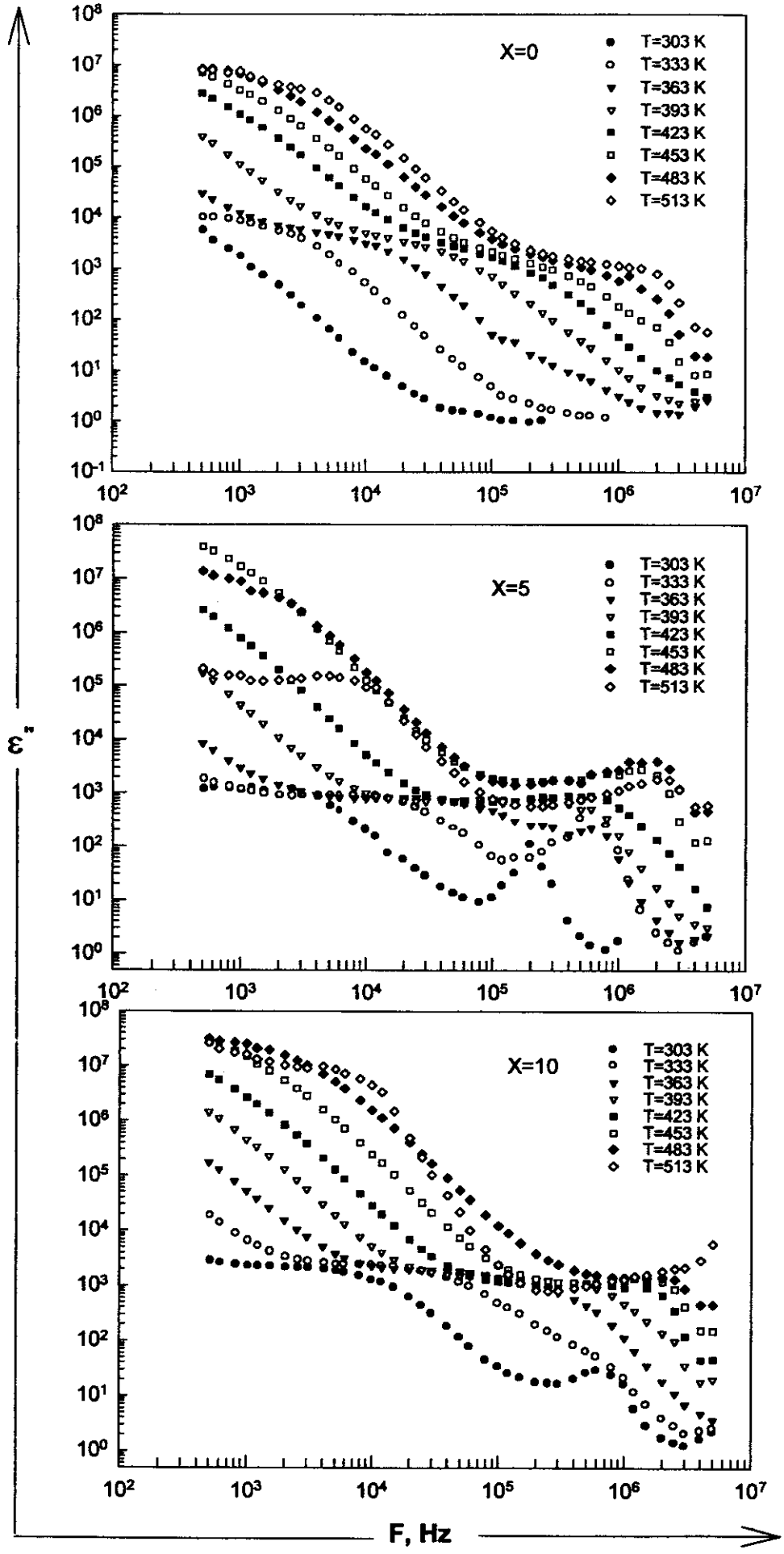

Figure [3.16(A)] : The frequency dependence of ε" for the glass system (50-x)P_2O_5-xAgI-40Ag_2O-10Fe_2O_3 , (x=0,5,10) at different ambient temperatures.

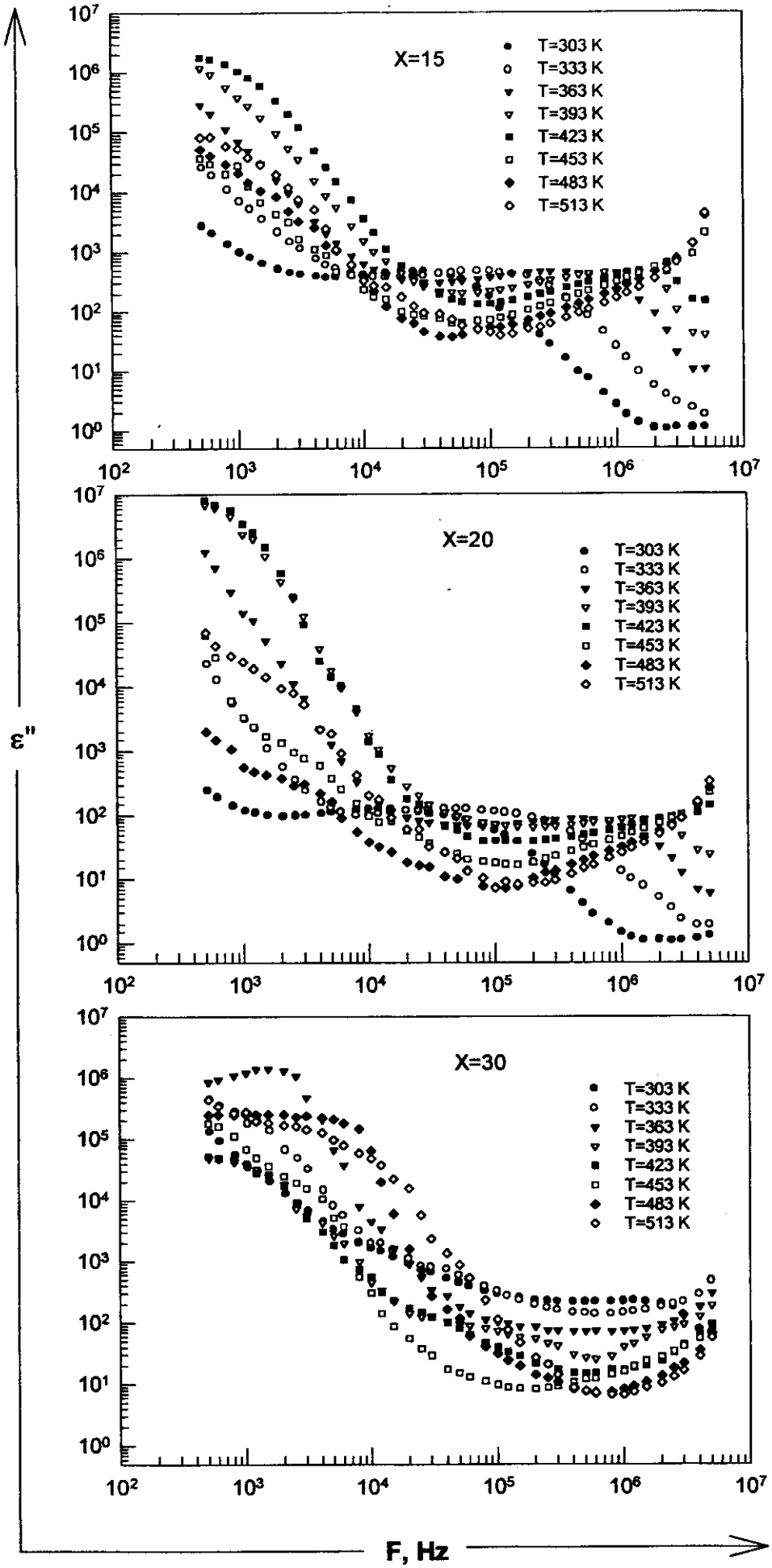

Figure [3.16(B)] : The frequency dependence of ε" for the glass system (50-x)P_2O_5-xAgI-40Ag_2O-10Fe_2O_3 , (x=15,20,30) at different ambient temperatures.

Table (3.8A) : The parameters A , m , and W_m for the glass system $(50-x)P_2O_5$-$xAgI$-$40Ag_2O$-$10Fe_2O_3$, [x=0,5,10].

X=0			
T , K	A	m	Wm , eV
303	2.52×10^4	1.903	0.054
333	1.11×10^6	1.978	0.058
363	5.33×10^2	0.964	0.129
393	9.58×10^5	1.712	0.079
423	2.01×10^7	1.760	0.082
453	2.35×10^8	1.832	0.085
483	1.12×10^9	1.825	0.091
513	9.21×10^9	1.944	0.091

X=5			
T , K	A	m	Wm , eV
303	6.07×10^4	1.724	0.060
333	2.17×10^3	1.120	0.102
363	9.26×10^2	1.224	0.102
393	6.47×10^5	1.797	0.075
423	4.55×10^7	1.995	0.073
453	1.01×10^9	2.004	0.078
483	1.14×10^9	2.126	0.078
513	4.53×10^7	1.798	0.098

X=10			
T , K	A	m	Wm , eV
303	1.27×10^5	1.534	0.068
333	7.58×10^4	1.281	0.089
363	4.02×10^5	1.659	0.075
393	2.66×10^7	1.925	0.070
423	1.12×10^8	1.859	0.078
453	8.62×10^8	1.879	0.083
483	1.70×10^{10}	1.990	0.083
513	8.97×10^{15}	3.285	0.053

Table (3.8B) : The parameters A , m , and W_m for the glass system $(50-x)P_2O_5$-$xAgI$-$40Ag_2O$-$10Fe_2O_3$, [x=15,20,30].

X=15			
T , K	A	m	Wm , eV
303	5.52×10^{2}	1.134	0.092
333	1.26×10^{5}	1.672	0.068
363	3.34×10^{7}	2.128	0.058
393	5.21×10^{8}	2.287	0.059
423	2.52×10^{10}	2.627	0.055
453	6.66×10^{5}	1.787	0.087
483	9.45×10^{5}	1.781	0.093
513	4.40×10^{6}	1.891	0.093

X=20			
T , K	A	m	Wm , eV
303	3.96×10^{6}	1.682	0.062
333	1.44×10^{7}	2.520	0.045
363	3.19×10^{10}	2.964	0.042
393	2.71×10^{11}	2.898	0.046
423	2.74×10^{12}	3.184	0.045
453	6.26×10^{5}	1.842	0.084
483	3.31×10^{2}	1.037	0.160
513	1.21×10^{6}	1.758	0.100

X=30			
T , K	A	m	Wm , eV
303	1.56×10^{5}	1.475	0.070
333	1.07×10^{7}	1.859	0.061
363	5.80×10^{10}	2.650	0.047
393	2.51×10^{5}	1.601	0.084
423	1.25×10^{6}	1.855	0.078
453	4.73×10^{10}	2.878	0.054
483	4.17×10^{12}	2.994	0.055
513	1.98×10^{10}	2.349	0.075

The samples had two dispersion regions in the investigated frequency range ; a low-frequency region centered below 10^4 Hz , and a high-frequency region at 10^6 Hz . The low-frequency dispertion of ε`` (the decrease of ε`` with the increase of the frequency)may be partly due to the intrinsic dc conductivity of the sample . At high frequencies,on the other hand,the behaviour of S is consistent only with stochastic-hoping models.No indication of a maximum is observed in ε`` in the region of frequency-dependent conductivity,σ_{tot} (after taking dc conduction into account).

The temperature dependence of the dielectric loss ε`` is studied for the glass system $(50\text{-}x)P_2O_5\text{-}xAgI\text{-}40Ag_2O\text{-}10Fe_2O_3$ ,[x=0,5,10,15,20,30] at different frequencies, Figure [(3.17)A,B] . It is clear that, the dielectric loss ε`` increases with increasing temperature for all tested samples but it decreases again at certain temperature for samples of composition x= 15,20,30. In addition, the peak in ε``-T relation is higher at low frequency ranges than that at the high frequency ranges . When the frequency was increased the dielectric loss decreases which can be attributed to the reduction to the diffusion of silver ions in the glass matrix with increasing frequency. Consequently, there is a phase lag between the applied field and the polarization of the glass leading to energy absorbed from the field to the dielectric material. No disperion relation in studing ε`` against frequency were recorded, only a decrease in the value of ε`` with frequency which suggested that the relaxation peak shifts towards lower temperature range . The obtaineed values of W_M (0.042 - 0.016 eV) are lower than the activation energies obtained using dc conductivity. This can be attributed to the remarkable contribution of the localized electrons of the amorphous matrix in conduction process.

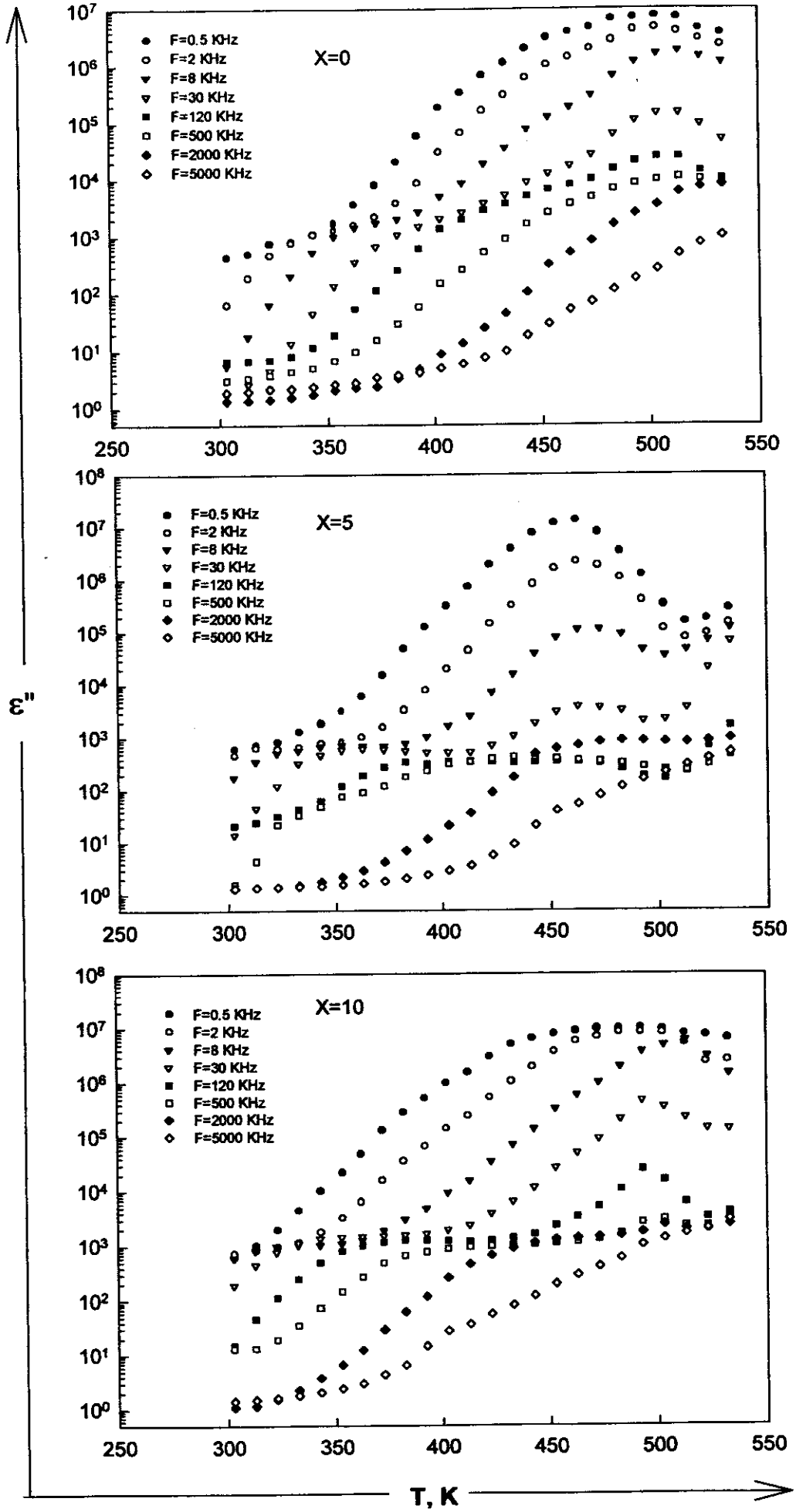

Figure [3.17(A)] : The temperature dependence of ε" for the glass system $(50-x)P_2O_5$-$xAgI$-$40Ag_2O$-$10Fe_2O_3$, (x=0,5,10) at fixed frequencies.

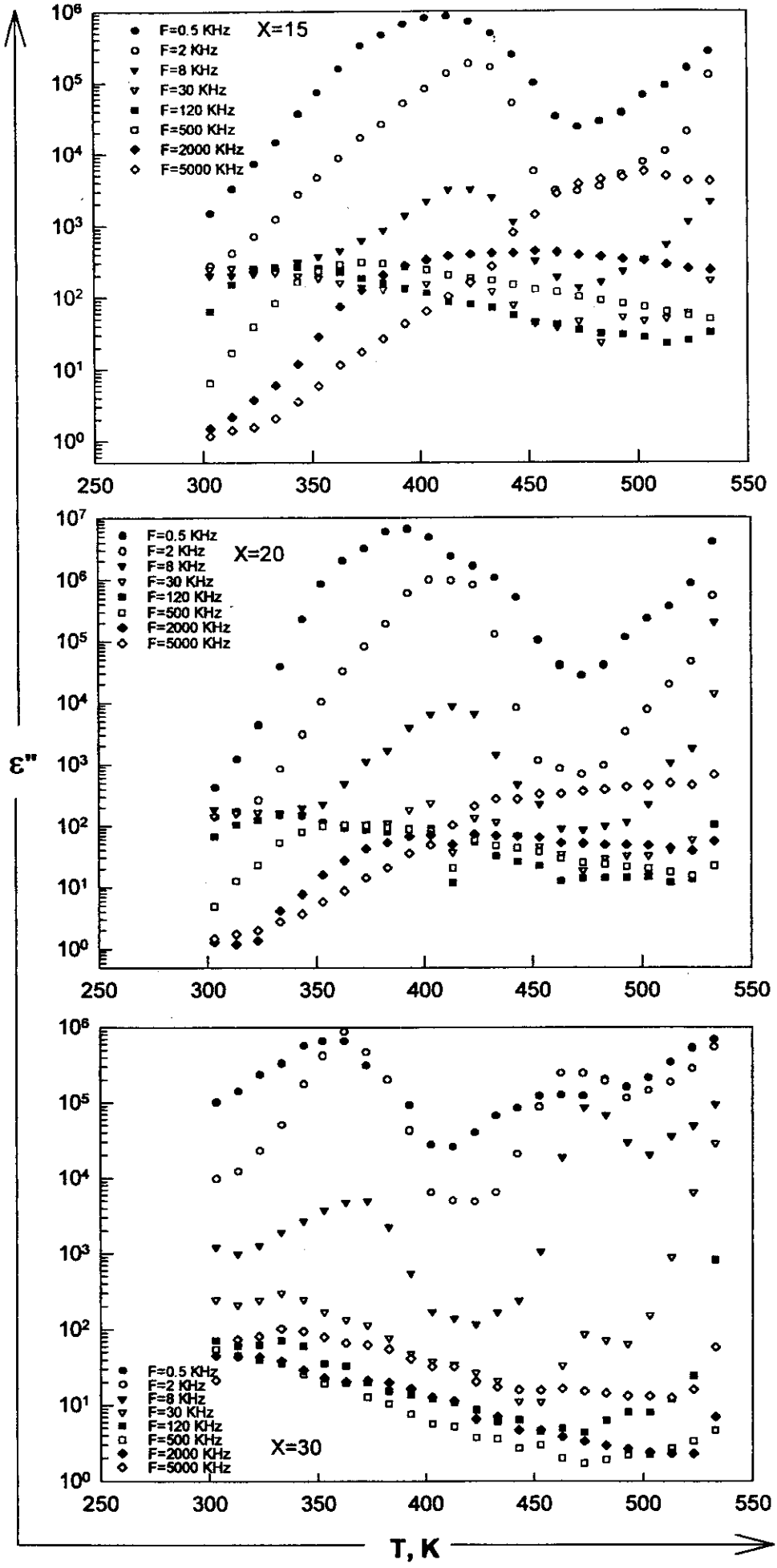

Fig.[3.17(B)] : The temperature dependence of ε" for the glass system (50-x)P_2O_5-xAgI-40Ag_2O-10Fe_2O_3 , (x=15,20,30) at fixed frequencies.

3.4.6 Effect of frequency and temperature on the dielectric loss tangent (tan δ) .

The frequency dependence of the dielectric loss tangent tan δ was studied for the glass system $(50\text{-}x)P_2O_5\text{-}xAgI\text{-}40Ag_2O\text{-}10Fe_2O_3$, [x = 0 , 5 , 10 , 15, 20, 30] at different ambient temperatures, Figure [(3.18)A,B]. It is clear that, the tan δ –F curves shows a maximum at certain frequency , f_{max} , which is shifted towards higher frequency with increasing temperatures. This behaviour characterizes the ionic glasses and consistent with Debye model for dielectric relaxition. In addition, the peak disappears at relatively higher temperature ranges except , the case of x=30. The temperature dependence of the f_{max} peak , Figure (3.19) , can be discribed by the following relation;

$$f_{max} = f_{o(max)} \exp(-E_{max}/KT) \qquad (3.12\ a)$$

$$\omega_{max} = 1/\tau \quad , \quad \omega_{max} = 2\pi f_{max} \qquad (3.12\ b)$$

where E_{max} is the activation energy for the relaxation process , ω_{max} is the angular frequency correspondes to the maximum absorption and τ represents the most probable value of spread of relaxation times . Such values of τ have been determined and lie in the range ($1.64 \times 10^{-8} - 1.95 \times 10^{-3}$ sec.) . The value of the activation energy is obtained by the least square fitting of equation (3.12a) and listed in Table (3.9). It is noticed that the values of E_{max} decreases with increasing xAgI content.

The temperature dependence of the dielectric loss tangent tan δ was studied for the glass system $(50\text{-}x)\ P_2O_5\text{-}xAgI\text{-}40Ag_2O\text{-}10Fe_2O_3$, [x = 0, 5, 10 , 15, 20, 30], Figure [(3.20)A,B]. It is clear that, when the temperature

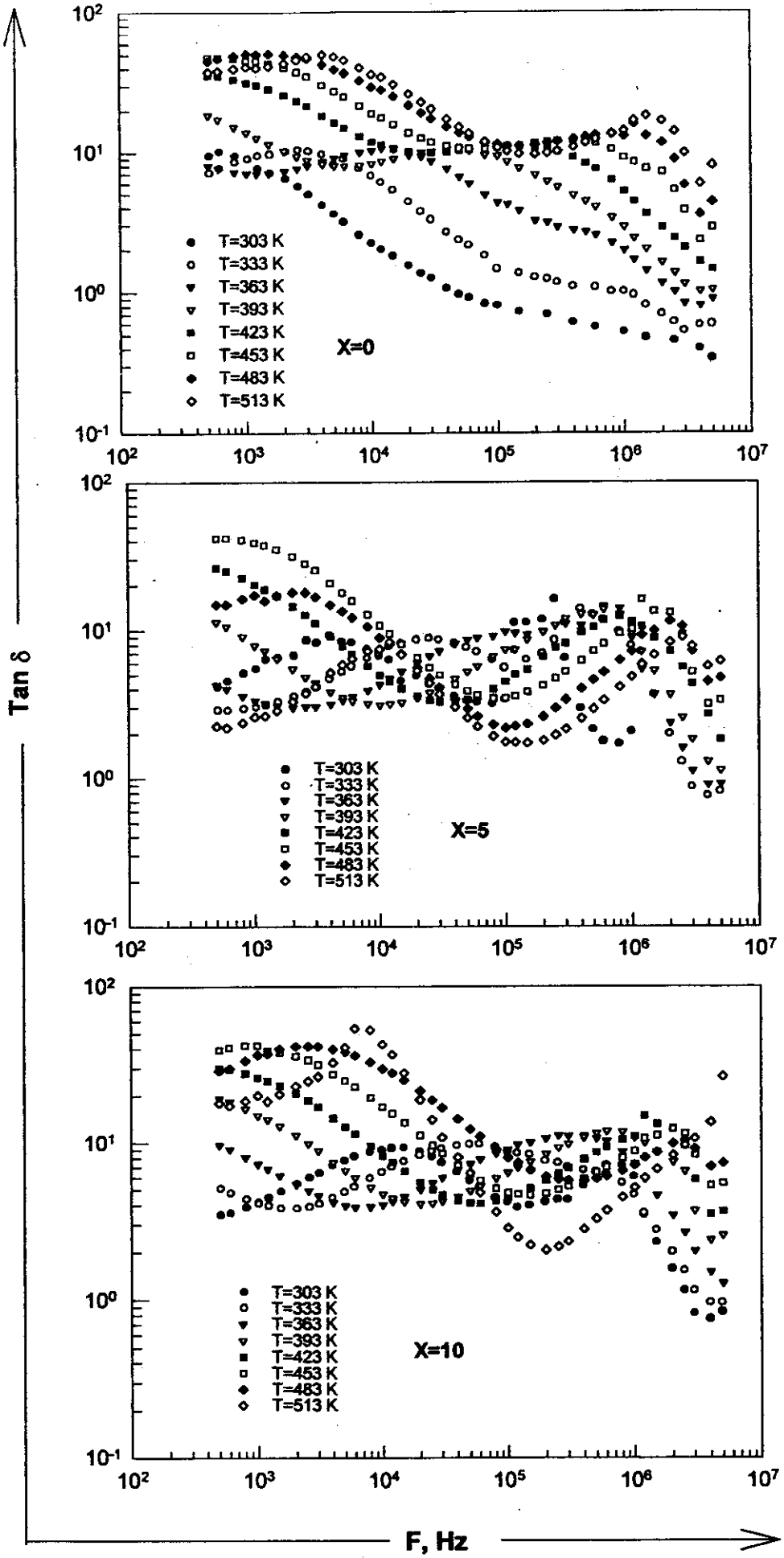

Figure [3.18(A)] : The frequency dependence of Tan δ for the glass system $(50-x)P_2O_5$-$xAgI$-$40Ag_2O$-$10Fe_2O_3$ (x=0,5,10) at different ambient temperatures..

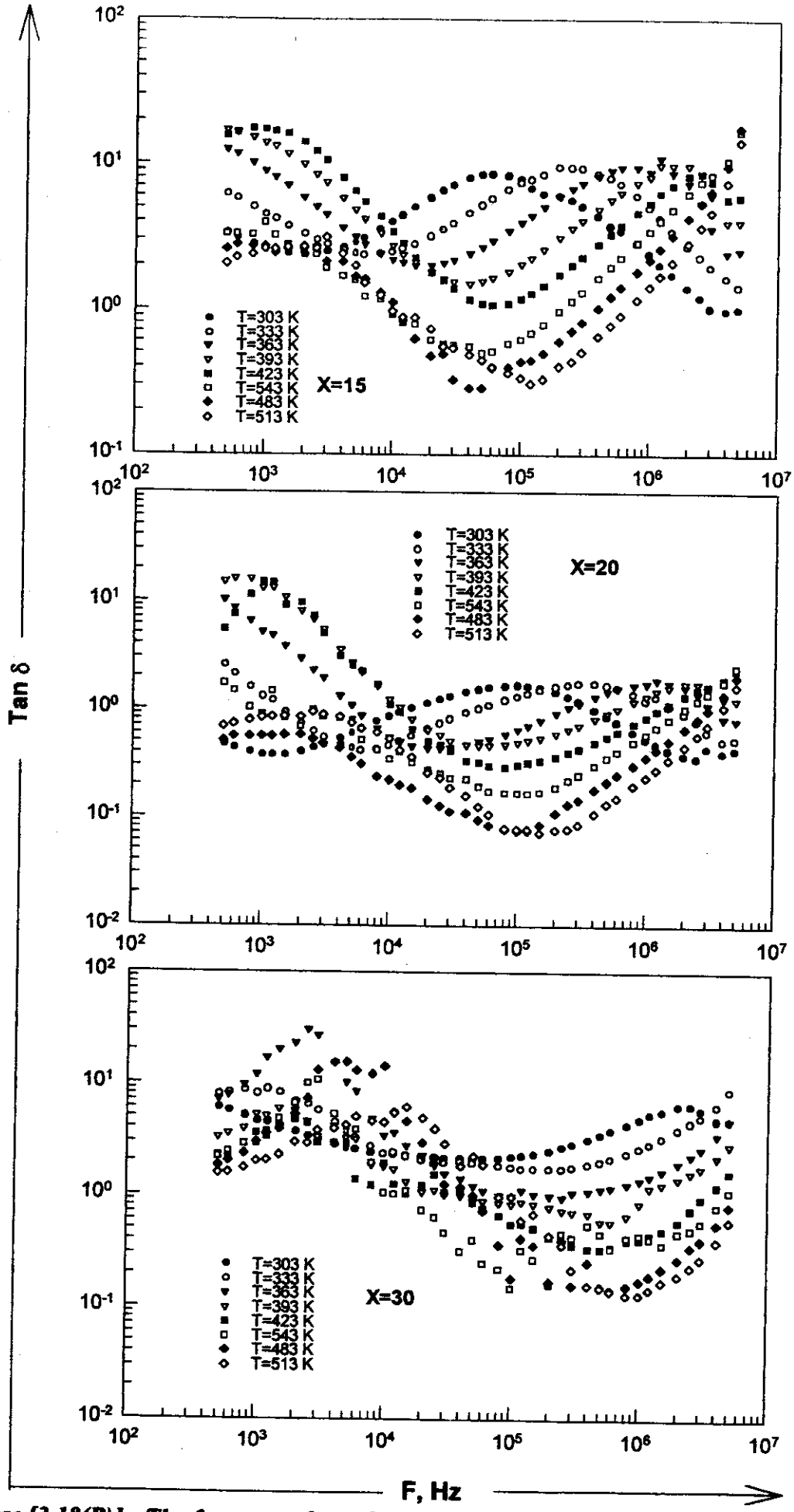

Figure [3.18(B)] : The frequency dependence of Tan δ for the glass system $(50-x)P_2O_5$-$xAgI$-$40Ag_2O$-$10Fe_2O_3$ (x=0,5,10) at different ambient temperatures..

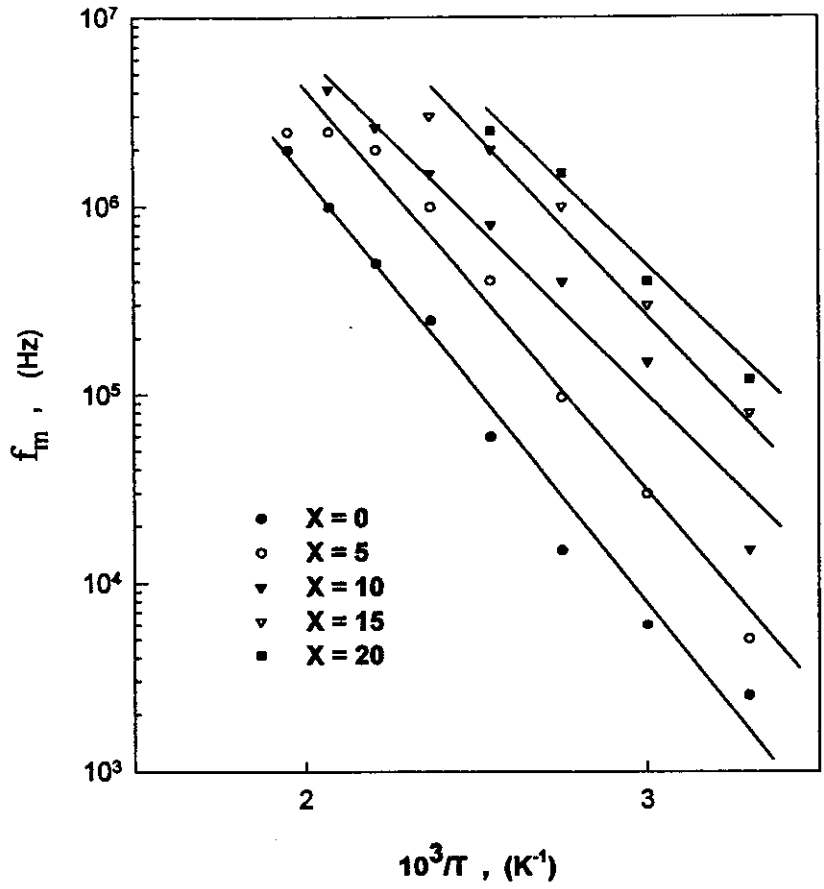

Figure (3.19) : The temperature dependence of f_m for the glass system (50-x)P_2O_5-xAgI-40Ag_2O-10Fe_2O_3, (x=0,5,10,15,20,30) .

Table (3.9) : The values of $E(f_m)$, E_τ , E_D , τ_o and F_o for the glass system $(50-x)P_2O_5$-$xAgI$-$40Ag_2O$-$10Fe_2O_3$,[x=0,5,10,15,20,30].

x AgI	E (f_{max}) , eV	E_τ , eV	τ_o , Sec.	F_o , Sec^{-1}	E_D , eV
0	0.495	0.329	8.36×10^{-11}	1.20×10^{10}	0.575
5	0.421	0.314	1.24×10^{-9}	8.06×10^{8}	0.597
10	0.397	0.321	7.63×10^{-9}	1.31×10^{8}	0.384
15	0.396	0.307	2.45×10^{-10}	4.08×10^{9}	0.403
20	0.359	0.294	5.38×10^{-11}	1.86×10^{10}	0.236
30	—	—	—	—	0.201

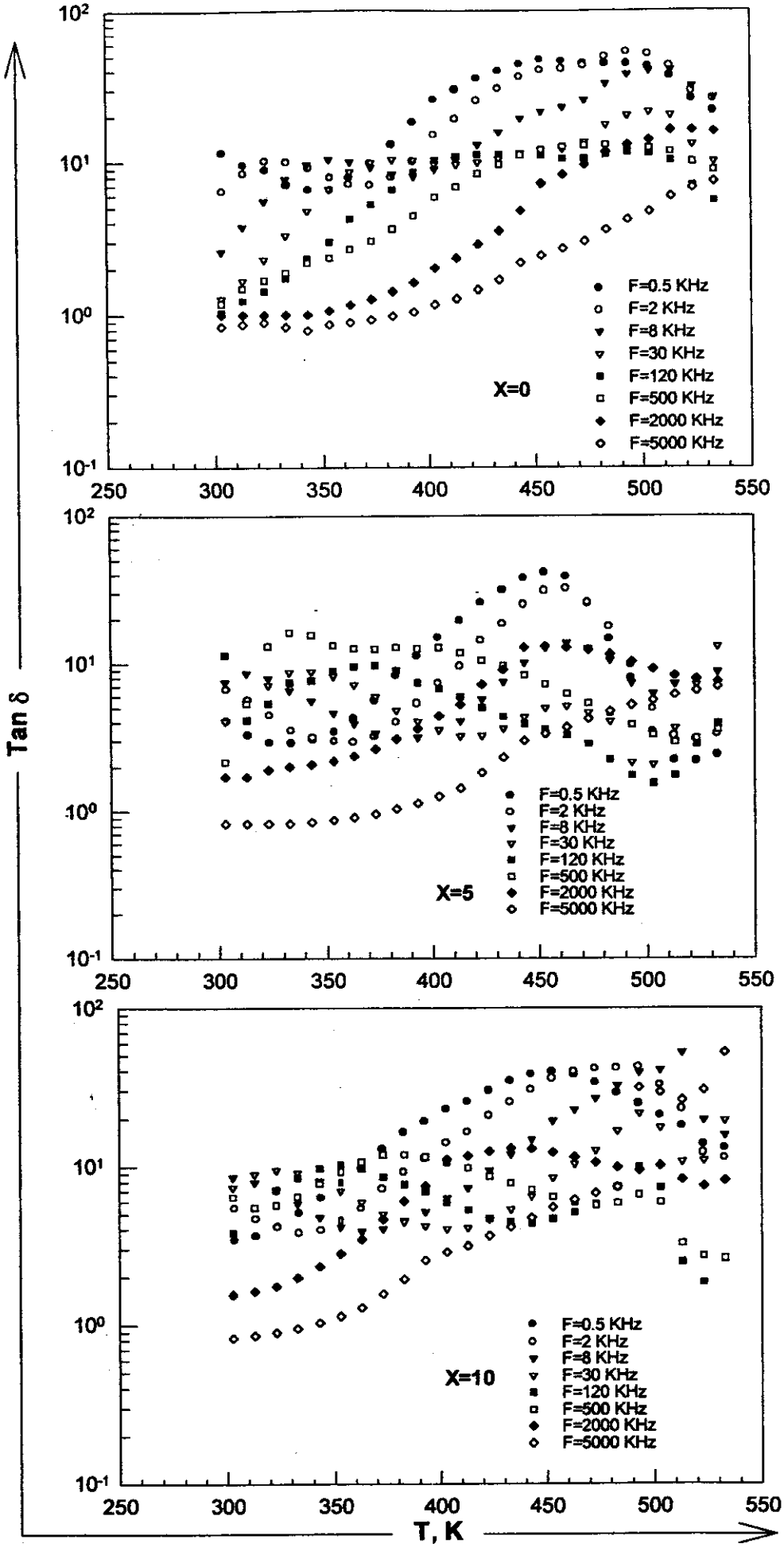

Figure [3.20(A)] : The temperature dependence of Tan δ for the glass system (50-x)P_2O_5-xAgI- 40Ag_2O-10Fe_2O_3 , (x=0,5,10) at different ambient temperatures .

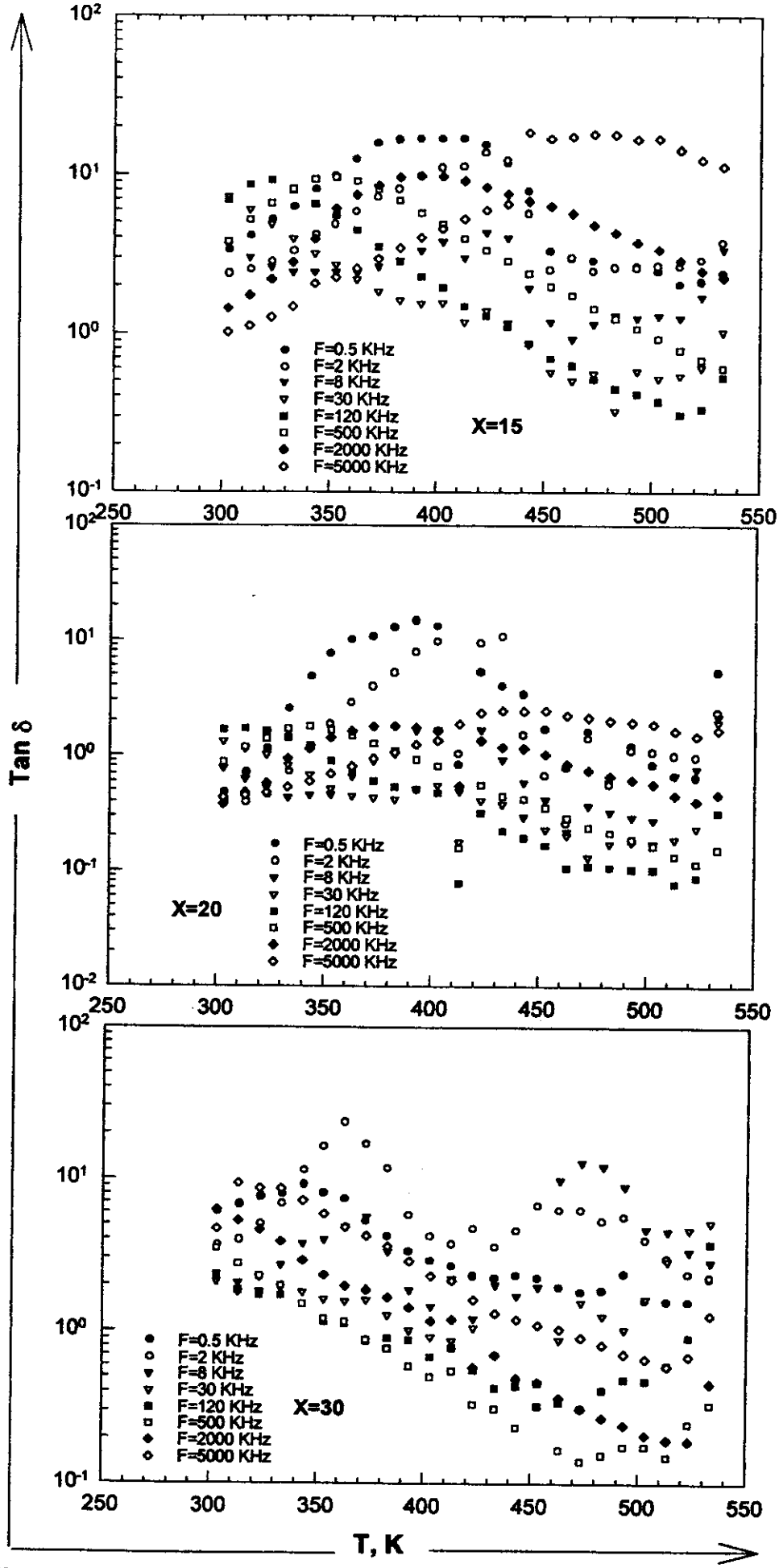

Figure [3.20(B)] : The temperature dependence of Tan δ for the glass system (50-x)P_2O_5-xAgI-40Ag_2O-10Fe_2O_3 , (x=0,5,10) at different ambient temperatures .

was increased the dielectric loss tangent tan δ has two distinguished regions, i.e at relatively low temperature range between 300 K and 400 K, the values of tan δ fluctuates with raising temperature. At higher temperature range, the tan δ increases sharply up to a maximum and increases again .It is also noticed that , the loss peak shifts to higher frequencies with increasing temperature .

In practice it is convenient to specify the absorption losses in a dielectric (at a given frequency and temperature) by the loss tangenet. At low frequency ranges most of Ag^+ ions in the glass matrix contribute to the ionic polarization. When the frequency was increased, the ionic polarization decreases which lead to the appearance of the peaks in tan δ - F curves , they shift towards higher frequencies with increasing temperature. At high frequency ranges, the vibration loss may contribute to the total dielectric loss.

3.4.7 Temperature dependence of relaxtion time τ.

Results of the complex impedence plane are shown schematically as in the Figure (3.11). The complex impedence Z``(Z`) can be described by the following relation;

$$Z = Z`-iZ`` = \frac{Z_s - Z_\infty}{1+(i\omega\tau)^{1-h}} \qquad (3.13)$$

where Z_S denotes the low-frequency limit of the impedence, τ is the time constant and ω is the angular frequency of the measuring field. It can be seen in the plot that the extrapolated high frequency limit of the impedence Z_∞ is equal to zero. The semicircles are due to a parallel combination of the bulk resistance Z_S and the geometric capacetance C_S of the sample. When the temperature increases , the experimental points are shifted towards the right side of the semicircle. This is a simple consequence of the fact that the time constant $\tau = Z_S C_S$ decreases with increasing temperature. Using the semicircles, the relaxation time τ of the all samples are obtained using the following relation[111] ;

$$\tau = \frac{1}{2\pi F}\left[\frac{(Z_S - Z`)^2 + Z^{`2}}{(Z` - Z_\infty)^2 + Z^{`2}}\right]^{\frac{1}{2(1-h)}} \qquad (3.14)$$

where h (=2α/180) <1,and α is the angle between Z` axis and the radius of the circle . Figure (3.21) illustrate temperature dependence of relaxation time τ . In general, the obtained values of τ is attenuated with increasing temperature which obeys the following exponential relation ;

$$\tau = \tau_0 \exp (E_\tau / KT) \qquad (3.15)$$

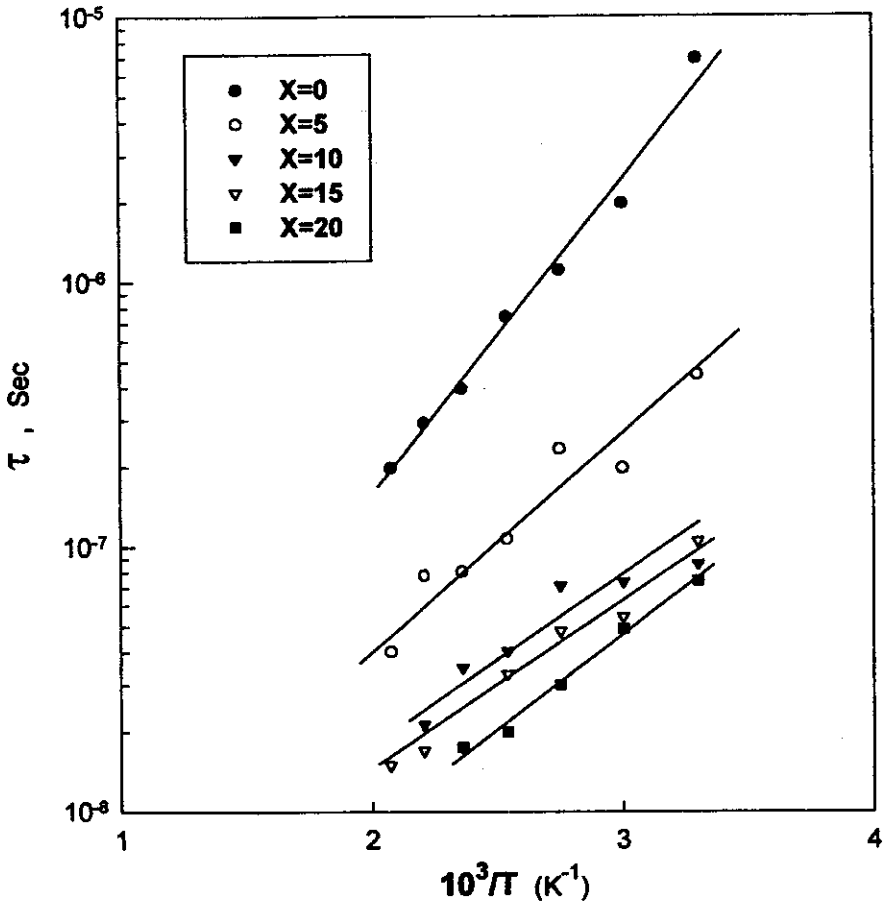

Figure (3.21) :Temperature dependence of τ for the glass system $(50-x)P_2O_5$-$xAgI$-$40Ag_2O$-$10Fe_2O_3$, (x=0,5,10,15,20,30).

Where E_τ is the activation energy of relaxation time. The values of E_τ and τ_o are deduced and listed in Table (3.9). It is noticed that, E_τ lies in the range (0.171-0.329 eV) , and τ_o lies in the range (3.36×10^{-11}-3.63×10^{-10} sec) which is in comparison equal to the inverse of expected phonon frequency ($F_o = 1/\tau_o$) which lies in the range (3.31×10^{9} - 3.33×10^{10} sec^{-1}) . A look at Fig.(3.21) and Fig.(3.19) reveals that there is a close proximity in the values of relaxation times determined from Cole-Cole diagrames and those estimated by using eq.(3.12b) . This is expected because both the two methods provide an average or most probable value of τ . This is in agreement with concept of molecular relaxation.

The relaxation time is interpreted as the average time which a molecule spends in one of the equilibrium positions before jumping to the other one. when the temperature was increased, the relaxation time decrease because of the raising of temperature leads to structure relaxes and to increase the probability of silver ions migration to the new sites.

3.4.8 Temperature dependence of diffusion coefficient , D .

The study of diffusion process in the ionic glass system $(50\text{-}x)P_2O_5$-$xAgI$-$40Ag_2O$-$10Fe_2O_3$, [x = 0 , 5 , 10 , 15, 20, 30] enables us to throw more light on conduction in such glasses.

According to Schutt et al[112], the charge carrier concentration n, can be given by the following relation ;

$$n = \left[\frac{\sigma_o}{3\varepsilon_o\varepsilon_s\omega_{10}}\right]^4 \frac{\varepsilon_o\varepsilon_s KT}{e^2 d^2} \qquad (3.16)$$

where ε_o is the free space permitivity , ε_s static dielectric constant , d thickness of smaple and ω_{10} is the frequency at which the dielectric constant $\varepsilon' = 10\ \varepsilon_s$. The carrier concentration of the present glass system are obtained and listed in Table [(3.10)A,B] . It is clear that, the carrier concentration lie in the range (1.73×10^{19} - 5.39×10^{24} cm^3) for all tested samples. In addition, the charge carrier concentration increases when the AgI content and or the temperature was increased. Also the values of charge carrier mobility μ had been obtained by using the values of n at any temperature which listed in Table [(3.10)A,B] .

The diffusion coefficient D is calculated using the values of charge carrier mobility μ and Nearnst-Eienstin relation ($D/\mu = kT/q$)[21]. It is noticed that, D increases with increasing temperature obeing the following relation ;

$$D = D_o \exp(-E_D/KT) \qquad (3.17)$$

Table (3.10A) : The parameters n , μ for the glass system $(50-x)P_2O_5$-$xAgI$-$40Ag_2O$-$10Fe_2O_3$, [x=0,5,10].

X=0		
T , K	n , cm^{-3}	μ , $cm^2 . v^{-2} . sec^{-1}$
303	5.58×10^{19}	2.95×10^{-1}
333	8.95×10^{19}	0.89×10^{-1}
363	7.23×10^{19}	2.92×10^{-2}
393	8.42×10^{20}	1.15×10^{-2}
423	1.24×10^{21}	2.83×10^{-3}
453	1.50×10^{21}	6.30×10^{-4}
483	2.71×10^{21}	8.78×10^{-4}
513	2.82×10^{21}	7.75×10^{-5}

X=5		
T , K	n , cm^{-3}	μ , $cm^2 . v^{-2} . sec^{-1}$
303	5.90×10^{19}	5.69×10^{-1}
333	7.88×10^{19}	2.81×10^{-2}
363	1.91×10^{20}	9.32×10^{-1}
393	9.80×10^{19}	1.42×10^{-2}
423	2.44×10^{20}	8.17×10^{-3}
453	1.02×10^{21}	3.01×10^{-3}
483	1.13×10^{21}	5.51×10^{-4}
513	1.90×10^{21}	4.68×10^{-4}

X=10		
T , K	n , cm^{-3}	μ , $cm^2 . v^{-2} . sec^{-1}$
303	1.73×10^{19}	1.31×10^{-1}
333	3.09×10^{20}	2.67×10^{-2}
363	1.00×10^{21}	2.21×10^{-1}
393	6.13×10^{20}	1.22×10^{-2}
423	2.97×10^{21}	3.05×10^{-3}
453	1.76×10^{22}	2.93×10^{-3}
483	2.16×10^{22}	4.93×10^{-3}
513	2.23×10^{22}	1.31×10^{-4}

Table (3.10 B) : The parameters n , μ for the glass system $(50-x)P_2O_5$-$xAgI$-$40Ag_2O$-$10Fe_2O_3$, [x=15,20,30].

X=15		
T , K	n , cm^{-3}	μ , $cm^2 . v^{-2}.sec^{-1}$
303	8.65×10^{19}	1.31×10^{-4}
333	3.78×10^{20}	8.58×10^{-3}
363	2.36×10^{21}	4.83×10^{-4}
393	7.87×10^{21}	1.77×10^{-4}
423	2.52×10^{22}	1.13×10^{-5}
453	2.23×10^{21}	3.06×10^{-6}
483	8.95×10^{22}	2.31×10^{-6}
513	4.78×10^{23}	7.86×10^{-6}

X=20		
T , K	n , cm^{-3}	μ , $cm^2 . v^{-2}.sec^{-1}$
303	4.55×10^{19}	4.98×10^{-3}
333	4.97×10^{21}	8.90×10^{-4}
363	3.59×10^{20}	3.98×10^{-5}
393	8.23×10^{21}	3.16×10^{-5}
423	3.34×10^{22}	1.05×10^{-6}
453	5.55×10^{23}	4.28×10^{-5}
483	4.77×10^{24}	3.58×10^{-6}
513	5.39×10^{24}	2.68×10^{-7}

X=30		
T , K	n , cm^{-3}	μ , $cm^2 . v^{-2}.sec^{-1}$
303	1.79×10^{21}	4.90×10^{-1}
333	1.38×10^{23}	4.50×10^{-2}
363	1.86×10^{24}	1.20×10^{-3}
393	1.18×10^{23}	2.72×10^{-5}
423	6.14×10^{23}	7.65×10^{-7}
453	9.17×10^{23}	9.13×10^{-6}
483	1.79×10^{24}	5.91×10^{-7}
513	1.88×10^{24}	9.52×10^{-7}

Where E_D is the activation energy concerning diffusion process, D_o ($= \nu a^2$) is the diffusion coefficient at T= ∞, ν is the probability of ion jumping between two sites and a is the diffusion distance. A semilogarithmic plots of D versus $10^3/T$, Figure (3.22) , shows straight lines. The values of E_D are obtained by using the least square fitting of equation (3.17) and listed in Table (3.9) . It is noticed that, the values of E_D decrease with increasing xAgI content . In superionic solids, the diffusion coefficient D lies in the range (10^{-4}-10^{-1}) cm^2. sec^{-1}[113] which is in agreement with the present results for the glass system (50-x)P_2O_5-xAgI-40Ag_2O-10Fe_2O_3 , [x = 0 , 5 , 10 , 15, 20, 30] .

Ionic diffusion rates in solids were assumed to result from the random motion or jump of ions by means of various defects in crystalline solids such as vacancies and interstitials whereas in glasses diffusion occurs through the glass network unoccupied sites or voids. Diffusion process depend on the change in carrier mobility μ and concentration of change carriers with temperature. There are two kinds of silver ions in the glass network , the first is attaching themselves to the non-bridging oxygens of the phosphate. This group of ions is termed " immobile " carrier population . The second is surrounded by halide ions represent the " mobile " carrier population . The bridging oxygen facilitates the formation of a rigid glass network whereas non-bridging oxygens break the rigidity of the network and the structure becomes loose. With increasing temperature , some of the bridging oxygen may convert to non-bridging oxygen and vice versa.[114] . According to the cluster-bypass model[115], a conducting glass framework can be regarded as consisting of short-range order microdomains or clusters embedded in a highly disordered medium referred to as connecting tissue for ion migration.

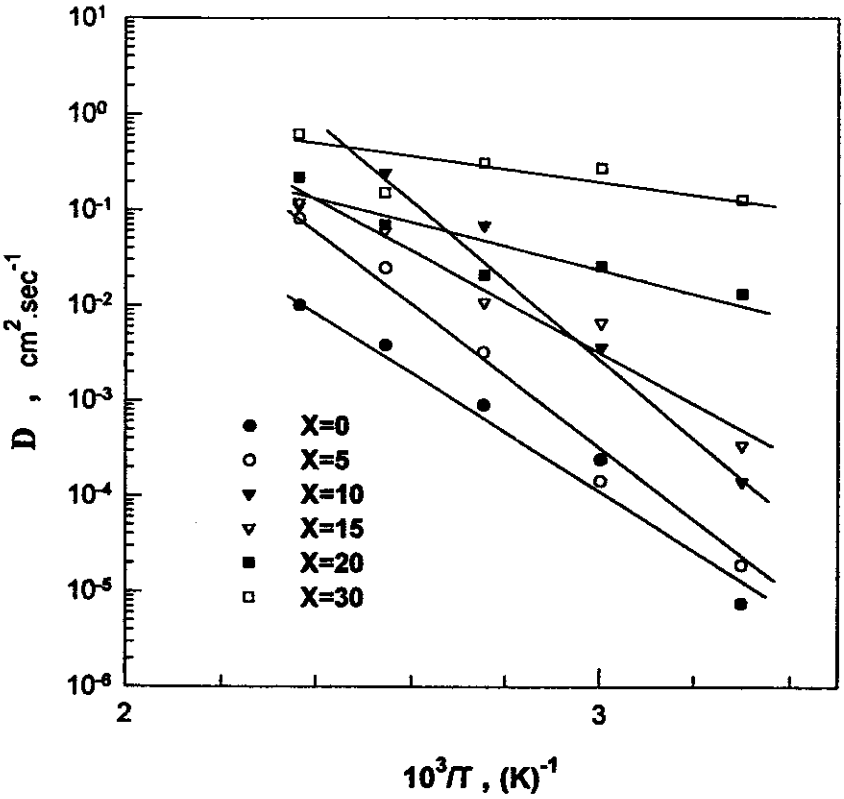

Figure (3.22): The temperature dependence of* D *for the glass system (50-x)P_2O_5-xAgI-40Ag_2O-10Fe_2O_3 , (x=0,5,10,15,20,30)..

These tissues constitute the preferred pathways as well as partial pathways. The partial pathways, which may arise due to the interconnection of some of the clusters to each other with bridging oxygen, blocks the pass for migration of the ions. In the case of our glass system, as the temperature increases, the Ag^+ ions "immobile" attached to the non-bridging oxygens are released and become "mobile" results in an increase in the mobile ion concentration n as well as the number of non-bridging oxygens . Many of these non-bridging oxygen convert into bridging oxygen by interconnecting the adjoining clusters. Consequently, the number of partial (blocking) pathways increases which results in a decrease in ion mobility μ with increasing temperature. In addition it is noticed that when AgI content increases the concentration of charge carriers n increases according to Stevels[116] which reasoned that as more alkali ions are add to the glass , fewer and fewer briding oxygen ions remain . The network " coherence " decreases and it is then easier for the ions to move.

3.5 Effect of asymmetric electrodes on conduction and dielectric properties of superionic solid electrolyte powder .

The Z``-Z` of the present solid electrolyte sample pressed powder at 37.8MPa using symmetric (Ag/SE/Ag) and asymmetric (Ag/SE/$Ag_2S$) electrodes was studied at different ambient temperatures , Figure (3.23) . The values of the bulk resistance (the semicircle intersection at Z`) were obtained from which the bulk conductivities were estimated.

Figure (3.24) illustrates the temperature dependence of the bulk coductivity (σ_{bl}) of the Ag/bulk SE/Ag solid elecrolyte , pressed powder Ag/SE/Ag solid electrolyte at 37.8 MPa and pressed powder Ag/SE/Ag_2S solid electrolyte at 37.8 MPa . All solid electrolytes were studied in the temperature range from room temperature up to 393 K . It is noticed that , for the Ag/bulk SE/Ag solid electrolyte, the conductivity increases with increasing temperature in the whole range of temperature. The conductivity of the Ag/SE/Ag pressed powder solid electrolyte increases with increasing temperature up to 373 K with mild change beyond such temperature.The conductivity of the Ag/SE/Ag_2S pressed powder solid electrolyte increases with increasing temperature up to 373 K whereas beyond such temperature it decreases with increasing temperature.The increase of the coductivity (σ_{bl}) with increasing temperature was interpreted previously in section (3.4.3) according to the structure model suggested by T.Minami[12].Also the kink in σ_{bL}-1/T relation at 373 K can be attributed to the dehydration of SE powder.The temperature dependence of the bulk coductivity (σ_{bl}) can be described by Arhinous relation (3.7) . The activation energy values ΔE_{bL} are estimated by using the least square fitting of relation (3.7) and listed in Table (3.11) . The values of the activation energy for the different electrolytes show the same value approximately.It can be concluded that

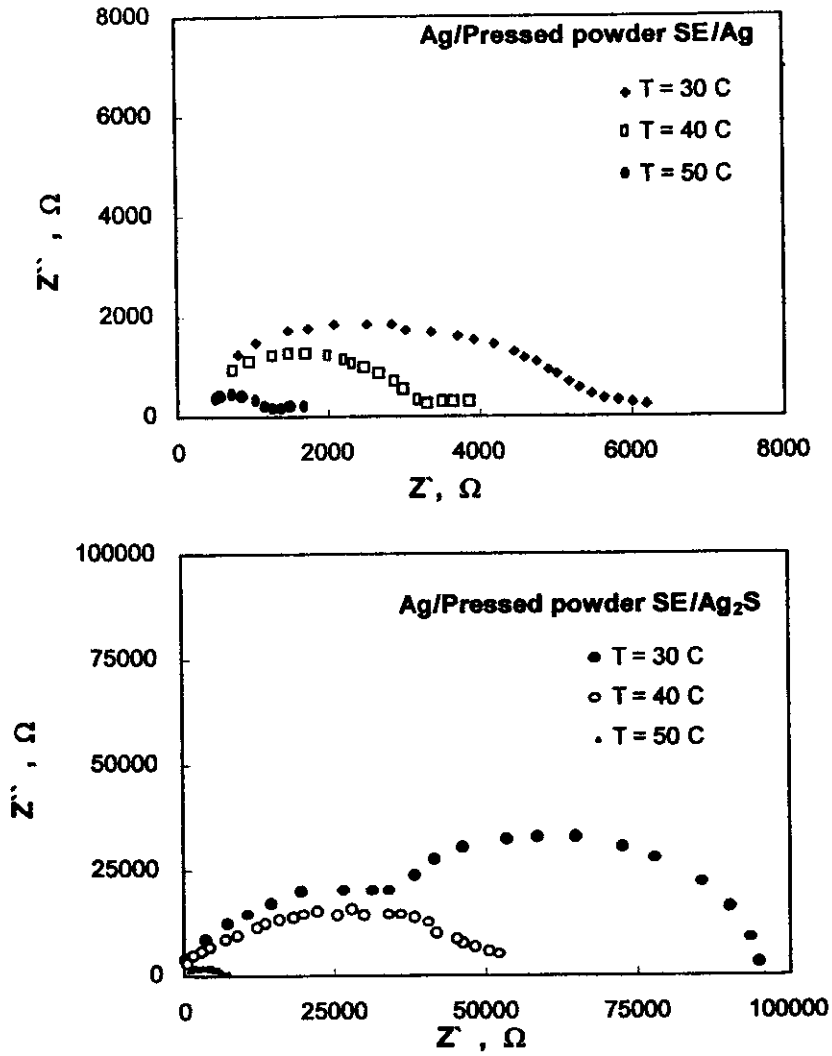

Figure (3.23) : Z`` versus Z` for the pressed powder Ag/SE/Ag and Ag/SE/Ag_2S solid electrolytes at different temperatures.

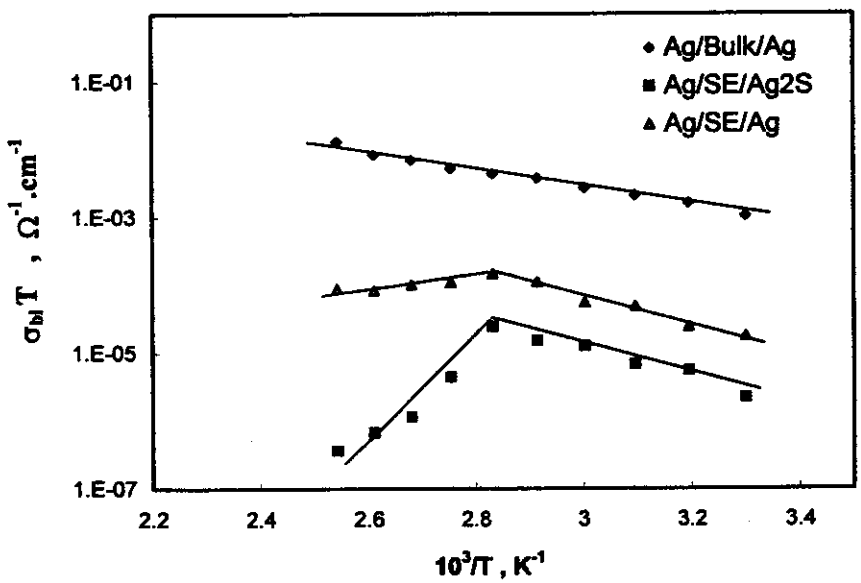

Figure (3.24) : Temperature dependence of σ_{bl} for the pressed powder Ag/SE/Ag and Ag/SE/Ag_2S solid electrolytes .

Table (3.11) : The activation energy values ΔE_{bL}, ΔE_{tot} and ΔE_{dc} for different solid electrolytes.

Solid electrolyte	ΔE_{bL} , eV	ΔE_{tot} , eV	ΔE_{dc} , eV
Ag/bulk SE/Ag	0.264	0.266	0.152
Ag/pressed powder SE/Ag	0.273	0.435	0.367
Ag/pressed powder SE/Ag_2S	0.281	0.512	0.411

grain boundary resistance at of the pressed powder electrolytes is negligible[79].

The resistance of the SE-Ag_2S interface was estimated using the complex impedance analysis . Figure (3.25) shows Z``- Z` diagram for the Ag/SE/$Ag_2S$ solid electrolyte at room temperature (30 °C) , it defines two arcs , the intersection of the first arc with Z` axis gives the bulk resistance R_b(= 44 KΩ) and the intersection of the second arc with Z` axis gives the resistance R_i (=96 KΩ) of the SE-Ag_2S interface.

Figure [(3.26)A,B] illustrates the logarithmic plots of $\sigma_{tot}(\omega)$ against frequency (50 Hz - 5 MHz) for the pressed powder Ag/SE/Ag and Ag/SE/Ag_2S solid electrolytes at different ambient temperatures. It is noticed that ,for two solid electrolytes, $\sigma_{tot}(\omega)$ is nearly constant at lower frequency range but it obeys a power relation (3.2) at higher frequency range.In addition $\sigma_{tot}(\omega)$, for Ag/SE/Ag solid electrolyte , is nearly unchanged with increasing frequency at higher temperatures in the whole frequency range. It is also noticed that , for two pressed powder solid electrolytes , $\sigma_{tot}(\omega)$ decreases beyond 373 K . The values of the power S obtained at different ambient temperatures are listed in Table (3.12) .

Figure (3.27) illustrates $\sigma_{tot}(\omega)$ against temperature for the Ag/bulk SE/Ag , pressed powder Ag/SE/Ag and pressed powder Ag/SE/Ag_2S solid electrolytes at 1KHz . It is noticed that , the general behaviour is the activation of $\sigma_{tot}(\omega)$ with increasing temperature while it decreases again beyond 373 K for pressed powder Ag/SE/Ag and Ag/SE/Ag_2S solid electrolytes. The activation energy values ΔE_{tot} are estimated by using the least square fitting of relation (3.7) and listed in the Table (3.11) . The value

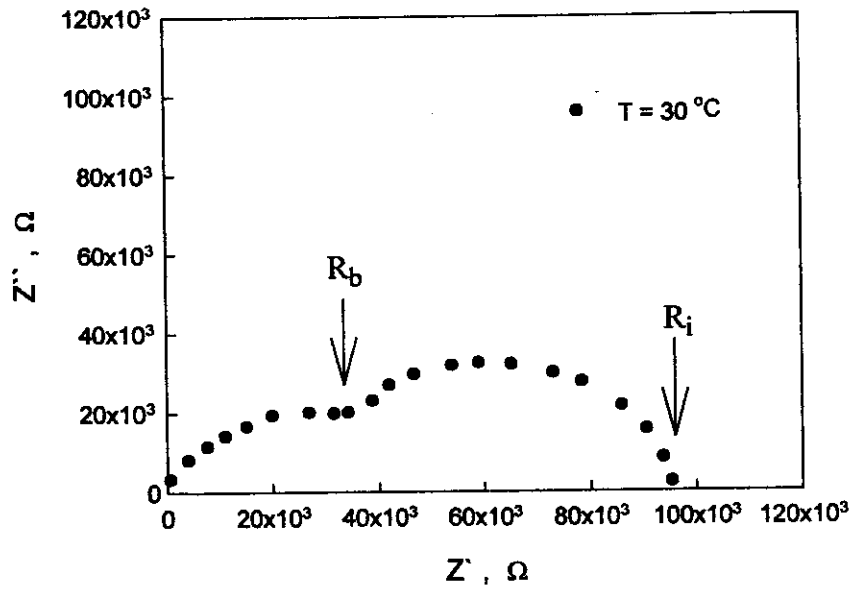

Figure (3.25) : Z`` versus Z` for the Ag/SE/Ag_2S solid electrolyte at room temperature (30 °C) .

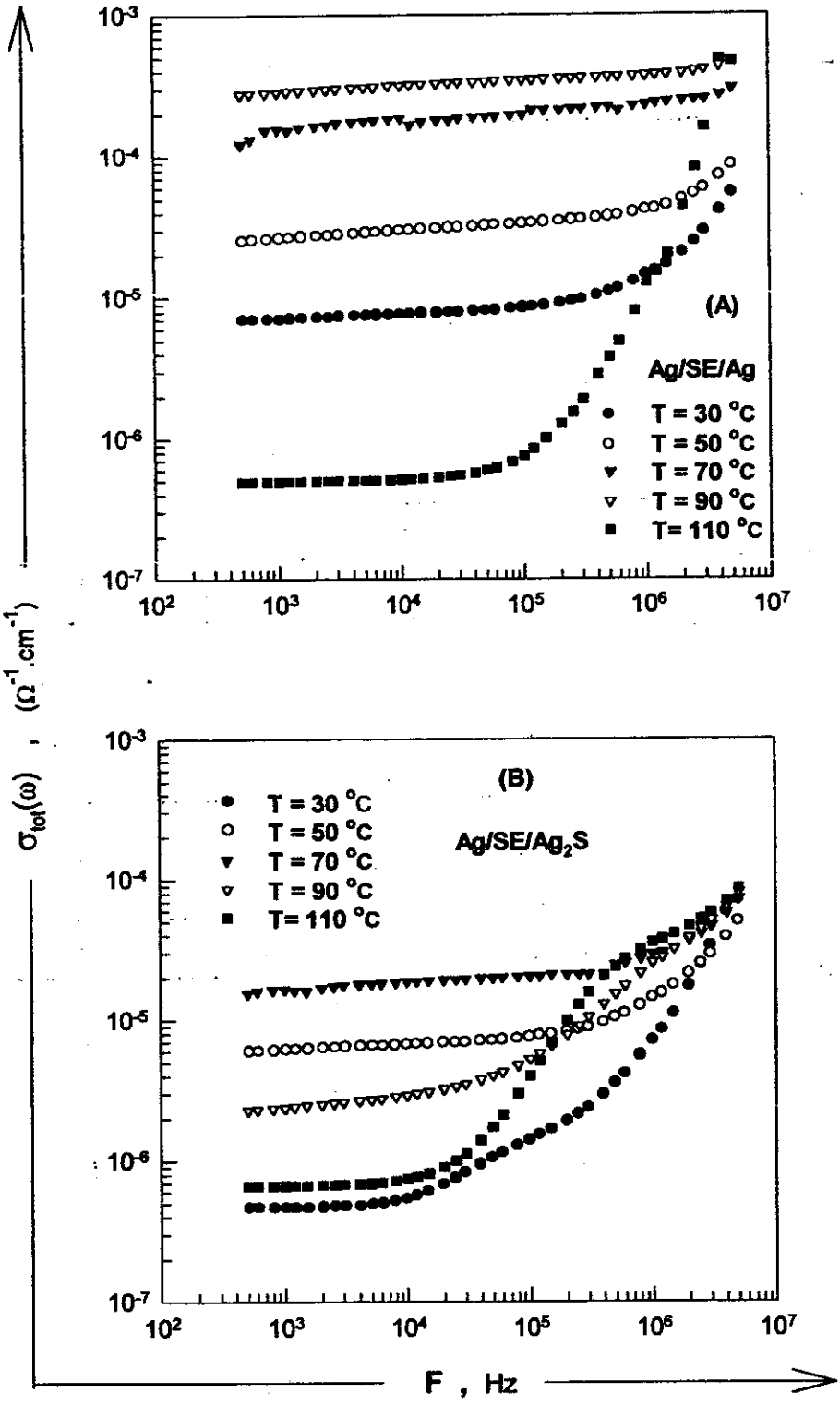

Figure [(3.26) A,B] : Temperature dependence of $\sigma_{tot}(\omega)$ for the pressed powder Ag/SE/Ag and Ag/SE/Ag_2S solid electrolytes at different temperatures.

Table (3.12) : The values of power S at different ambient temperatures for different solid electrolytes.

Temp. K	Ag/SE/Ag	Ag/SE/Ag_2S
	S	S
303	1.06	1.29
323	0.68	0.69
343	------	0.81
363	------	0.72
383	1.55	1.23

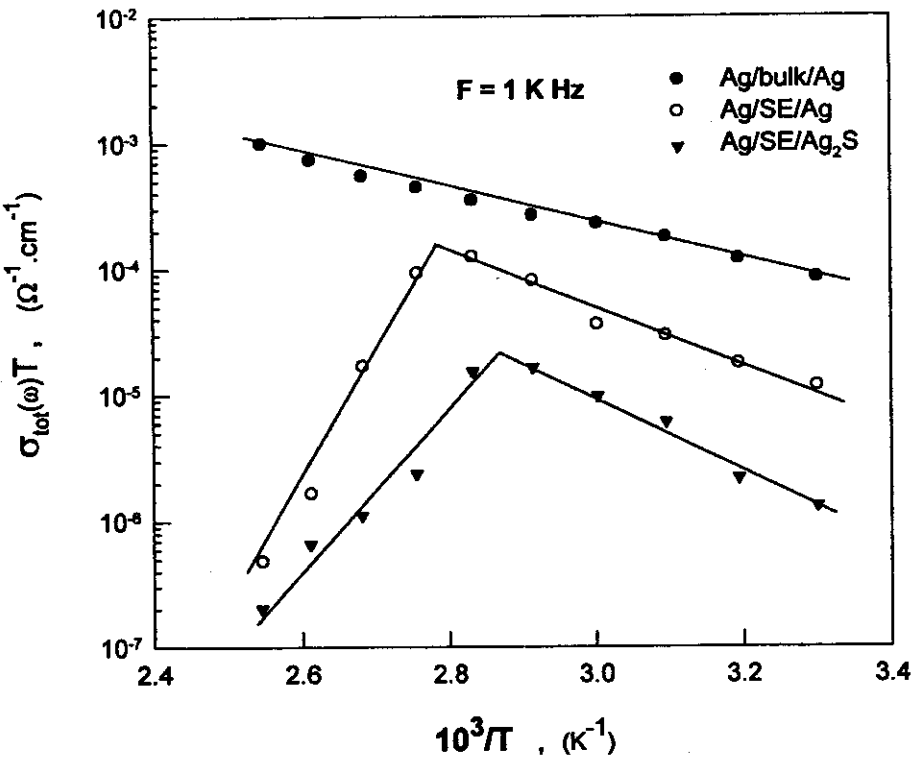

Figure [(3.27)] : Temperature dependence of $\sigma_{tot}(\omega)$ for the Ag/bulk/Ag , Ag/SE/Ag and Ag/SE/Ag_2S solid electrolytes at fixed frequency(1 K Hz).

of ΔE_{tot} for bulk sample Ag/bulk SE/Ag with symmetric electrodes is lower than that of pressed powder Ag/SE/Ag solid electrolyte with the same electrode configuration . This can be attributed to the contribution of the interface resistance of powder grains . In addition , the value of ΔE_{tot} of pressed powder Ag/SE/Ag_2S solid electrolyte with asymmetric electrodes is higher than both bulk and or powder SE with symmetric electrode configuration . This is also attributed to the contribution of Ag_2S/SE interface resistance .

Figure (3.28) illustrates the temperature dependence of σ_{dc} at zero frequency for the Ag/bulk SE/Ag , pressed powder Ag/SE/Ag and pressed powder Ag/SE/Ag_2S solid electrolytes. It is noticed that , the general behaviour is the activation of σ_{dc} with increasing temperature but it decreases again beyond 373 K for pressed powder Ag/SE/Ag and pressed powder Ag/SE/Ag_2S solid electrolytes. The activation energy values ΔE_{dc} are estimated by using the least square fitting of relation (3.7) and listed in Table (3.11).

Figure (3.29) illustrates the dielectric constant ε' against frequency (50 Hz - 5 MHz) for the pressed powder Ag/SE/Ag and pressed powder Ag/SE/Ag_2S solid electrolytes at different ambient temperatures.It is noticed that , the general behaviour is the decrease of ε' with increasing frequency. The attenuation of ε' with increasing frequency can be explained by equation (3.9) , section (3.4.4) . It is also noticed that , ε' increases with increasing temperature up to 373 K and thereafter that it decreases again . The large values of ε' for the pressed powder Ag/SE/Ag and pressed powder Ag/SE/Ag_2S solid electrolytes which could be attributed to the interfacial polarization effect [53,108,109].

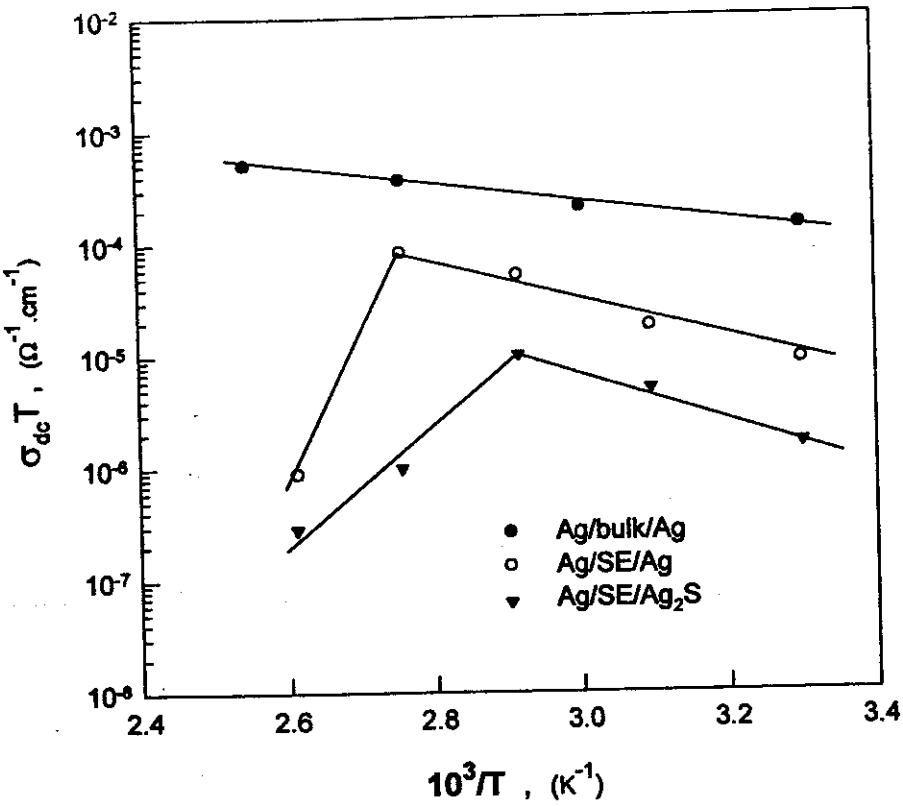

Figure [(3.28)] : Temperature dependence of σ_{dc} for the Ag/bulk/Ag , Ag/SE/Ag and Ag/SE/Ag_2S solid electrolytes .

Figure (3.30) illustrates the dielectric loss ε`` against frequency (50 Hz - 5 MHz) for the pressed powder Ag/SE/Ag and pressed powder Ag/SE/$Ag_2S$ solid electrolytes at different ambient temperatures.It is noticed that , the general behaviour is the decrease of ε`` with increasing frequency. This can be explained by equation (3.10) , section (3.4.5).It is also noticed that , ε`` increases with increasing temperature up to 373 K and it decreases sharply.

Figure (3.31) illustrates temperature dependence of relaxation time τ obtained for the pressed powder Ag/SE/Ag and pressed powder Ag/SE/Ag_2S solid electrolytes. In general , the values of τ is attenuate with increasing temperature and obeys relation (3.15). The values of E_τ deduced and listed in Table (3.13) .

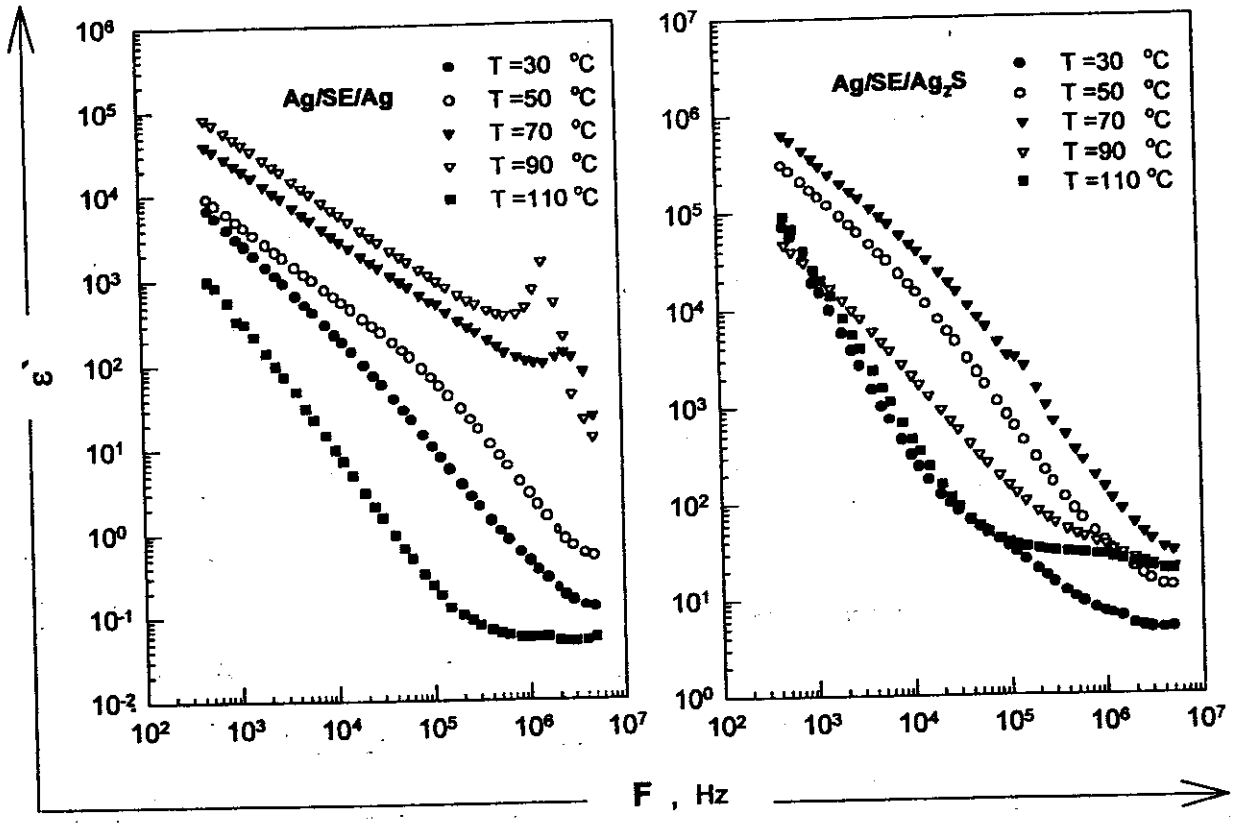

Figure (3.29) : Frequency dependence of dielectric constant ε` for the Ag/SE/Ag and Ag/SE/Ag_2S solid electrolyts.

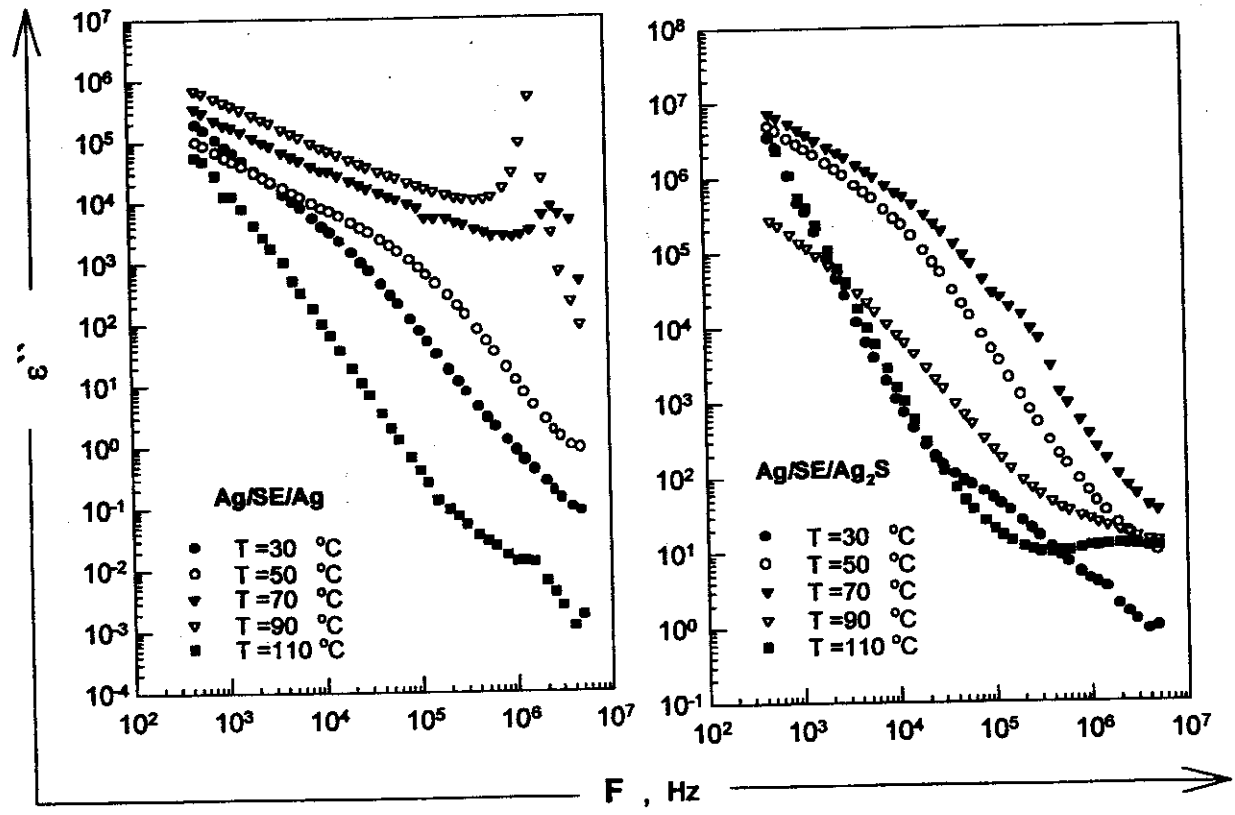

Figure (3.30) : Frequency dependence of dielectric loss ε`` for the Ag/SE/Ag and Ag/SE/Ag_2S solid electrolyts.

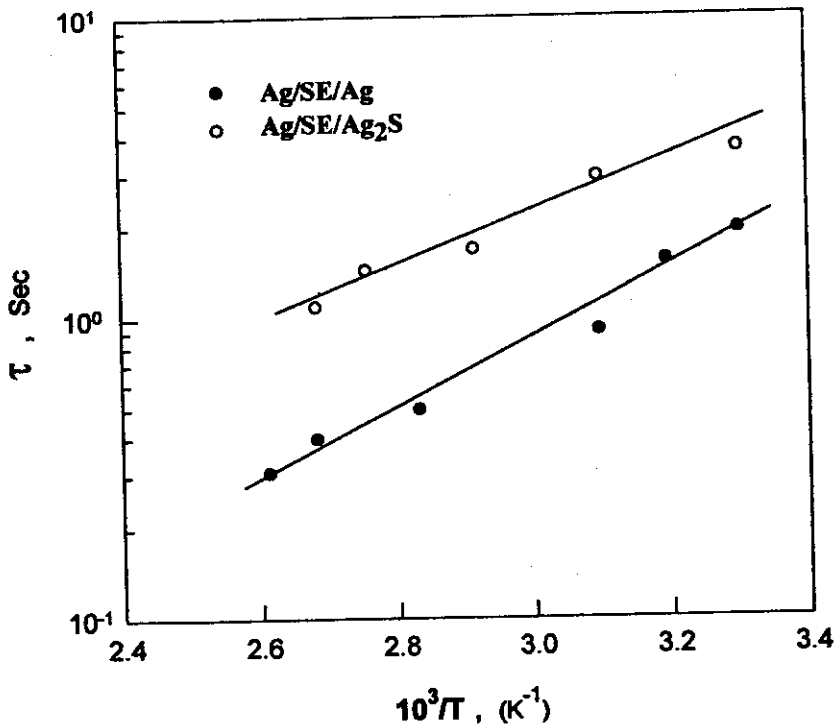

Figure (3.31) : Temperature dependence of Relaxation time for the Ag/SE/Ag and Ag/SE/Ag_2S solid electrolytes.

Table (3.13) : The values of activation energy $\Delta E\tau$ for different solid electrolytes.

Solid electrolyte	ΔE_{τ} , eV
Ag/Pressed powder SE/Ag	0.292
Ag/Pressed powder SE/Ag_2S	0.234

3.6 I-V characteristic of the superionic solid electrolyte (SE).

In the present section , it is interesting to study I-V characterestic relationships by using asymmetrical electrodes for the present glass electrolyte (Ag/SE/Ag_2S) , Ag_2S electrode forms blocking . Figure (3.32) illustrates a plot of current I against voltage V in the forward and backward direction at different ambient temperatures. It is noticed that , in the case of forward direction , the current increases nonlinearly with increasing applied voltage . The voltage dependence of current can be expressed by the following Schottky diode equation [32] ;

$$I_F = I_o(e^{qV_F / KT} - 1) \qquad (3.18)$$

$$I_o = C e^{-q\phi_B / kT}$$

where C is the proportionality constant , ϕ_B is the barrier hight and V_F is the applied voltage in the forward direction. In addition the current in the forward direction activates by increasing the ambient temperature because of the more excitation charge according to eq.(3.18) . Figure (3.33) illustrates the temperature dependence of I_F at different applied voltages. The temperature dependence of I_F can be discussed according to the Arhenius relation ;

$$I_F = I' e^{-E_F / KT} \qquad (3.19)$$

where E_F is the activation energy of I_F under the influence of applied voltage and I`=I_F at T= ∞ . The values of E_F are obtained at 1,2 and 3 V respectively and listed in Table (3.14) . One notices that , E_F decreases by increasing applied voltage , this can be interpreted as the applied voltage was increased the potential barrier height reduces which leads to more flow of charge carriers across the effective area of Ag_2S-solid electrolyte contact.

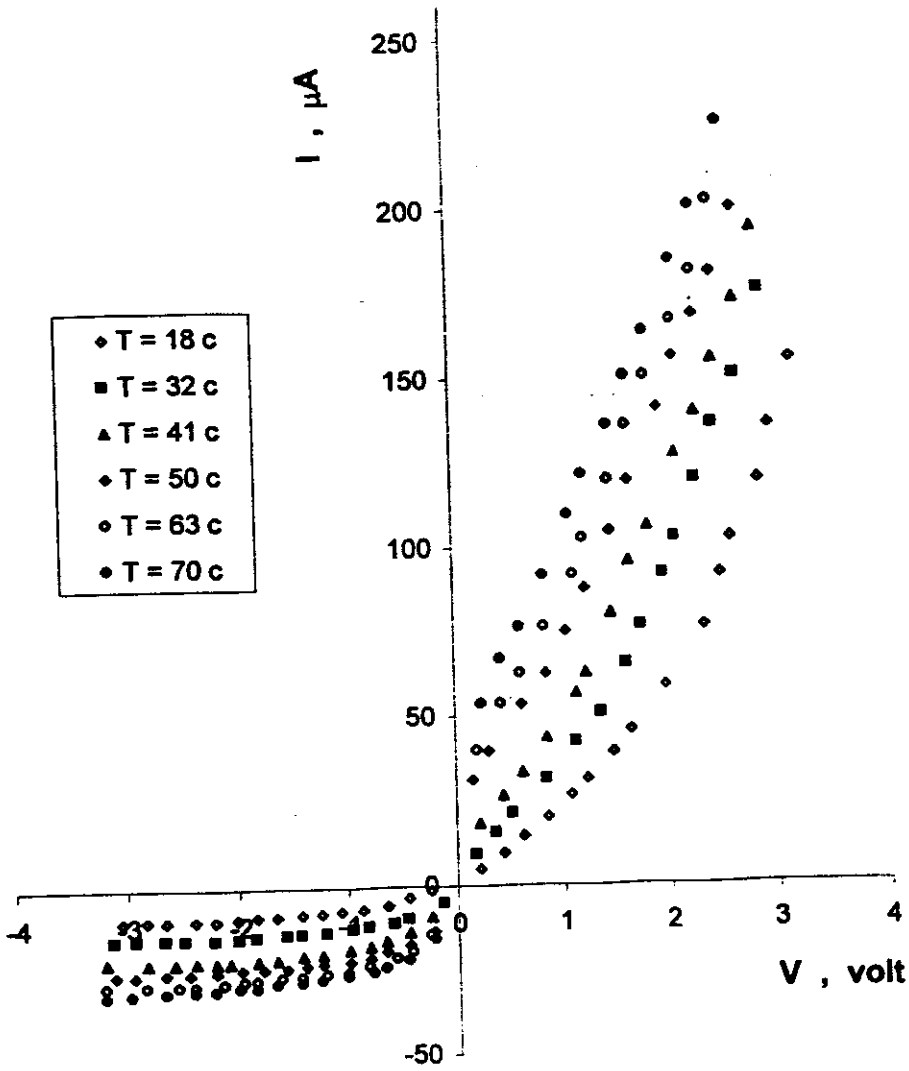

Figure(3.32): I-V characterestic curves for the Ag/SE/Ag_2S solid electrolyte in the forward and backward directions

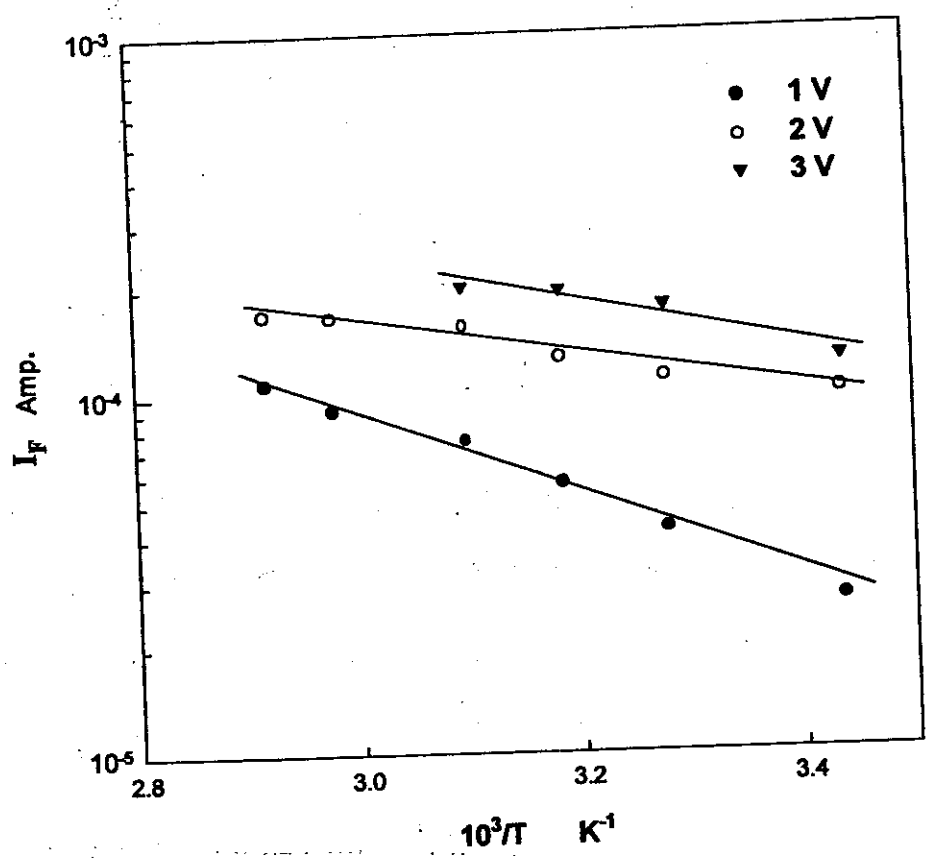

Figure (3.33) : Temperature dependence of the forward current (I_F) ***at different applied voltages .***

Table (3.14) : The values of activation energy E_F at different applied voltage.

Applied voltage , volt	E_F eV
1	0.232
2	0.214
3	0.126

As the direction of applied field was reversed , the I-V relationships illustrate a little increase of the current I_{rev} with increasing applied voltage until a saturation of current is attained , this can be attributed to the movement of minority carriers under the influence of external applied potential . The voltage dependence of I_{rev} could be expressed by the following equation ;

$$I_{rev} = I_s(e^{-qV_R/KT} - 1) \qquad (3.20)$$

where V_R is the applied voltage in the backward direction and I_s is the saturation current which can be expressed as follows ;

$$I_s = AT^2 e^{-q\phi_B/KT} \qquad (3.21)$$

where A is the effective Richardson constant and ϕ_B is the equilibrium contact barrier height which prevent further charge carrier diffusion between the solid electrolyte and Ag_2S ;

$$\phi_B = \phi_{electrode} - \phi_{SE} \qquad (3.22)$$

where $\phi_{electrode}$ is the work function of electrode material and ϕ_{SE} is the work function of the solid electrolyte .

The saturation current I_s is thermally activated by increasing temperature obying equation (3.21) . The plot of I_s/T^2 versus 1/T shows straight line , Figure (3.34). The value of ϕ_B (0.082 eV) was obtained using the least square fitting of relation (3.21).

In the absence of any external field on Ag/SE/Ag_2S , the charge carrier density gradient at both sides around the SE - Ag_2S interface results in a self diffusion of the majority carriers producing a depletion region at the interface. The main part of the depletion region arised at SE side.The potential barrier arised at interface is attributed to the present of the negative

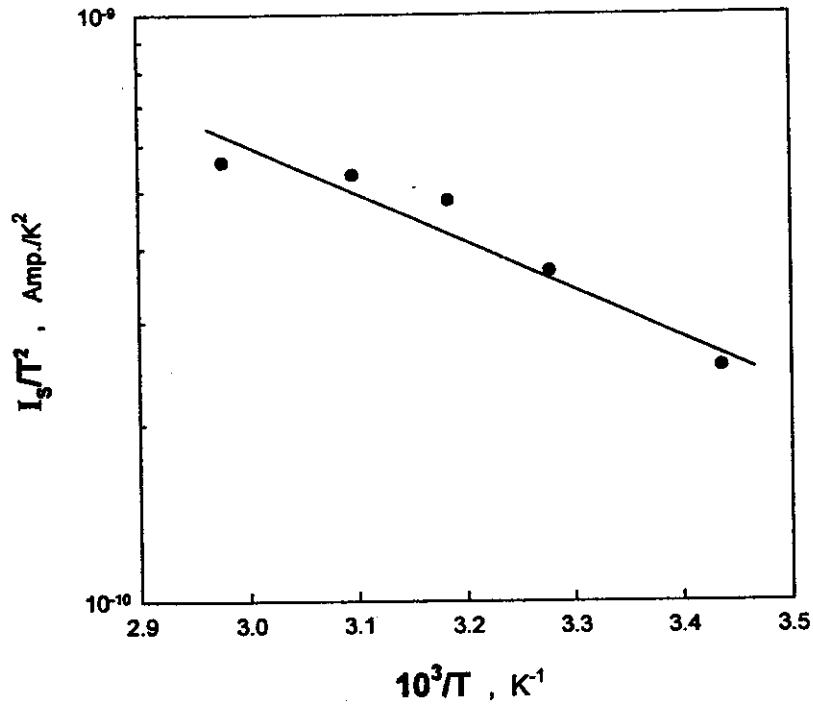

Figure (3.34) : I_s/T^2 versus $10^3/T$ for the Ag/SE/Ag_2S solid electrolyte.

fixed ions inside SE and we neglect the depth of depletion region in Ag_2S side because of its high concentration of charge carriers ($1x10^{22}$ cm^{-3}).The generation of PO_4^- groups in SE is due to break of O-Ag bonds and consequently a reduction reaction occurs as follows ;

$$Ag^+ + e^- \longrightarrow Ag \qquad \text{(Reduction)}$$

The electrons whish attack silver ions at SE side generates from oxidation reaction at Ag_2S side as follows ;

$$S^{2-} \longrightarrow 2e^- + S \qquad \text{(Oxidation)}$$

The built-in potential height (V_{bi}) arised at Ag_2S – SE interface can be expressed by the following equation[32] ;

$$V_{bi} = \frac{KT}{q} Ln \frac{N_{SE}}{N_{Ag2S}} \qquad (3.23)$$

where N_{SE} , $N_{Ag2S(electrode)}$ are the concentration of charge carriers of solid electrolyte and Ag_2S electrode respectively. The value of V_{bi} has been estimated using N_{SE}(=$1.8x10^{21}$ cm^{-3}) and N_{Ag2S}(=$1x10^{22}$ cm^{-3})[111] . It is noticed that , the estimated value of V_{bi}(=0.061 eV) is lower than the value of the barrier hight from solid electrolyte to Ag_2S electrode (ϕ_B = 0.082 eV).

3.7 Superionic Solid electrolyte glass for rechargeable battery application.

3.7.1 Effect of thickness on the charging and discharging of solid electrolyte Ag/SE/Ag_2S battery.

In the present section, the study of the effect of thickness on the charge-discharge processes of the solid electrolyte Ag/SE/Ag_2S battery was performed at room temperature (30 °C). Figure (3.35), illustrates charge current I versus time t for the solid electrolyte Ag/SE/Ag_2S battery (reverse direction) for samples of different thicknesses of solid electrolytes prepressed at pressure (37.8 MPa) using applied voltage 3V . It is noticed that, the charge current decays exponentialy to stationary after long duration.The attenuation of charge current with time can be attributed to the polarization process as follows[75], the application of electric field assists the migration of silver ions and leads to produce local field opposing the external field. Therefore, the actual field is reduced and results in lowering conduction in the solid electrolyte Ag/SE/Ag_2S battery with time. It is also noticed that the initial value of the charge current in the case of thickness =1 mm is greater than that of the electrolyte thickness =1.8 mm which can be attributed to the decrease of the electrolyte resistance.The attenuation of charge current with time can be described by the following empirical relation;

$$I = I_o \, e^{-t/C} \qquad (3.24)$$

where I_o is the initial charge current and C is the circuit time constant. The values of time constant C was obtained by using the least square fitting of equation (3.24) and listed in Table (3.15) .The increase of the time constant

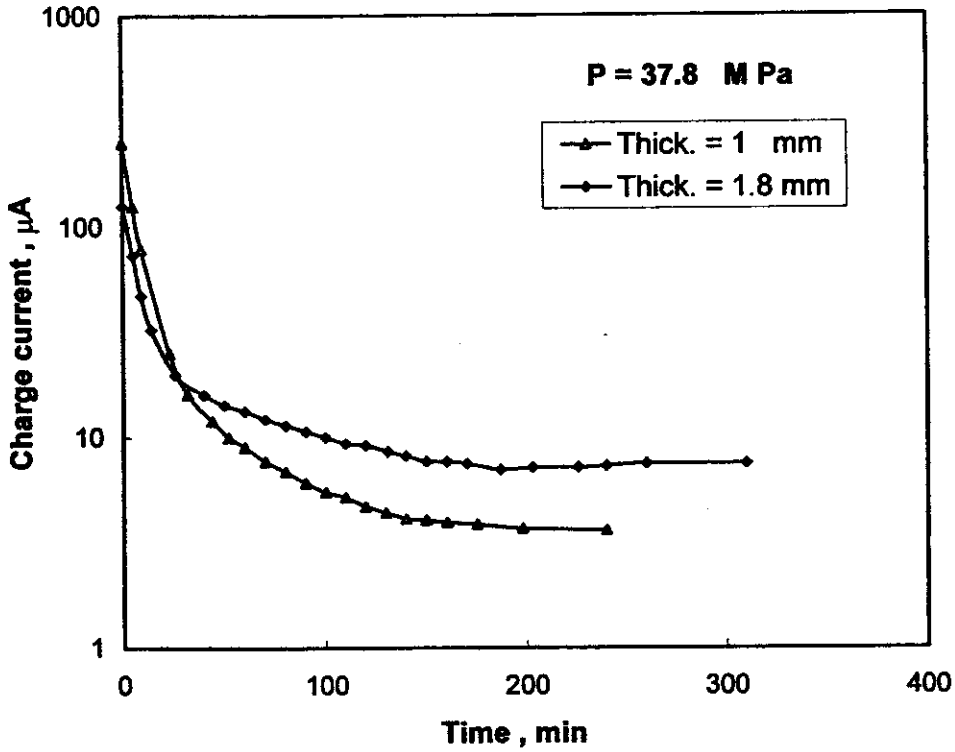

Figure (3.35) : Charge current versus Time for the solid electrolyte battery Ag/SE/Ag_2S charged at a constant voltage 3V .

Table (3.15) : The values of circuit time constant C at different thickness.

Thickness , mm	*Charge process*	*Discharge process*	
	C , Sec	C_1 , Sec	C_2 , Sec
1	665	2500	10000
1.8	1250	1666	5000

with increasing thickness confirms the expectation of the change of electrolyte resistance by increasing sample thickness.

Figure (3.36) illustrates the cell voltage of the solid electrolyte Ag/SE/Ag_2S battery versus electerical capacity [Q=I x t μAh][78] at constant load resistance equal to 5KΩ . It is noticed that , the cell voltage is decreases , in general , to nearly stationary value . It is also noticed that, as the electrolyte thickness increases the cell voltage decreases because of resistance reduction due to the sample thickness decrease leading to an facilitate polarization and/or silver ion migration in the charging process. Consequently this leads to an increase of depelation region at the interface. Figure (3.37) illustrates the discharge current against time at load resistance equal to 5kΩ . The general behaviour is the decrease of the values of the discharge current to a stationary value. It is also noticed that, the values of the discharge current for sample of thickness 1mm is higher than that of the 1.8 mm thickness. The attenuation of discharge currrent with time can be attributed to the re-diffusion of electric charges of opposite signs at both sides of an interface.The values of circuit time constant C was obtained by using the least square fitting of equation (3.24) and listed in Table (3.15). The values of time constant shows decreasing with increasing thickness in both of two regions. This can be explained as follows ; (i) the circuit rate constant depends on the total circuit resistance , (ii) the decreases because the reverse of the current direction and (iii) the higher the cell voltage leads to larger initial current.

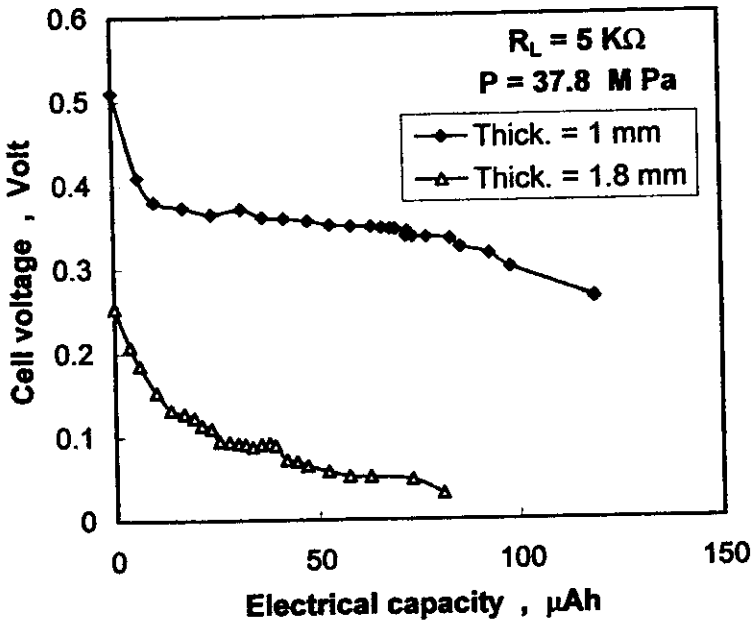

Figure (3.36) : Cell voltage versus electrical capacity for the solid electrolyte battery Ag/SE/Ag_2S .

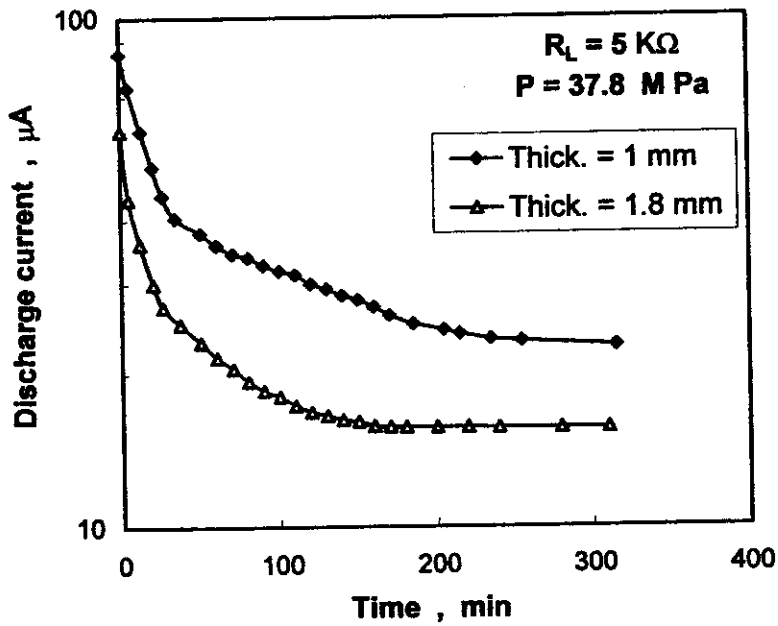

Figure (3.37) : Discharge current versus Time for the solid electrolyte battery Ag/SE/Ag_2S .

3.7.2 Effect of pressure on the charging and discharging of solid electrolyte batteries.

The effect of pressure on the charge-discharge process of the solid electrolyte Ag/SE/Ag_2S battery , prepared under different pressures and constant thickness equal to 1mm , was performed at room temperature (30 °C). Figure (3.38) illustrates the charge current against time of the solid electrolyte Ag/SE/Ag_2S battery at constant voltage 3V. it is noticed that, the charge current decays with increasing charge duration to a stationary value.

Figure (3.39) illustrates the cell voltage against elecrical capacity of the solid electrolyte Ag/SE/Ag_2S battery by using load resistance of 2 MΩ . It is noticed that, the general behaviour of the cell voltage-electric capacity relation shows a slight decrease of the value of discharge voltage down to stationary value. In addition , the value of cell voltage increases with increasing pressure of preparation . Figure (3.40) illustrates the discharge current against time for the solid electrolyte Ag/SE/Ag_2S battery using load resistance 2 MΩ . The general behaviour shows a remarkable decrease of the value of discharge current followed by a mild decrease to a stationary value. It is also noticed that, the value of discharge current shifts upward as the value of the preparation pressure increases. This can be explained as follows, the higher pressure accumulates grains together leading to a lower of the contact resistance at grain boundaries.The value of the circuit time constant R was obtained by using the least square fitting of equation (3.24) and listed in Table (3.16) .The values of time constant showed two regions , the first region showed decreasing of C_1 with increasing pressure and the seconed region showed increasing of C_2 with increasing pressure.

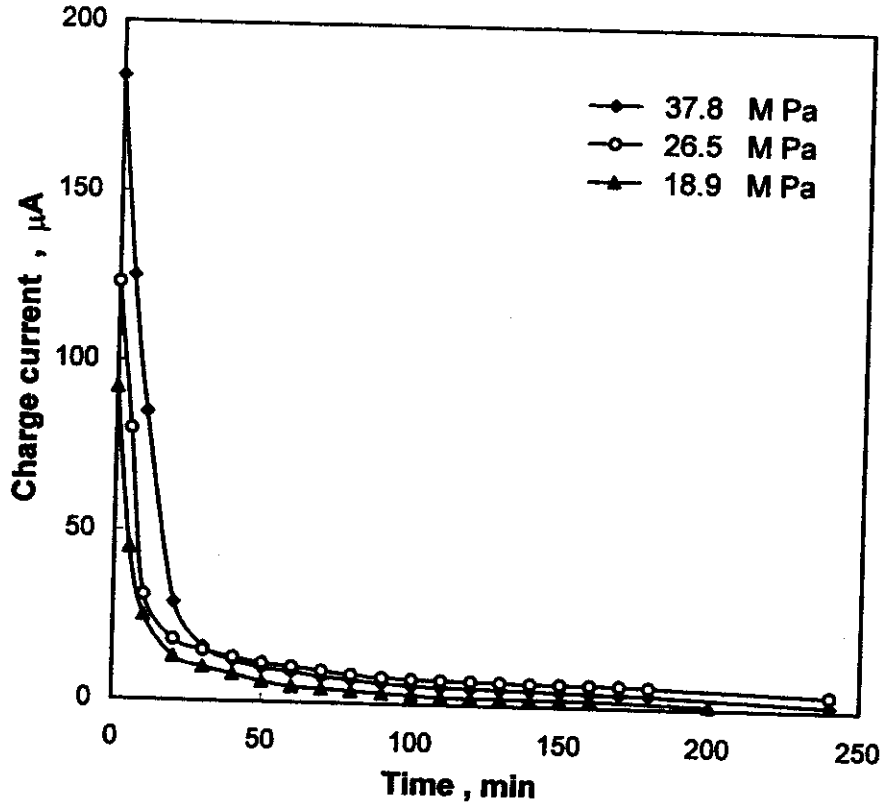

Figure (3.38) : Charge current versus Time for the solid electrolyte battery Ag/SE/Ag_2S at different pressures charged at constant voltage 3V .

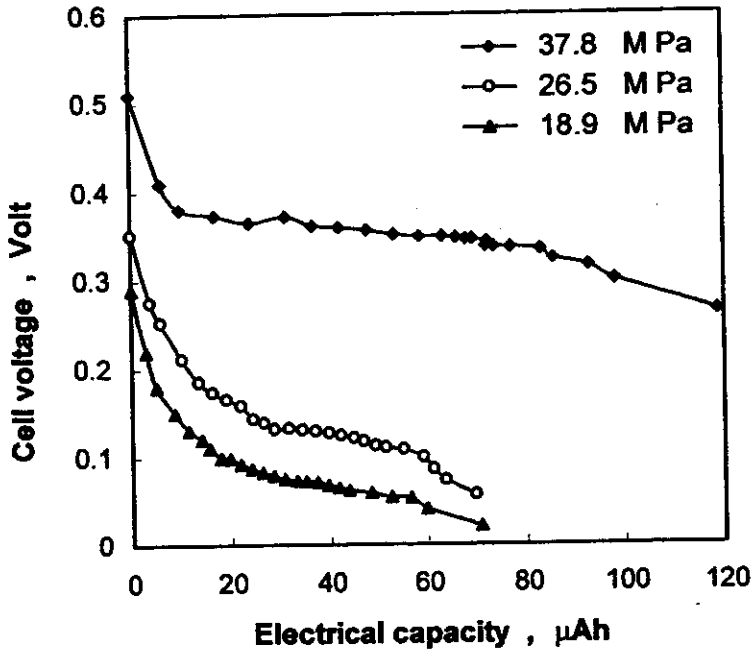

Figure (3.39) : Cell voltage versus electrical capacity for the solid electrolyte battery Ag/SE/Ag_2S discharged at a constant load resistance 2 MΩ.

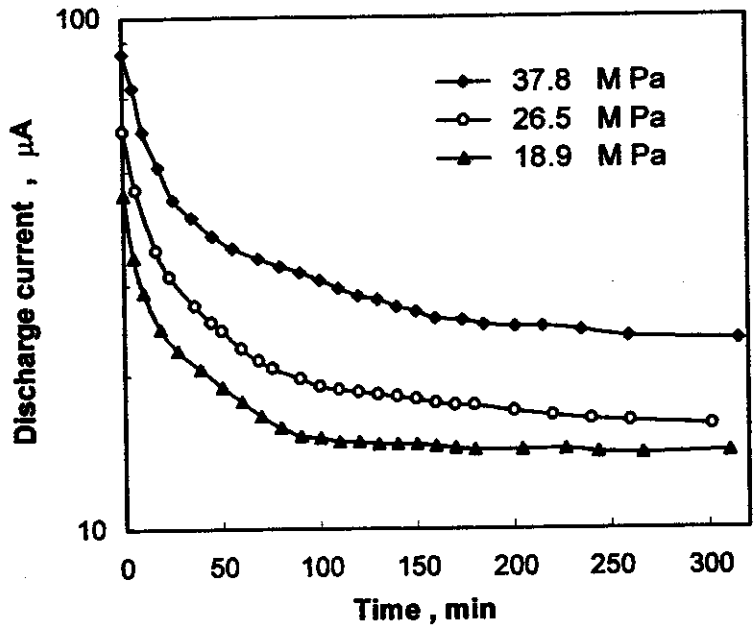

Figure (3.40) : Discharge current versus Time for the solid electrolyte battery Ag/SE/Ag_2S discharged at a constant load resistance 2 MΩ.

Table (3.16) : The values of circuit time constant C at different pressures.

Pressure , MPa	C_1 , Sec	C_2 , Sec
18.9	2000	10000
26.5	2776	16665
37.8	3343	20000

3.7.3 Study of the charge-discharge processes by using different load resistances[81].

In the present section we study the effect of load resistance on the cell voltage and discharge current at room temperature (30 °C). Figure (3.41) illustrates the charge current versus time for the solid electrolyte Ag/SE/Ag_2S battery , thickness (1 mm) and preparation pressure (37.8 MPa) at constant applied voltage 3V. it is noticed that, the charge current decays with increasing time to stationary value.

Figure (3.42) illustrates the cell voltage against the electrical capacity for the solid electrolyte Ag/SE/Ag_2S battery at different load resistances . It is noticed that, as the load resistance increases the cell voltage shifts upward . This can be attributed to the load resistance control of the battery current drain. It is also noticed that, the value of electrical capacity in the case of 2MΩ is higher than that in the case of 1 and/or 5KΩ because at higher load resistance , 2 MΩ , the discharge current spend long time at higher values in the whole range of discharge time.This means that the battery supplies smaller current for longer time. Figure (3.43) illustrates the discharge current against time for the solid electrolyte Ag/SE/Ag_2S battery at different load resistances. The general behaviour is the decrease of discharge current untill a stationary values. The values of the circuit time constant C was obtained by using least square fitting of equation (3.24) and listed in Table (3.17) .

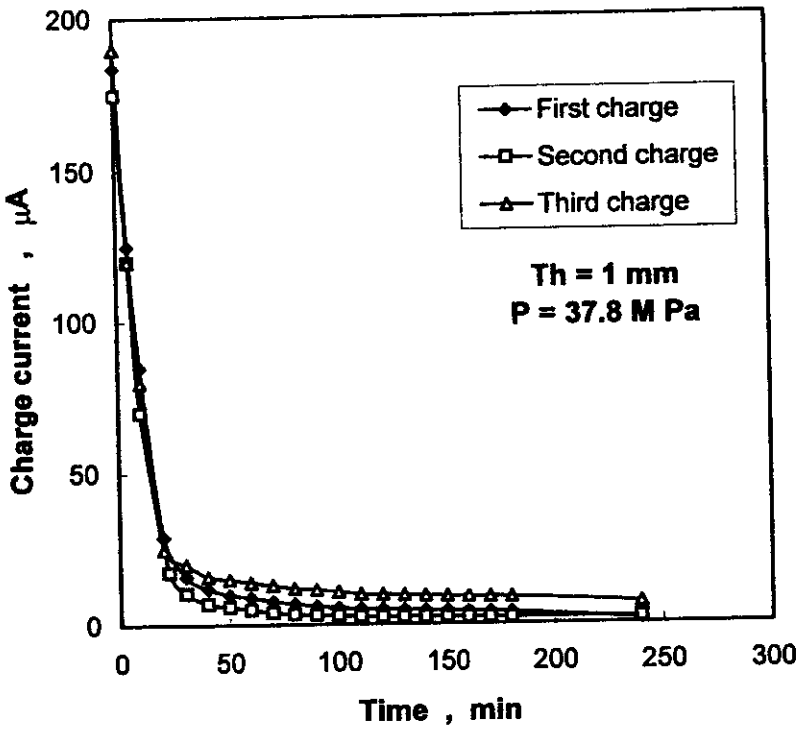

Figure (3.41) : Charge current versus Time for the solid electrolyte battery Ag/SE/Ag_2S charged at constant voltage 3V .

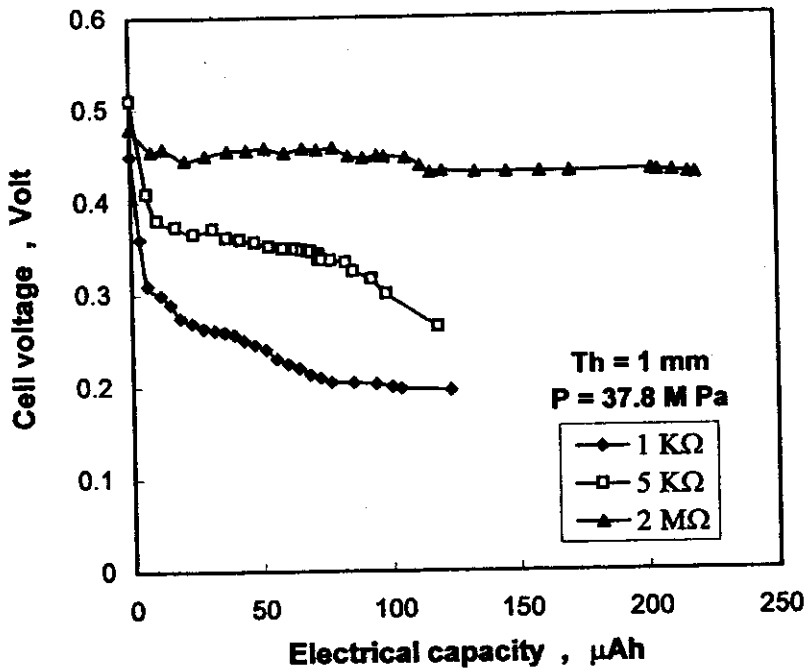

Figure (3.42) : Cell voltage versus electrical capacity for the battery Ag/SE/Ag_2S discharged at a different load resistances .

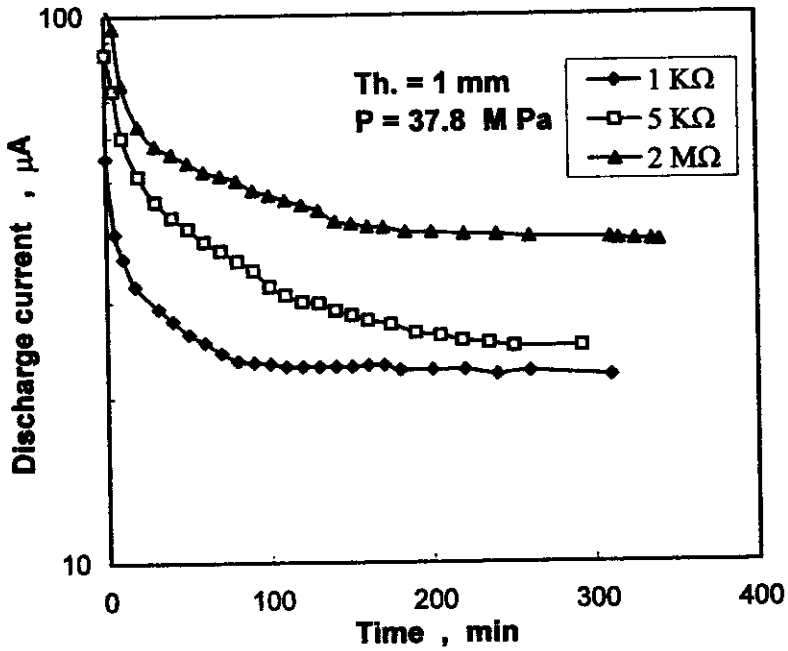

Figure (3.43) : Discharge current versus Time for the battery Ag/SE/Ag_2S discharged at different load resistances .

Table (3.17) : The values of circuit time constant C at different load resistances.

Load resistance , KΩ	C_1 , Sec	C_2 , Sec
1	2575	244
5	2334	374
2000	2941	361

3.7.4 Effect of ambient temperature on the charge-discharge processes of the Ag/SE/Ag_2S battery .

The charge-discharge processes of the solid electrolyte Ag/SE/Ag_2S battery was carried out at different ambient temperatures. Figure (3.44) illustrates the charge curves at different temperatures and at fixed applied voltage 3V. It is noticed that , the charge current decays with time to stationary value. In addition , as the ambient temperature was increased the initial value of charge current increases which can be attributed to the temperature assisting silver ion migration. The stationary value of charge current shifts downward by raising the ambient temperature , this is due to ease of ion movement leading to the fast polarization process.

Figure (3.45) illustrates the cell voltage against the electric capacity for the solid electrolyte Ag/SE/Ag_2S battery at different ambient temperatures by using a load resistance equal to 2MΩ. It is noticed that, discharge voltage decreases slightly to stationary value.In addition the behavior shifts down by increasing ambient temperature. Figure (3.46) illustrates the discharge current versus time at different ambient temperatures. The general behaviour is the attenuation of the discharge current with time to stationary value. In addition, the initial discharge current value shifts towards higher values by increasing temperature because of the structure relaxation which assists silver ion migration. Figure (3.47) illustrates logarithmic plot between circuit time constant , C , and reciprocal of temperature . It is noticed that , two regions in lnI – t relation appear , Figure (3.47) . The values of circuit time constant obtained decrease by increasing ambient temperature. This can be

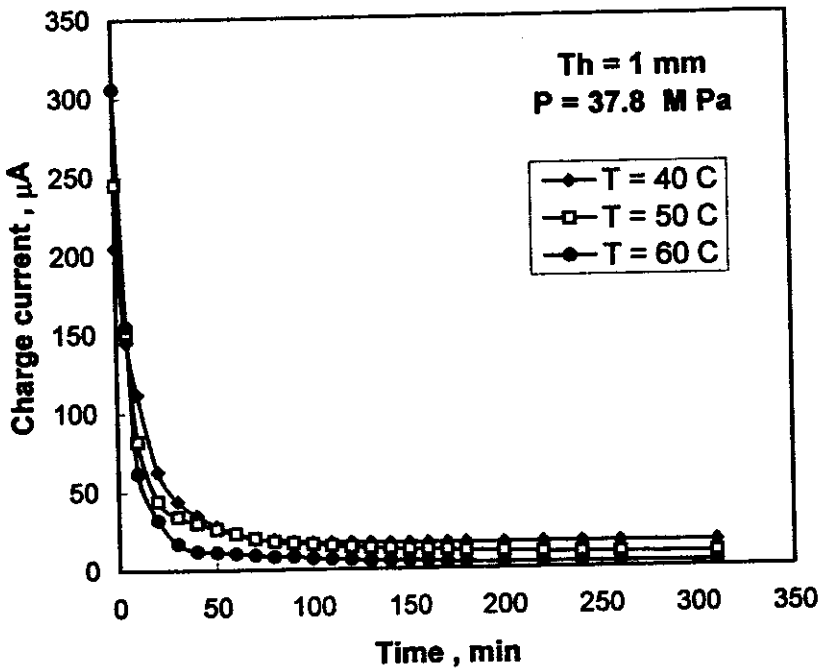

Figure (3.44) : Charge current versus Time for the Ag/SE/Ag_2S solid electrolyte battery charged at constant voltage 3V .

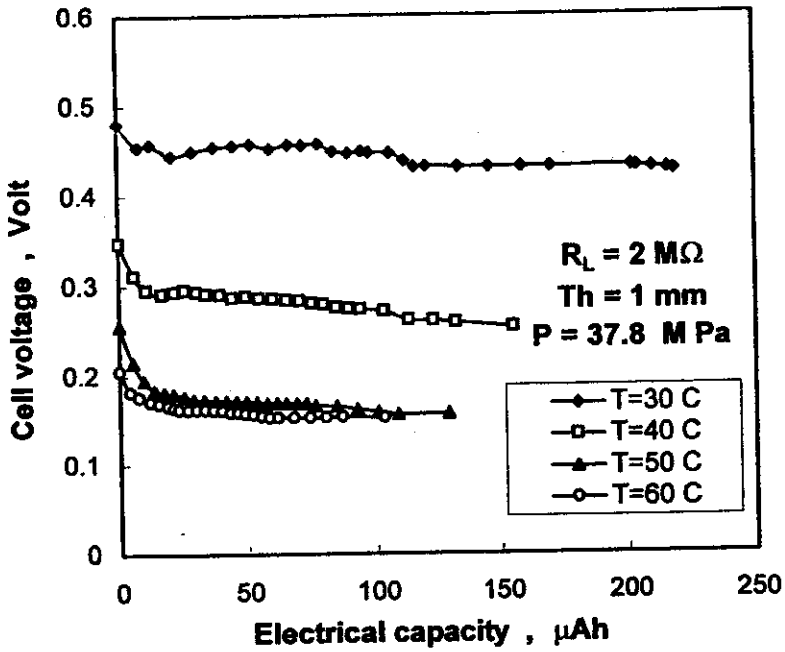

Figure (3.45) : Cell voltage versus electrical capacity for the solid electrolyte batteryAg/SE/Ag_2S .

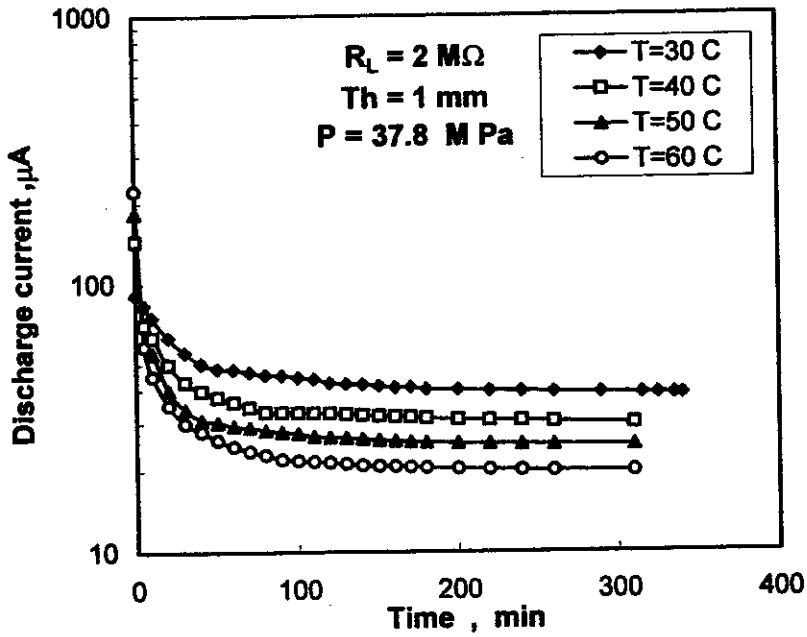

Figure (3.46) : Discharge current versus Time for the solid electrolyte battery Ag/SE/Ag_2S .

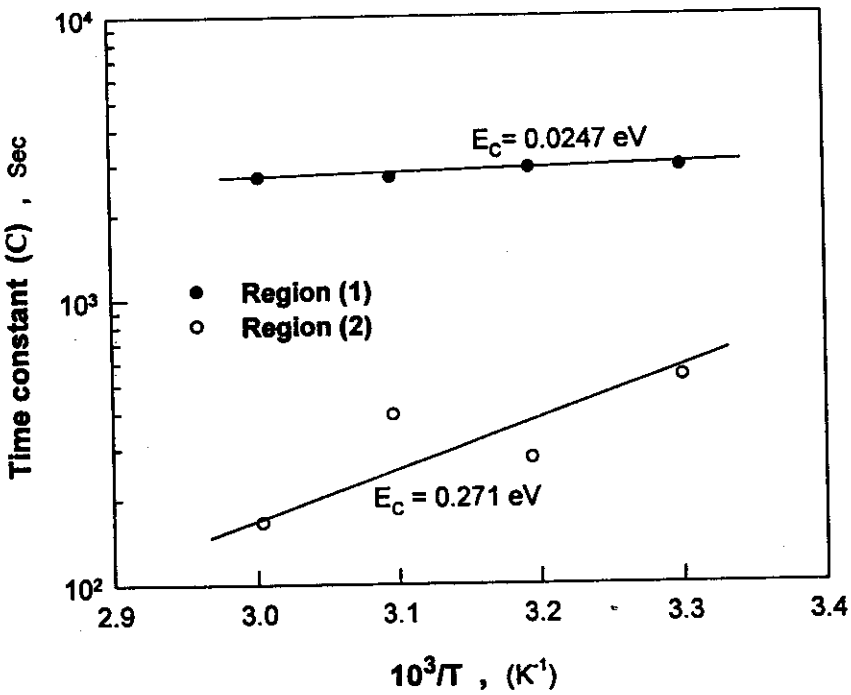

Figure (3.47) : Temperature dependence of time constant* (C) *for the solid electrolyte battery Ag/SE/Ag_2S .

explained as the temperature raises the electrolyte resistance decreases. The time constant C can be expressed by the following Arhenios relation;

$$C = C_o \exp (E_C / KT) \qquad (3.25)$$

where C_o is the time constant at $T = \infty$ and E_C is the activation energy of ion migration rate process.

3.7.5 Effect of annealing on the charging and discharging of solid electrolyte Ag/SE/Ag_2S battery.

In the present section , it is interesting to study the effect of the durability of the solid electrolyte battery. Figure (3.48) illustrates the effect of annealing at crystallization temperature ($T_C = 255\ ^\circ C$) on the charge process of the solid electrolyte Ag/SE/Ag_2S battery,charge current against time at room temperature. The general behaviour is the decay of charge current with time to a stationary value. The attenuation of charge current with time can be attributed to the polarization process. It is also noticed that , the initial value of the charge current for the virgin sample is higher than that for heat treated. This may be attributed to the following , *(i)* change of the nature of Ag_2S – SE barrier height and *(ii)* solid electrolyte amorphous-amorphous transition (this has been confirmed using X-ray diffraction)

Figures [(3.49)A,B] illustrate the cell voltage against electrical capacity for the virgin and annealed solid electrolyte Ag/SE/Ag_2S battery for different time of annealing. It is noticed that , the cell voltage decreases with electrical capacity , In addition , the value of cell voltage for virgin sample is higher than that for samples annealed . Figures [(3.50)A,B] illustrate the discharge current of virgin and annealed solid electrolyte Ag/SE/Ag_2S battery , the general behaviour is the decrease of the values of discharge current to stationary value with increasing time of discharge. The values of C was obtianed by using the least square fitting of equation (3.24). Figure (3.51), illustrates the circuit time constant , C , against time of annealing for the solid electrolyte Ag/SE/Ag_2S battery . Two regions in LnI-annealing time relation was observed . The first show an increase of C with increasing time of annealing while the second shows an attenuation of C with increasing the time of annealing.

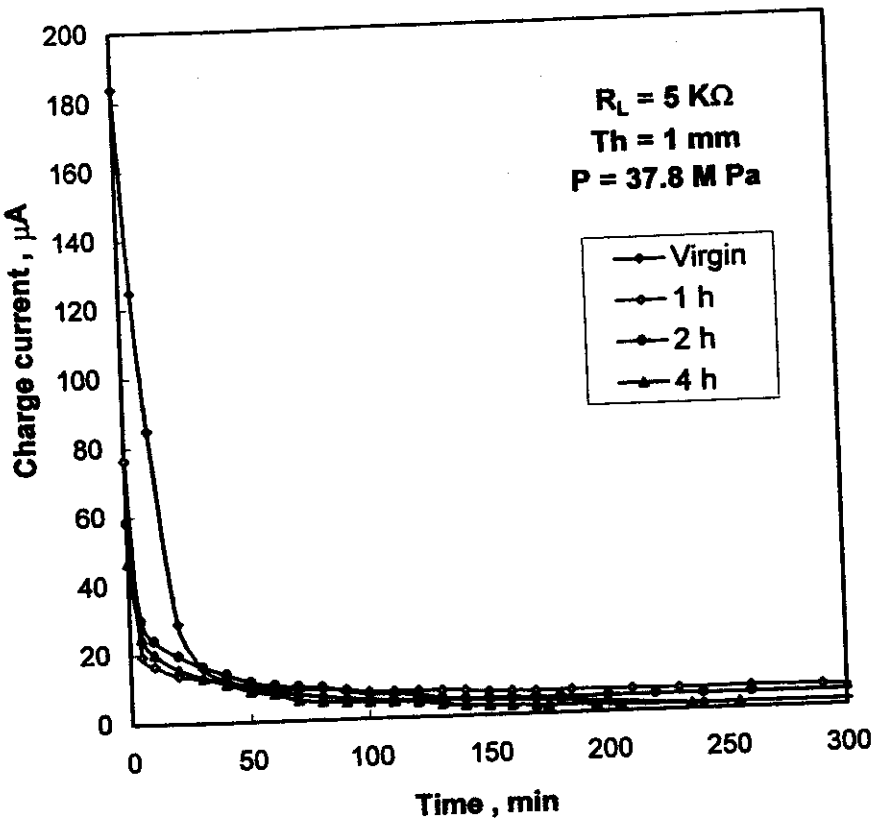

Figure (3.48) : Charge current versus Time for the solid electrolyte batteryAg/SE/Ag_2S charged at constant voltage 3V and different annealing time. .

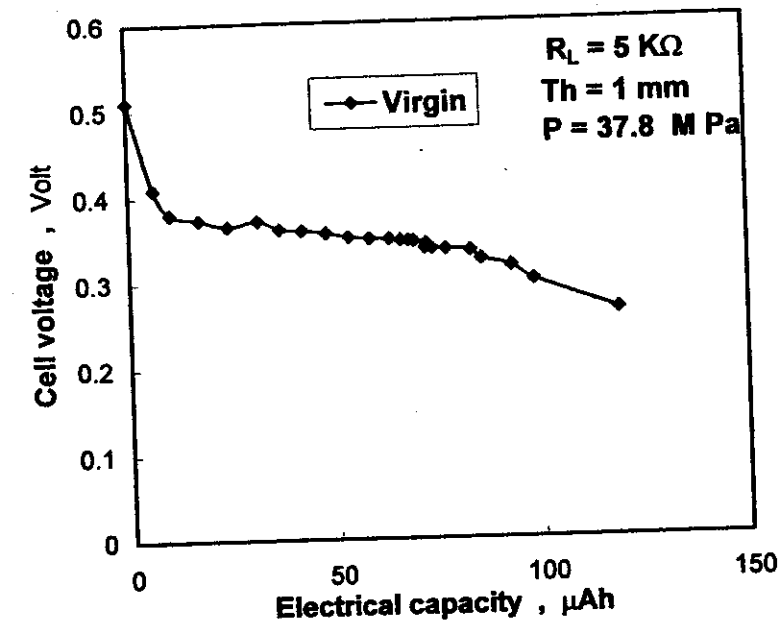

Figure (3.49A) : Cell voltage versus electrical capacity for the virgin solid electrolyte battery Ag/SE/Ag_2S .

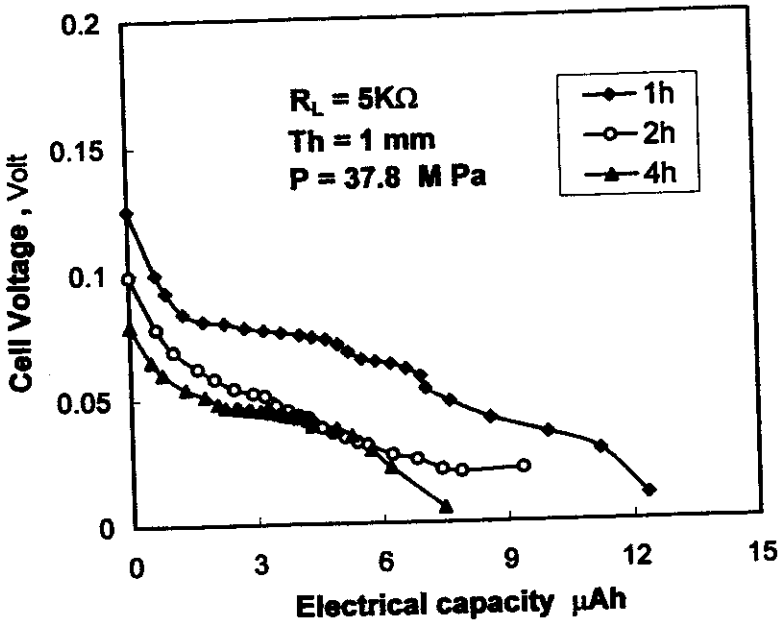

Figure (3.49B) : Cell voltage versus electrical capacity for the annealed solid electrolyte battery Ag/SE/Ag_2S .

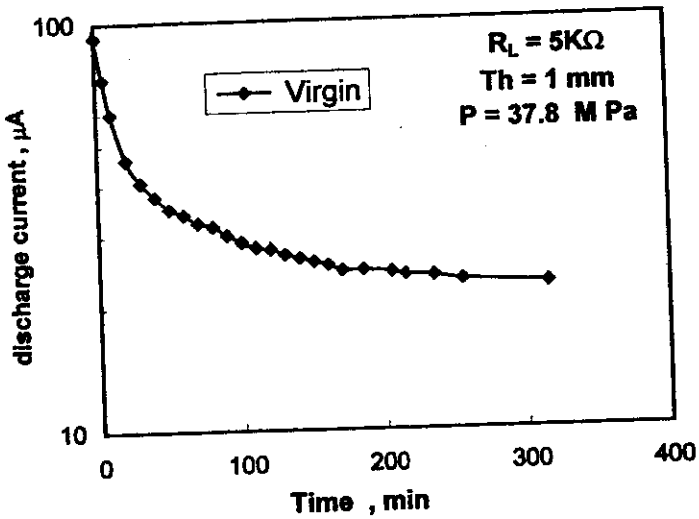

Figure (3.50A) : Discharge current versus Time for the virgin solid electrolyte battery Ag/SE/Ag_2S.

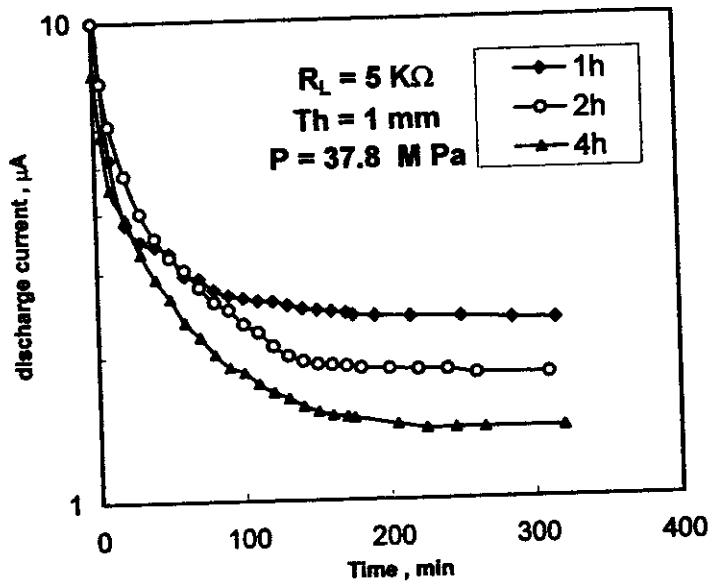

Figure (3.50B) : Discharge current versus Time for the annealed solid electrolyte battery Ag/SE/Ag_2S .

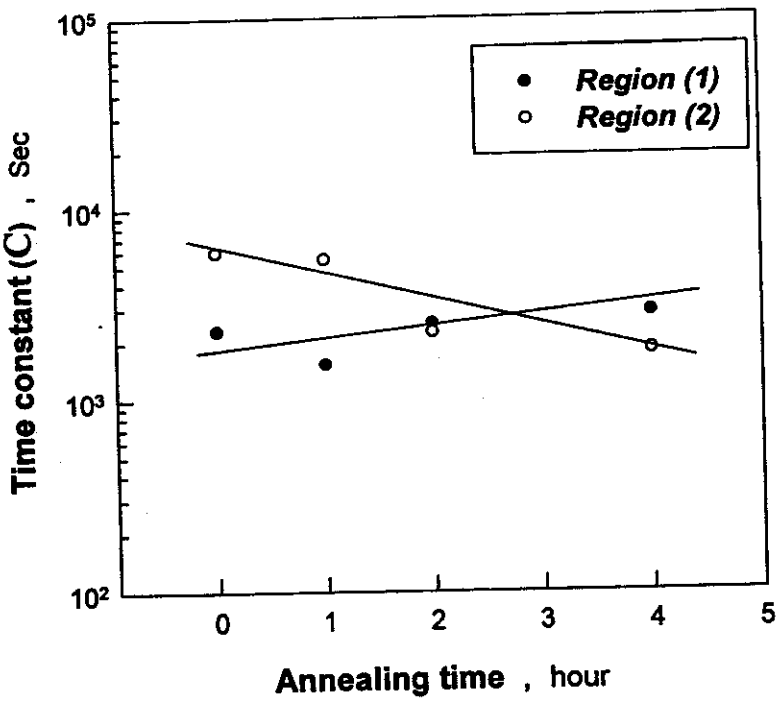

Figure (3.51) : Time constant (C) versus annealing time for the solid electrolyte battery Ag/SE/Ag_2S .

3.7.6 Effect of solid electrolyte Ag/SE/Ag_2S battery storage on the charging and discharging process[75].

The discharge processes of the solid electrolyte Ag/SE/Ag_2S battery was performed after different storage times at room temperature. Figure (3.52) illustrates the cell voltage against elecrical capacity of the solid electrolyte Ag/SE/Ag_2S battery by using load resistance equal to 2MΩ. It is noticed that , the cell voltage shows remarkable decrease down to stationary value . It is also noticed that , the values of cell voltage decreases as the storage time increased which can be attributed to the charge leakage (recovery process) . Figure (3.53) illustrates the discharge current time dependence of battery left charged for different times. The general behaviour shows an attenuation of discharge current with time to stationary value. In addition, the values of discharge current lowers by increasing storage duration because of the mentioned leakage of stored charges. The value of circuit time constant C was obtianed by using least square fitting of equation (3.24). Figure (3.54) , illustrates the time constant C against storage time for the solid electrolyte Ag/SE/Ag_2S battery. It is notices that, the values of C increase by increasing storage time which can be attributed to the increase of the solid electrolyte resistance as a result of the ionic diffusion .

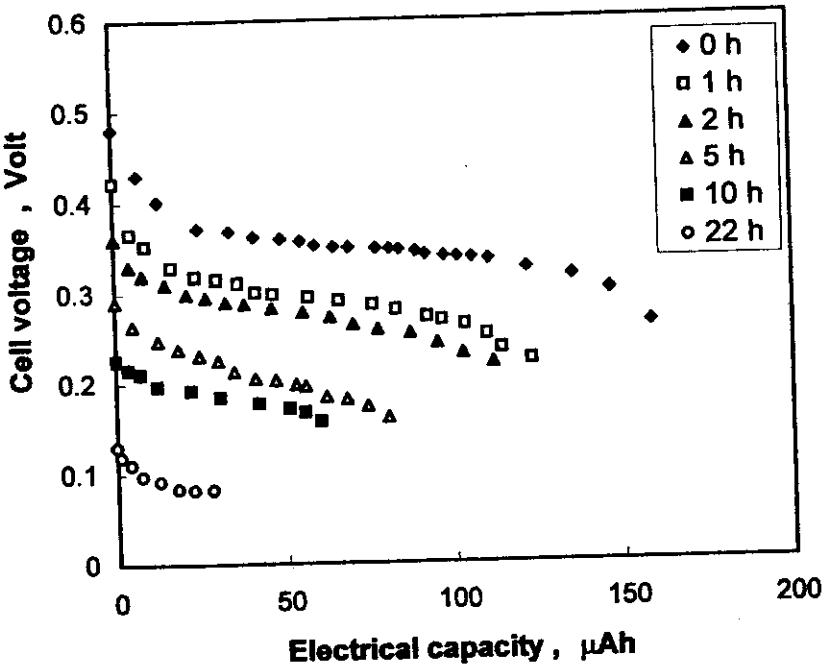

Figure (3.52) : Cell voltage versus electrical capacity for the solid electrolyte battery Ag/SE/Ag_2S discharged at a constant load resistance 2 MΩ.

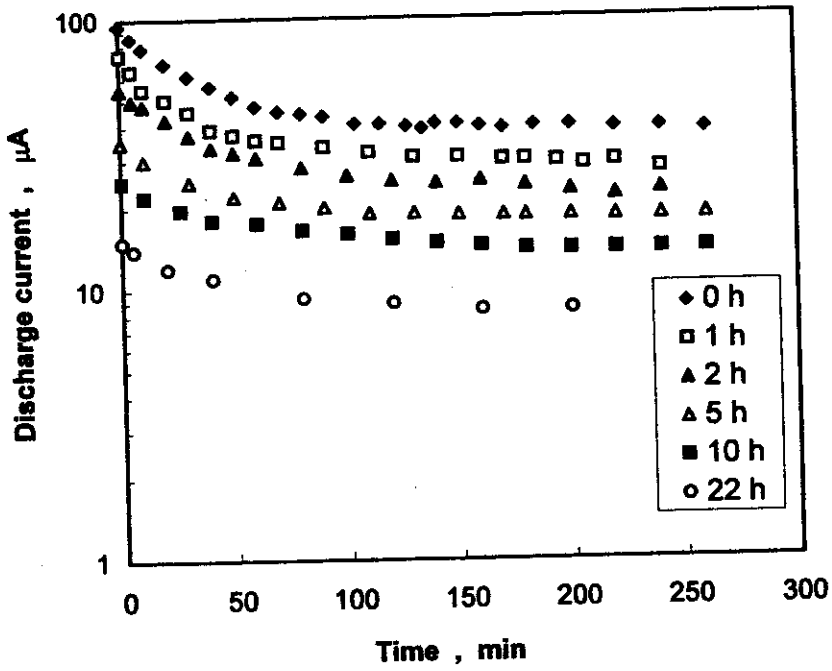

Figure (3.53) : Discharge current versus Time for the solid electrolyte battery Ag/SE/Ag_2S discharged at a constant load resistance 2 MΩ.

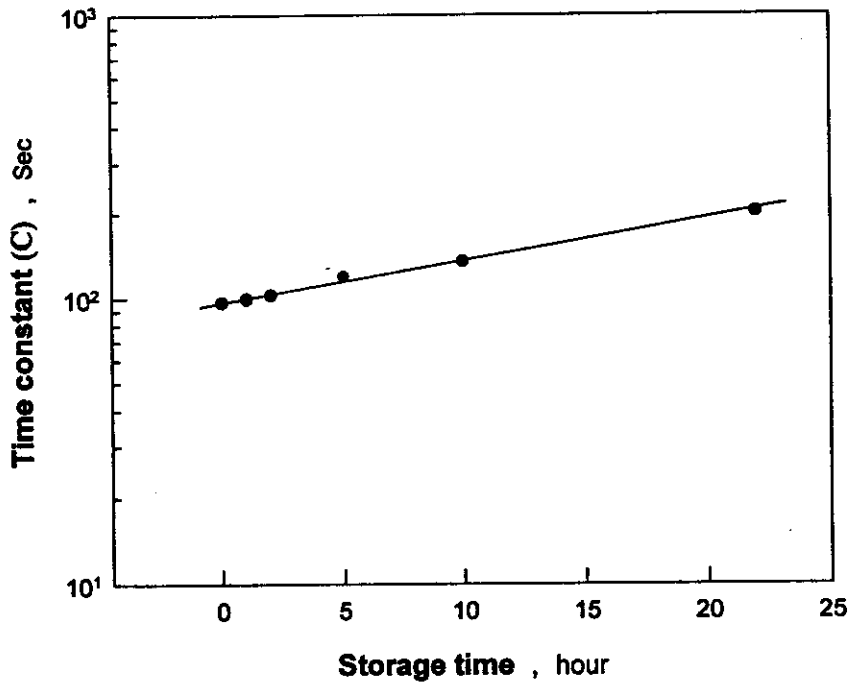

Figure (3.54) : Time constant (C) versus storage time for the solid electrolyte battery Ag/SE/Ag_2S .